BEFORE THE OFFICE OF ADMINISTRATIVE HEARINGS
FOR THE
MINNESOTA PUBLIC UTILITIES COMMISSION
STATE OF MINNESOTA

IN THE MATTER OF AN APPLICATION OF NORTHERN STATES POWER COMPANY FOR AUTHORITY TO INCREASE RATES FOR ELECTRIC SERVICE IN THE STATE OF MINNESOTA	MPUC Docket Nos. E002/GR-12-961 E002/GR-13-868
IN THE MATTER OF THE REVIEW OF THE ANNUAL AUTOMATIC ADJUSTMENT REPORTS FOR ALL ELECTRIC UTILITIES	E999/AA-13-599 E999/AA-14-579 E999/AA-16-523 E999/AA-17-492 E999/AA-18-373

OAH Docket No. 65-2500-38476

DIRECT TESTIMONY OF

ANTHONY A. TIPTON

On Behalf of

NORTHERN STATES POWER COMPANY

June 16, 2023

Exhibit___(AAT-1)

Failure Investigation

Table of Contents

Schedules

I. INTRODUCTION AND QUALIFICATIONS

Q. PLEASE STATE YOUR NAME AND BUSINESS ADDRESS.

A. My name is Anthony Allen Tipton. My business address is 82 Boulder Drive in Barrington, New Hampshire.

Q. WHAT IS YOUR EDUCATIONAL BACKGROUND?

A. I have a bachelor's degree in metallurgy and materials science from Lehigh University in Bethlehem, Pennsylvania. I also have a master's degree in metallurgy and materials engineering from Rensselaer Polytechnic Institute in Troy, New York. My qualifications and experience are more fully described on Exhibit___(AAT-1), Schedule 1

Q. WHAT IS YOUR WORK EXPERIENCE?

A. I have 40 years of metallurgical engineering experience, the vast majority of which was spent addressing issues associated with the design, manufacture, operation and repair of gas and steam turbines, including commercial and military aircraft engines, space shuttle auxiliary power units, Titan IV and other missile hydraulic power units, undersea propulsion turbines for torpedoes, land-based gas turbines, and steam turbines ranging from 50 horsepower to over 950 megawatts.

Q. BY WHOM ARE YOU EMPLOYED AND WHAT IS YOUR POSITION?

A. I am the owner and operator of New England Metallurgical.

Q. HOW LONG HAVE YOU OWNED AND OPERATED NEW ENGLAND METALLURGICAL?

A. Six years, since March 2017.

Q. WHERE WERE YOU EMPLOYED PRIOR TO NEW ENGLAND METALLURGICAL?

A. Thielsch Engineering.

Q. WHERE IS THIELSCH ENGINEERING LOCATED AND WHAT IS THE NATURE OF ITS BUSINESS?

A. Thielsch Engineering is located in Cranston, Rhode Island, and has been primarily a consulting firm for most of its existence supporting the utility industry, everything from boiler systems, to piping systems, to turbomachinery. Their customers are primarily insurance companies, attorneys, and end users such as equipment operators.

Q. WHAT WAS YOUR TITLE AT THIELSCH ENGINEERING?

A. I was a Senior Staff Engineer.

Q. FOR WHOM ARE YOU TESTIFYING?

A. I am testifying on behalf of Northern States Power Company, d/b/a Xcel Energy (Xcel Energy or the Company).

Q. WHAT IS THE PURPOSE OF YOUR TESTIMONY IN THIS PROCEEDING?

A. My testimony will explain my involvement in determining the root cause of the November 19, 2011 catastrophic failure of Unit 3 at the Sherburne County generating plant (the Event); detail the nature of the Event; identify the equipment involved in the Event; describe the critical design features of that equipment as well as detail the operational and maintenance history of that

equipment; and ultimately provide my expert opinion on the root cause of the Event.

II. ROOT CAUSE INVESTIGATION

Q. WHILE AT THIELSCH ENGINEERING, WERE YOU CONTACTED ABOUT AN INCIDENT AT A POWER PLANT IN MINNESOTA, AND IF SO, WHEN AND WHAT WERE YOU TOLD?

A. Yes, a week or two before Christmas of 2011, I received a call from our vice president of engineering services informing me that there was a failure at the Company's Sherburne County power generation facility in Becker, Minnesota (Sherco). The event involved Sherco's third turbine-generator train (Unit 3). The Company wanted to interview someone from Thielsch Engineering to see if they wanted to hire us to perform a failure analysis/root cause analysis.

Q. WHAT WAS YOUR INVOLVEMENT IN THIS MATTER?

A. Thielsch Engineering was contracted by the Company to perform a root cause analysis of the Sherco Unit 3 turbine event which occurred on November 19, 2011. I arrived on-site on January 4, 2012 to begin the investigation.

Q. WHAT QUALIFICATIONS DO YOU HAVE TO PERFORM ROOT CAUSE ANALYSES?

A. I have performed over 300 failure analyses and root cause analyses of gas and steam turbines. These investigations have involved components fabricated from a wide variety of structural alloys. Damage mechanisms have included creep, creep rupture (high temperature exposure), fatigue (cyclic operation) and stress corrosion cracking, hydrogen embrittlement, and other liquid/metal

embrittlement mechanisms as a result of operating in an aggressive environment.

A. Background on Sherco Unit 3 Turbine-Generator Train

Q. DESCRIBE THE LAYOUT OF SHERCO UNIT 3'S TURBINE GENERATOR AS RELEVANT TO THE NOVEMBER 2011 EVENT.

A. Unit 3 is a steam turbine generator designed and manufactured by General Electric (GE). It consists of a high pressure turbine module, a double-flow reheat intermediate pressure turbine module, two double-flow low pressure turbine modules (LP-A and LP-B), a two-pole 1,043,000 kVA generator, and a two-pole 3255 kVA alternator-exciter. The low pressure turbines are relevant to the 2011 failure, and in particular LP-B. A depiction of Sherco Unit 3's turbine generator and its components can be found on Exhibit___(AAT-1), Schedule 3, Figure 1.

Q. DESCRIBE THE LAYOUT OF SHERCO UNIT 3'S TWO LOW PRESSURE TURBINES.

A. The Sherco Unit 3 LP-A turbine rotor with blades attached is shown in Figure 1 below. Each low pressure turbine module contains a rotor comprised of two shaft ends and twelve disks to which blades are attached at the periphery of each disk. The turbine rotor starts out as a large solid forging and is machined radially to form the twelve disks and two shaft ends. The turbine modules are fed steam from a coal-fired recirculating drum boiler which "pushes" on the blade airfoils causing the rotor to rotate. The rotor shaft end is connected to the generator, where the rotational mechanical energy is converted to electrical energy. The LP turbine disks are numbered with the end stage being L-0, the next row in being L-1, and so on. Figure 2 below depicts the blade rows, with the L-5 being at the center of the turbine, and the L-0 being at the end of the

turbine. Figure 2 further depicts the blade attachment design for the L-0 and L-1 blade rows versus the L-2 through L-5 blade rows.

Figure 1
Photograph of Unit 3 low pressure turbine rotor "A" in stands at the Event site

Figure 2
Schematic of low pressure turbine rotor, disks, and blading

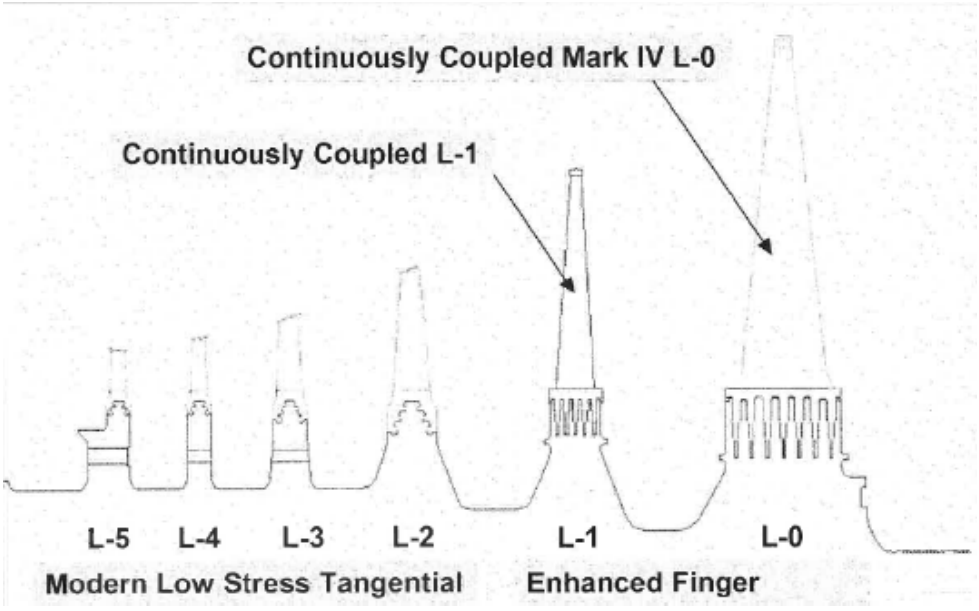

The L-0 and L-1 blade rows use a finger-pinned style attachment[1] wherein the periphery of each rotor disk contains fingers that interlock with matching fingers on the blade[2] roots, not unlike a mortise and tenon joint. Metal pins are press fit into holes in the fingers of the blade and disk to secure each blade to the rotor disk. Figure 3 below provides a view of the finger-pinned style attachment design and the placement of the metal pins.

Figure 3
Depiction of finger-pinned style attachment

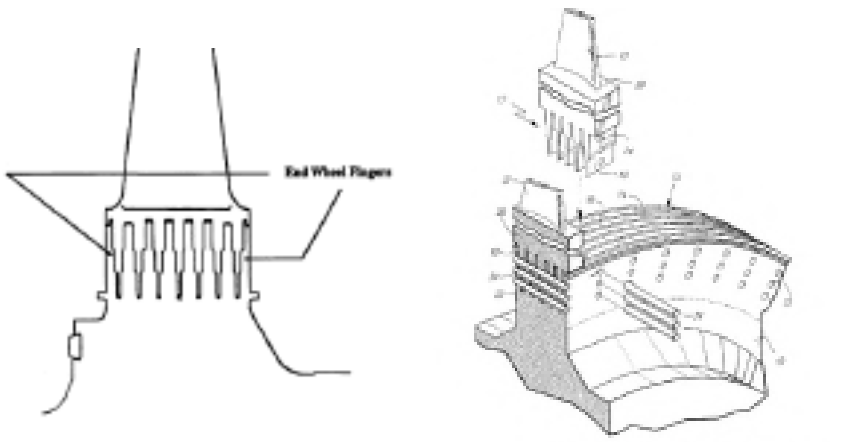

B. The Event

Q. WHAT WAS THE NATURE OF THE EVENT?

A. The turbine-generator train for Unit 3 suffered extensive damage during the Event. The turbine-generator train was started up on November 17, 2011 at the conclusion of a planned outage during which the Company replaced the high pressure and intermediate pressure turbine modules and performed routine maintenance and inspections. Trial start-ups were conducted on November 17,

[1] The finger-pinned style attachment between the rotor disk and the blade has been referred to by GE as a "Finger Dovetail." I find the language "finger-pinned" to describe the style of attachment more accurately as this attachment style is not a dovetail but more akin to a mortise and tenon joint.
[2] General Electric refers to turbine blades as "buckets" in their technical documents.

2011 and November 18, 2011. On November 19, 2011, as the Company conducted a mandatory overspeed test, the unit experienced an explosion-like event—the turbine-generator train began to vibrate violently resulting in fracturing of components with some being liberated from the unit.

Specifically, the steam turbine was disengaged from turning gear at 10:00 a.m. on November 17, 2011 and slowly brought up in speed. The turning gear is an external piece of equipment used to rotate the turbine at very low speed when steam flow is turned off. The train reached approximately 1000 RPM during the day and encountered a slight rub and was brought down in speed and put back on turning gear. A rub occurs when the turbine rotor deflects/bows and contacts a stationary seal usually as a result of nonuniform temperature profile around the turbine rotor. The steam turbine was disengaged from turning gear at about 6:30 p.m. that evening and brought up to 3578 RPM by 7:50 p.m. without load (meaning steam flow to the steam turbine was minimal and just enough to increase turbine speed. It was held at 3578 RPM for about 30 minutes and then brought back down in speed and put on turning gear at 9:20 p.m. It remained on turning gear until 8:35 a.m. the next morning, November 18, 2011, when it was brought up to nominally 3580 RPM without load and held at that speed until 2:37 p.m. At this time, the steam flow to the turbine was increased, the generator breaker was closed, and the unit was loaded. The unit was slowly loaded reaching nominally 240 MW at 10:06 p.m. The unit ran at nominally 3580 RPM producing 240 MW until 7:20 a.m. on November 19, 2011. The inlet flow was cut back and the unit was disconnected from the grid at approximately 9:14 a.m. on November 19, 2011. The unit was put back on turning gear at 11:00 a.m. that same morning.

At approximately 11:55 a.m. on November 19, 2011, the unit was being brought up to speed for a planned test of the overspeed trip system. The mechanical overspeed device consists of a spring-loaded piston (bolt) mounted in a shaft, mounted to the front of the turbine rotor. When turbine speed reaches an overspeed condition (i.e., 10% above running speed), the centrifugal force on the bolt overcomes the spring force, the bolt moves out and hits a lever which moves the oil dump valve causing depressurization of the oil supply to all steam valves. This results in all valves immediately closing and steam flow to the turbine stops. Without steam flow the turbine speed slowly decreases and eventually the turbine will coast to rest. The first trip point was set at 3082 RPM, and the unit tripped at 12:04 p.m. The second trip point was set at 4100 RPM. The unit was brought up in speed and reached 3889 RPM at 12:39 p.m. at which point the unit instantaneously and without warning began to vibrate violently. The generator shaft fractured transversely adjacent to the generator collector ring and the exciter shaft fractured transversely at three locations. The exciter is the power source that supplies the dc magnetizing current to the field windings of the generator. The fracture of the exciter shaft adjacent to the Alterex collector, the collector is a portion of the generator containing the slip rings and brushes, resulted in liberation of the exciter collector with sufficient energy to burst through the generator enclosure (see Exhibit___(AAT-1), Schedule 3, Figure 8) then skip across the turbine deck and through two glass windows of a nearby conference room before coming to rest on the floor of the control room, (see Exhibit___(AAT-1), Schedule 3, Figure 110). The unit immediately tripped, due to high bearing vibration, but required approximately 2½ minutes to coast down; the coast down time was estimated from vibration data recorded on the nearby Boiler Feedwater Turbines. All vibration instrumentation and speed sensors on Unit 3 were destroyed within 12 seconds of the event start.

Two fires resulted from the event, one a hydrogen fire due to escaping hydrogen from the generator and the other due to oil line leaks on the high-pressure and intermediate-pressure steam turbine bearing areas.

C. The Root Cause Analysis

Q. WHAT IS A ROOT CAUSE ANALYSIS (RCA) AND WHAT DOES IT ENTAIL?

A. A root cause analysis is an investigation into an event to determine the cause of the event and identify solutions to avoid a similar event from happening in the future. What is done during a root cause analysis depends on the nature of the event. It could include non-destructive and destructive inspection, material testing, design review, review of maintenance documentation, operation and witness interviews.

Q. WHAT WAS THE PROCESS FOR THE RCA FOLLOWING THE SHERCO UNIT 3 EVENT?

A. The Unit 3 turbine-generator train and surrounding turbine deck were visually inspected, and observations documented photographically, prior to disassembly of the unit. Then, the steam generator was disassembled and inspected. Some components were disassembled and inspected on-site at Sherco, while others had to be transferred to another facility for disassembly and inspection. During the inspection phase, photographs were taken and samples of surface deposits/residue on the various components of the steam generator were collected and sent for a forensic metallurgical examination. A full description of the disassembly and inspection process is detailed at pages 7 through 12 of Exhibit___(AAT-1), Schedule 2: Root Cause Analysis Steam Turbine Generator Event of November 19, 2011.

III. DETERMINED CAUSE OF FAILURE

Q. WHAT DID YOUR INVESTIGATION IDENTIFY REGARDING UNIT 3?

A. Unit 3's LP-B turbine suffered a catastrophic failure which caused significant damage to Unit 3 rendering it inoperable. Upon opening the inner casing of Unit 3's LP-B turbine, I observed a large portion of the blades from the L-1 row had liberated from the rotor, and the remaining blades were severely damaged. I observed fractures and cracks in the finger-pinned blade attachment areas of the L-1 stage disks. The fractures and cracks were due to tensile overload which progressed from pre-existing stress corrosion cracks. Some of the stress corrosion cracks had progressed through the entire cross-section of a given finger in the finger-pinned blade attachment area.

The presence of the stress corrosion cracks in the finger-pinned blade attachment area of the L-1 row disks reduced the load-carrying capability to a degree that centrifugal loads during the overspeed test exceeded the load-carrying capability of the compromised finger-pinned blade attachment areas. The fractures in the finger-pinned blade attachment areas of the L-1 row disk were the primary failure.

As a result of the fracture of the finger-pinned blade attachment areas in the rotor disk, the attached blades, blade pins, and associated fractured portion of disk liberated from the rotor and caused impact damage to surrounding structures, including the remaining L-1 stage blades and the L-0 stage diaphragm. The liberation of blades resulted in a large imbalance which created severe vibration of the entire turbine train causing the other turbines' rotors and shafts to deflect.

Q. WHAT IS STRESS CORROSION CRACKING?

A. Stress corrosion cracking (SCC) is a time-dependent progressive damage mechanism that requires three components: a susceptible material, a specific chemical environment, and a tensile load/stress. SCC occurs at stress levels below the yield strength of the material. Considerable time, measured in years, may be required for cracks to initiate and propagate to the point of component failure.

Q. HOW DOES SCC FORM?

A. The SCC phenomenon is very complex and not completely understood. Several theories have been proposed, and some have gained wider acceptance than others. Gaining a complete understanding is difficult because mechanisms vary with material type and conditions, and the mechanisms active in one system may not be active in another. One generally accepted theory for SCC can be simplified as anodic dissolution of the crack tip and passivation of the crack walls. An applied stress initiates the process by locally rupturing the passive film on a metal surface. The bare metal that is revealed is then subject to anodic dissolution, which extends the crack further. An environmental condition allows the crack walls to repassivate. Film formed at the crack tip then ruptures allowing the cycle to continue and the crack to propagate. Once SCC begins it will continue to propagate provided the tensile load/stress and specific chemical environment remains.

Q. WHAT IS THE WILSON LINE IN A TURBINE AND HOW DOES IT IMPACT SCC?

A. The Wilson Line is the region in the energy extraction process where the steam pressure and temperature are reduced so that the steam becomes wet. In other words, it is where the steam condensates into liquid form. The Wilson Line,

now more typically referred to as the Phase Transition Zone, typically occurs in the last few rows of the blades of the LP turbine, and specifically, rows L-0 and L-1. The increased moisture can contribute to corrosion issues, including stress corrosion cracking, because the condensate may contain increased concentration of certain chemical species present in the boiler water.

As the boiler water goes from steam back to liquid, any impurities concentrate in the droplets that attach to the surfaces of the LP turbine. These impurities can contribute to stress corrosion cracking. To mitigate the risk associated with impurities, it is important to have water chemistry controls in place to decrease, if not eliminate, the presence of impurities.

Q. DID YOU IDENTIFY SCC ON THE L-1 FINGER-PINNED BLADE ATTACHMENTS?

A. Yes. Stress corrosion cracking was identified emanating from the pin holes and stepped ledges of the finger attachment area of the low pressure turbine L-1 rotor disks.

Q. WHAT DID YOU INVESTIGATE AS POTENTIAL CAUSAL FACTORS RESPONSIBLE FOR THE SCC AND BLADE LIBERATION OF THE L-1 ROW BLADE IN THE LP-B TURBINE?

A. I identified three major categories as potential causal factors responsible for the SCC and fractures of LP-B's finger-pinned blade attachments on row L-1. The categories were design, operation, and maintenance. All three were investigated. Regarding design factors, my investigation included the suitability of the rotor material for the intended application and the static design stresses in the finger-pinned blade attachments at normal operating conditions. Regarding operational factors, my investigation included the influence of part-load

operation and boiler water chemistry. Finally, past maintenance and inspection practices were scrutinized for potential influences.

Q. WHAT DID YOUR REVIEW OF THE MAINTENANCE AND INSPECTION HISTORY OF SHERCO UNIT 3 DETERMINE?

A. My review is detailed in Exhibit___(AAT-1), Schedule 2 at pages 65 through 76. However, the following findings merit emphasis here. First, Unit 3 was inspected on rotating major and minor outages every three years. In 1996, Unit 3's blade tie wires were removed following an industry-identified issue with tie-wire cracking.

The Company followed GE's recommendations and replaced all L-1 blades during an outage in 1999. With the blades removed, the Company engaged GE to perform the magnetic particle inspection prescribed in Technical Information Letter (TIL) 1121-3AR1 of the L-1 rotors. The unit was reassembled and returned to service.

During the next major outage in 2005, the L-2 and L-3 rows of the LP turbines were examined by linear phased array ultrasonic inspection and found to have no indications of cracking. Because rows L-2 and L-3 have tangential entry blade attachments, the ultrasonic inspection could be completed without removing the blades. In contrast, due to the finger-pinned style blade attachment design in the L-1 row, magnetic particle inspection and/or ultrasonic inspection could only be accomplished by removing the blades. Such examination was not performed in 2005.

In 2008, during a minor inspection, the last-stage blades on the L-0 row, which are visible at the end of the turbine and also employ a finger-pinned style attachment design, were observed and found to be in generally good condition with only light deposits.

Finally, Unit 3 was taken offline on September 15, 2011, for the installation of new high pressure and intermediate pressure turbines. While offline, Unit 3's LP turbines received a minor inspection.

Q. IN YOUR EXPERT OPINION, WHAT WAS THE EFFECT OF THE MAINTENANCE HISTORY OF UNIT 3 ON THE STRESS CORROSION CRACKING OF ROW L-1'S ROTOR DISK FINGERS?

A. No maintenance procedures performed would have contributed to the stress corrosion susceptibility of the LP turbine components. The Company performed all GE required inspections.

Q. WHAT DID YOUR REVIEW OF THE OPERATIONS AND WATER CHEMISTRY OF SHERCO UNIT 3 DETERMINE?

A. Unit 3 operated at varying power levels depending on grid demands and cycled offline for planned and forced outages. During part load operation, the Wilson Line would move slightly upstream resulting in the L-1 row of blades becoming "wetter." However, there are no GE limitations on part load operation and no technical papers in the open literature or any industry guidelines indicating that part load operation adversely affects corrosion and/or stress corrosion susceptibility of LP steam turbine disks.

The Company utilized an on-line water chemistry monitoring system, and they also took "grab" samples of the boiler water at approximately 2-week intervals since startup in 1987. The samples were analyzed on-site for sodium by atomic emission spectroscopy. Sodium in the boiler water could result in the formation of sodium hydroxide which if sufficiently high in concentration is known to result in stress corrosion cracking of low alloy steel such as the steel used for the Sherco Unit 3 turbine rotors. From start-up to November 19, 2011, the water chemistry of the boiler water in Unit 3 conformed to Electric Power Research Institute (EPRI) guidelines. The significance of monitoring boiler water sodium, as well as a full discussion of Sherco Unit 3's water chemistry practices and history are discussed in the testimony of Company witness Mr. David G. Daniels.

Q. IN YOUR EXPERT OPINION, WHAT WAS THE EFFECT OF OPERATIONS, INCLUDING STEAM AND WATER CHEMISTRY CONTROLS, ON THE STRESS CORROSION CRACKING OF ROW L-1'S ROTOR DISK IN THE FINGER-PINNED BLADE ATTACHMENT AREA?

A. The operating parameters of Unit 3 were not a causal factor contributing to stress corrosion cracking of finger-pinned blade attachment areas of the LP turbine rotor L-1 disks. There was no evidence of abnormal operating conditions that would have contributed to the stress corrosion susceptibility of the aforementioned rotor disks. Additionally, the water chemistry controls were not a factor contributing to the stress corrosion cracking observed in the finger-pinned blade attachment area of the LP turbine's L-1 disks.

Q. IN YOUR INVESTIGATION, DID YOU RESEARCH THE DESIGN STRESSES AND MATERIALS USED FOR THE FINGER-PINNED BLADE ATTACHMENTS USED ON THE L-1 ROW OF SHERCO UNIT 3, AND IF SO, WHAT DID YOU LEARN?

A. Yes, my investigation included an analysis of the materials used. The rotor disk was identified as a Nickel-Chromium-Molybdenum-Vanadium low-alloy steel commonly used by steam turbine manufacturers for operating conditions similar to those of Sherco Unit 3. The Finite Element Analysis indicates that localized steady stresses in Unit 3's LP turbines' finger-pinned blade attachments at the pin holes, ledges and at the base of the fingers is very high and approaches or exceeds the yield strength of the rotor material. At these calculated tensile stress levels the subject alloy has been shown to be susceptible to stress corrosion cracking even in "pure water" environments (Exhibit___(AAT-1), Schedule 3, Figure 501). The susceptibility of the design to stress corrosion cracking is supported by GE TIL 1121-3A (Exhibit___(AAT-1), Schedule 3, Appendix E1-E15) and a patent granted to GE for an improved finger-pinned blade attachment design to reduce the localized stresses and increase the resistance to stress corrosion cracking.

Q. IN YOUR EXPERT OPINION, WHAT WAS THE EFFECT OF THAT DESIGN ON THE STRESS CORROSION CRACKING OF THE L-1 ROTOR DISK FINGERS?

A. GE's equipment design was the primary causal factor responsible for the stress corrosion cracking and fracture of the Unit 3 LP turbine rotor L-1 disks resulting in the liberation of the blades from the LP-B turbine rotor. The design stresses at the LP L-1 finger-pinned blade attachment area of the LP L-1 rotor disks were sufficiently high to render the rotor material susceptible to caustic stress corrosion cracking under normal operating conditions.

IV. ADDITIONAL OBSERVATIONS AND OPINIONS

Q. IN YOUR EXPERT OPINION, IS THE DESIGN ALONE SUFFICIENT TO CAUSE LATENT SCC IN THE L-1 FINGER-PINNED BLADE ATTACHMENTS EVEN UNDER PERFECT OPERATING AND STEAM CHEMISTRY CONDITIONS?

A. Yes.

Q. IN YOUR EXPERT OPINION, IS SCC IN THE FINGER-PINNED BLADE ATTACHMENT AREA OF THE L-1 DISK OF A LOW PRESSURE TURBINE MANUFACTURED TO THE SAME DESIGN STANDARDS AS SHERCO UNIT 3 UNAVOIDABLE EVEN WITH PRUDENT OPERATIONS AND MAINTENANCE OF THE TURBINE AND OF THE STEAM CHEMISTRY?

A. Yes.

Q. DOES THIS CONCLUDE YOUR DIRECT TESTIMONY?

A. Yes, it does.

Anthony A. Tipton
82 Boulder Drive
Barrington, NH 03825
(603) 380-5807

Curriculum Vitae

EDUCATION:

1983: Lehigh University, Bachelor of Science in Metallurgy and Materials Engineering
1987: Rensselear Polytechnic Institute, Master of Science in Metallurgy and Materials Science

EXPERIENCE:

2011-Present *Senior Metallurgical Engineer*
Thielsch Engineering
Cranston, RI

Project Management, root cause analysis, engineering consulting, failure analysis and condition assessment of turbomachinery, boiler components and balance of plant equipment within the power generation industry. Customers include end users and insurance companies/legal counsel.

2008-2011 *President/Owner*
Tipton Consultants
Barrington, NH

Engineering consulting, failure analysis and condition assessment of turbomachinery within the power generation and petrochemical industries. Customers include end users, insurance companies/legal counsel and third party repair facilities.

2004-2008 *Technical Engineering Lead, Materials and Welding Group*
Westinghouse Electric
Newington, NH

Responsibilities included directing, planning and reviewing all materials and weld engineering activities during proposal stage and manufacturing. Products included Control Element Drive Mechanisms, Reactor Coolant Pumps and Reactor Vessel Internals for Nuclear Power Plants. Six direct reports.

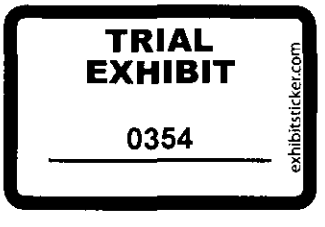

2002-2004 *Principal Engineer/Supervisor, Specialty Roll Shop*
Lehigh Heavy Forge
Bethlehem, PA

Responsible for planning and directing heat treatment and non-destructive inspection activities during contract execution of forged back-up and work rolls for steel rolling mills. Responsible for developing technical and manufacturing process flow. Eight direct reports.

1989-2002 *Manager-Advanced Engineering and Development*
Dresser-Rand
Wellsville, NY

Responsibilities included recommending and implementing technological research and development to advance technical capabilities, enhance product offerings and reduce manufacturing cost/cycle time for new products and the aftermarket. Product lines included steam turbines, gas turbines and hot gas expanders. Department consisted of core technical disciplines relevant to turbomachinery design and manufacture: aerodynamics, rotordynamics, stress and vibration, materials science and manufacturing engineering. Sixteen direct reports.

1986-1989 *Senior Materials Engineer*
Sundstrand Aviation
Rockford, IL

Accountable for selecting materials/processes for new products during design development as well as support of product in field. Product lines included: Space Shuttle APU's, Missile System HPU's, Undersea Propulsion Systems, Ram Air Turbines and Mechanical Actuation Systems.

1983-1986 *Material Engineer*
Pratt & Whitney Aircraft
East Hartford, CT

Primarily responsible for failure analysis of commercial/military fleet and experimental gas turbine engine hardware.

TECHNICAL SOCIETY MEMBERSHIPS:

American Society for Testing and Materials (ASTM)

American Society of Mechanical Engineers (ASME)

PUBLICATIONS:

Tipton, A.A. and Connors, W.C., "Computer Analysis of SEM Striation Spacing Data", *International Symposium on Testing and Failure Analysis*, Los Angeles, CA.,

A. A. Tipton, "Steam Turbine Rotor Weld Repair Development Based Upon Fitness for Purpose Philosophy", *1991 International Joint Power Generation Conference*, San Diego, CA.

A. A. Tipton, M. P. Singh and C. D. Shepherd, "Applying the Probabilistic Fitness-for -Service Concept for Assessing Reliability of Weld Repaired Steam Turbine Rotors", *21st Turbomachinery Symposium*, Dallas, TX.

A. A. Tipton, "The Effect of Gamma Prime Precipitate Size on the Mechanical Properties of a Cast Nickel-Base Superalloy", *8th International Conference on Fracture*, Kiev, Ukraine.

A. A. Tipton, "The Use of Fracture Mechanics for Assessing Reliability of Weld Repaired Steam Turbine Rotors", *8th International Conference on Fracture*, Kiev, Ukraine.

A. A. Tipton, "Fatigue Failure of an Aluminum Turbine Impeller", **Handbook of Case Histories in Failure Analysis. Vol. II**, American Society for Metals, Metals Park.

A. A. Tipton, "Method for Estimating the Remaining Life of Steam Turbine Casings from a Creep Rupture Standpoint", *The Fifth Conference on Materials for Advanced Power Engineering*, Liege, Belgium.

A. A. Tipton, "Repair Technologies to Extend the Service Life and Improve the Reliability of Steam Turbine Components", *Thailand's First Chemical & Refining Plant Maintenance Conference*, Bangkok, Thailand.

A. A. Tipton, "The Effect of Thermal Expansion Mismatch on the High Cycle Fatigue Behavior of a HVOF Sprayed Martensitic Stainless Steel", *The 8th National Thermal Spray Conference*, Houston, Texas.

A.A. Tipton, "Design Considerations of Thermal Sprayed Coatings", Struers Aerospace Alloys Workshop and Symposium, Brea, CA.

A. A. Tipton, "Space Shuttle APU Turbine Blade Failure Analysis-A Retrospective", ASME NEE Chapter Presentation, Durham, NH.

THIELSCH ENGINEERING, INC.
195 FRANCES AVENUE
CRANSTON, RHODE ISLAND 02910

ROOT CAUSE ANALYSIS
STEAM TURBINE GENERATOR EVENT
OF NOVEMBER 19, 2011
UNIT NO. 3
SHERBURNE COUNTY
XCEL ENERGY
BECKER, MINNESOTA

Ara Nalbandian, P.E.

Anthony Tipton

May 29, 2013

Report No. 14439

TABLE OF CONTENTS

Page

EXECUTIVE SUMMARY

The Unit 3 Steam Turbine Generator event of November 2011 was precipitated by the fracture of multiple finger pinned blade attachments in the Low Pressure Turbine "B" turbine end L-1 stage disk rim. The fractures resulted in liberation of portions of the finger pinned blade attachments and associated L-1 blades. The loss of mass, due to the liberation of these blades and disk sections, created a significant imbalance at the affected stage, resulting in high amplitude vibration throughout the steam turbine generator train. This vibration was responsible for the fracture of the generator shaft, fractures of the exciter shaft at three locations and extensive additional damage to the steam turbine generator train and other plant equipment.

The fractures of the finger pinned blade attachments in the low pressure turbine L-1 turbine end disk were due to the presence of pre-existing caustic stress corrosion cracks at the pin holes, ledges and at the base of the finger pinned blade attachments. The chemical species responsible for stress corrosion cracking could not be positively identified but sodium hydroxide (NaOH) is suspected. Although the exact age of the stress corrosion cracks could not be determined, it is likely that they initiated a few years ago. The propagation and "linking-up" of the stress corrosion cracks during subsequent operation incrementally reduced the load carrying capability of the finger pinned blade attachments. By November 2011, the load carrying capability of the finger pinned blade attachments had been reduced to the point that they could no longer sustain the centrifugal stresses generated during the planned overspeed test and fractured due to tensile overload. Investigation also revealed numerous similar stress corrosion cracks in the finger pinned blade attachments of the Low Pressure Turbine "B" generator end L-1 disk and the generator and turbine end L-1 disks of the Low Pressure Turbine "A".

The primary causal factor responsible for the stress corrosion cracking of the low pressure turbine L-1 disks was the high static stresses generated during normal operation at the pin holes, ledges and at the base of the fingers of the finger pinned blade attachments in the low pressure turbine L-1 stage disks. The stresses in the finger

pinned blade attachments are solely a function of the original design and operation at design conditions.

The water chemistry of Unit 3 conformed to EPRI guidelines and was not a significant factor contributory to the stress corrosion cracking observed in the finger pinned blade attachments of the L-1 stage disks. There was no evidence of abnormal operating conditions or maintenance practices that would have contributed to the stress corrosion susceptibility of the finger pinned blade attachments in the L-1 disks.

The material of the low pressure turbine rotors conformed to the mechanical and chemical requirements of ASTM A470 Grade C, Class 7 low alloy steel. There was no apparent material or processing anomalies observed in the disk sections examined.

INTRODUCTION

The Unit 3 steam turbine generator at the Sherburne County Power Plant is a tandem compound train consisting of a high pressure turbine module, double flow reheat intermediate pressure turbine module, two double flow low pressure turbine modules, a two pole 1,043,000 KVA generator and a two pole 3255 KVA alternator-exciter. Designed and manufactured by General Electric, the turbine train arrived on site in late 1979 but remained in storage for a number of years and was not placed into initial operation until July 1987 and commercial operation in November 1987. General Electric provided instructions, consult and inspection audit services for the stored components. The low pressure turbine rotors were stored indoors in a heated environment per General Electric standard GEZ-5691C (Ref 1) with Tectyl 506 applied to all surfaces. General Electric performed inspection audits of the stored turbine components from 1979 through 1982 and Northern States Power performed inspection audits from late 1978 through 1984. The inspection audits occasionally revealed light oxidation and shallow pitting on the journals of the low pressure turbine rotors where they had rested on supports. The oxidation and pitting was removed by light buffing. No other conditions were noted during the inspection audits with regard to the low pressure turbine rotors.

Original design rated conditions were 936 MW at an inlet temperature of 1000°F, inlet pressure of 2520 psig, exhaust pressure of 1.5" HG absolute and speed of 3600 RPM (Ref 2). Details of the original steam turbine generator train are presented in Table 1.

The steam turbine generator is typically operated as a base load unit although it has operated at part load depending on system demands. The unit has not been cycled completely offline except for forced and planned outages.

Table 1

Unit No. 3 Steam Turbine Generator Details-Original Design

Module	Unit S/N	Rotor S/N	Type	Number of Stages
High Pressure Turbine	170X819	3487V1	First Stage - Double Flow. Remaining Stages - Straight Through	7
Reheat Intermediate Pressure Turbine	170X819	125A529VA1	Double Flow	6
Low Pressure A Turbine	170X819	3583V1	Double Flow	6
Low Pressure B Turbine	170X819	3567V1	Double Flow	6
Generator	180X819	123A204VA1	N/A	N/A
Alterex Exciter	316X270	N/A	N/A	N/A

The generator was uprated twice over its lifetime. It was originally shipped as a 956 MVA unit, but was upgraded to 1000 MVA and in fall of 2011 was upgraded to 1043 MVA.

No major upset or abnormal events were reported during the operating history of the Unit 3 steam turbine generator until the incident of November 19th, 2011.

In the fall of 2011, the Unit 3 steam turbine generator was retrofitted with a new high pressure turbine module and intermediate pressure turbine module. The low pressure turbine modules were not replaced. The new high pressure turbine module and intermediate pressure turbine module were designed and manufactured by Alstom Power, Inc. and included features to increase efficiency and overall power output of the steam turbine train. A pictorial of the steam turbine train after the retrofit is shown in Fig. 1. A comparison of rated operating conditions for the original and new steam turbine train is presented in Table 2.

Table 2

Operating Parameters of Unit No. 3

Train	Power (MW)	Inlet Temperature (°F)	Inlet Pressure (psig)	Speed RPM)	Steam Flow ($x10^6$ lbm/hr)
Original (Ref 3)	936	1000	2520	3600	6.3
Retrofit (Ref 4)	957	1000	2520	3600	6.3

Beginning in the year 2000, the instrumented operating data from Unit 3 has been electronically archived using PI® system software from OSIsoft®, LLC. Unless otherwise noted, reference to any operating parameters such as turbine speed, vibration amplitude, bearing temperatures, etc., are taken directly from the PI® archival database supplied by Xcel Energy.

The steam turbine train was started up on November 17, 2011 at the conclusion of the uprate outage to install the retrofitted HP and IP turbine modules. The steam turbine was disengaged from turning gear at 10:00 AM on November 17th and slowly brought up in speed. The train reached approximately 1000 RPM during the day and encountered a slight rub and was brought down in speed and put back on turning gear. It was disengaged from turning gear at about 6:30 PM that evening and brought up to 3578 RPM by 7:50 PM without load. It was held at 3578 RPM for about 30 minutes and then brought back down in speed and put on turning gear at 9:20 PM. It remained on turning gear until 8:35 AM the next morning, November 18th, when it was brought up to nominally 3580 RPM without load and held at that speed until 2:37 PM. At this time the inlet flow was increased, the generator breaker was closed and the unit was loaded. The unit was slowly loaded reaching nominally 240 MW at 10:06 PM. The unit ran at nominally 3580 RPM producing 240 MW until 7:20 AM on November 19th. The inlet flow was cut back and the unit was disconnected from the grid at approximately 9:14 AM on November 19th. The unit was put back on turning gear at 11:00 AM that same morning. At approximately 11:55 AM the unit was being brought up to speed for a planned test of the overspeed trip system. The first trip point was set at 3082 and the unit tripped at 12:04 AM. The second trip point was set at 4100 RPM. The unit was brought up in speed and reached 3889 RPM at 12:39 PM at which point the unit instantaneously and

without warning began to vibrate violently. The generator shaft fractured transversely adjacent to the generator collector ring and the exciter shaft fractured transversely at three locations. The fracture of the exciter shaft adjacent to the Alterex collector resulted in liberation of the exciter collector with sufficient energy to burst through the doghouse enclosure then skip across the turbine deck and through two glass windows of a nearby conference room before coming to rest on the floor of the control room. The unit immediately tripped, due to high bearing vibration, but required approximately 2½ minutes to coast down; the coast down time was estimated from vibration data recorded on the nearby Boiler Feedwater Turbines. All vibration instrumentation and speed sensors on Unit 3 were destroyed within 12 seconds of the event start. Two fires resulted from the event, one a hydrogen fire due to escaping hydrogen from the generator and the other due to oil line leaks on the HP and IP steam turbine bearing areas.

Thielsch Engineering was contracted by Xcel Energy to perform a root cause analysis of the Sherco Unit 3 turbine event which occurred on November 19, 2011. Thielsch Engineering arrived on-site January 4, 2012 to begin the investigation.

TEARDOWN AND DISASSEMBLY OBSERVATIONS

Site clean-up had already commenced prior to Thielsch Engineering's arrival at the plant. The clean-up was limited to debris generated from two localized fires, broken glass from the overhead lighting, displaced insulation and a few fasteners that had backed out of the outer casings and were lying on the turbine deck floor. Photographs of the unit and turbine deck prior to disassembly are shown in Figs. 2 through 4.

The damage to the front standard at the high pressure end of the steam turbine train, resulting from the lube oil fire, is shown in Figs. 5 and 6. Damage resulting from the hydrogen fire in the vicinity of the generator and exciter doghouse enclosure is shown in Figs. 7 and 8. Also evident in these photographs is a hole in the exciter doghouse from the liberated exciter collector. External damage to bearing and coupling covers/ structures is shown in Fig. 9. Many of the outer casing fasteners were sheared or had backed partially/completely out during the failure event. An example of a casing fastener that had partially backed out is shown in Fig. 10. Detailed observations of the steam turbine teardown follow.

High Pressure Turbine

A photograph of the high pressure turbine is shown in Fig. 11. The high pressure inner casing could not be opened at the site and the turbine was shipped intact to Alstom Power, Inc. in Richmond, VA for disassembly. Alstom Power, Inc. opened the casing using hydraulic jacks. It reportedly took over 600 tons of force to separate the upper and low inner turbine casings. The rotor and diaphragms were removed from the casing. The packing seal surfaces on both ends of the rotor were grit blasted and the horizontal split surfaces on both the upper and lower half of the inner casing were "cleaned-up". The HP rotor was placed on stands as shown in Fig. 12. The integral blade shrouds on all stages exhibited moderate to heavy rub damage as shown in Figs. 13 to 15. The interstage seal surfaces exhibited light rub damage from contact with the labyrinth seals as shown in Figs. 16 to 19. Severe galling was evident in the diaphragm fit areas of the inner casing as shown in Figs. 20 to 21. The inlet gland casing exhibited severe galling where the casing mates with the turbine inner casing as shown in Fig. 22. In one galled area a piece of the inner casing had adhered to the inlet gland casing from the

combination of frictional heat and contact pressure accompanying galling; adhesion due to galling is similar to and commonly referred to as "cold welding". During disassembly the "cold weld" between the inner casing and inlet gland casing fractured as shown in Figs. 23 to 24. The inlet gland bolts were severely deformed as shown in Fig. 25. Greyish deposits were observed on blade airfoil surfaces. These deposits were collected and submitted to Engel Metallurgical for deposit analysis as part of the forensic metallurgical analysis.

Reheat Intermediate Pressure Turbine

The reheat intermediate pressure turbine inner casing was opened at the Sherco plant. The inner casing exhibited a number of areas on the horizontal split sealing surface which exhibited characteristics indicative of melting as shown in Figs. 26 to 28. Similar "melted" appearing areas were observed on the outer surface of the outer casing at the alignment lug as shown in Figs. 29 to 30. The rotor was removed and shipped to Alstom Power, Inc. in Richmond, Virginia for further inspection. The rotor was placed on stands for examination as shown in Fig. 31. The blade integral shrouds exhibited moderate to heavy rub damage as shown in Figs. 32 to 33. Heavy greyish colored deposits were evident at base of airfoils and on the underside of the integral shrouds. These deposits were collected and submitted to Engel Metallurgical for inclusion in the forensic metallurgical analysis. The packing and interstage seal surfaces exhibited light rub damage as shown in Figs. 34 to 39. The machined contact faces of both the generator end and turbine end integral couplings exhibited small pits which had the visual characteristics of melted material as shown in Figs. 40 to 43.

Low Pressure Turbine "A"

The Low Pressure Turbine "A" inner casing was opened and the rotor placed on stands at the plant for examination as shown in Figs. 44 to 47. The generator end blading exhibited light to moderate rub damage to all blade covers and tenons with the heaviest being on the L-3, L-4 and L-5 stages as shown in Figs. 48 and 49. The turbine end L-2, L-3, L-4 and L-5 blade covers and tenons exhibited moderate rub damage with the L-3 stage blading exhibiting a few bent and torn blade cover edges as shown in Figs. 50, 51 and 52. Light to moderate impact damage to blade leading and trailing edges was noted. Turbine and generator end diaphragm vanes exhibited moderate impact

and rub damage to trailing and leading edges, Figs. 53 and 54. Moderate rub damage and transferred metal was noted on all interstage seal surfaces. Journal bearing surfaces and inlet seal surfaces exhibited moderate to heavy rub damage with substantial transferred metal present. The low pressure turbine "A" rotor was shipped to the General Electric Service Center in Chicago, Illinois for further inspection.

Low Pressure Turbine "B"

Upon opening the Low Pressure Turbine "B" inner casing it was observed that a large portion of the turbine end L-1 disk rim and associated blading was missing as shown in Fig. 55. The rotor was removed and placed in stands for further examination as shown in Fig. 56. Dark powdery deposits were present on all surfaces of the rotor including the fractured L-1 disk rim. These deposits were collected at a number of locations and submitted to Engel Metallurgical for inclusion in the forensic metallurgical examination. The aforementioned turbine end L-1 disk rim had fractured circumferentially for approximately 180°. The fractures occurred in the four internal finger pinned blade attachments; the outer fingers, which form the side faces of the disk rim, were not fractured. Figs. 57 to 59 show the extent of the L-1 disk rim fracture. The remaining intact turbine end L-1 blades were severely damaged and some had fractured outboard of the midspan attachments as shown in Figs. 60 and 61. The liberated L-1 stage blades and fractured sections of L-1 disk rim were found throughout the inner casing, Fig. 62.

A number of the turbine end last stage blades were fractured transversely through the airfoil and all exhibited severe impact damage as shown in Figs. 63 to 65. The majority of the blade covers were missing. The turbine end L-2, L-3, L-4 and L-5 stage blades exhibited severe rub damage to the covers and tenons with some covers missing and others torn. All blading exhibited severe impact damage to leading and trailing edges of airfoils. Damage to L-2, L-3, and L-4 and L-5 blading is shown in Figs. 66 to 68.

The generator end last stage blades exhibited severe impact damage with a number of blade covers damaged or missing. Impact damage was evident along the stellited leading edges of the last stage blades. The L-1, L-2, L-3, L-4 and L-5 blades exhibited severe rub damage to the integral blade shrouds, covers and tenons. Some covers on

the L-2 stage blades were missing. The damage to the generator end blading is shown in Figs. 69 to 74.

The turbine end and generator end diaphragms exhibited significant impact damage to the vane airfoils. The L-2 turbine end diaphragm exhibited a radial crack completely through the inner wall as shown in Figs. 75 to 76. The crack had not resulted in any liberated diaphragm material. The crack was wide enough to allow limited visual examination on the shop floor. The crack surfaces were coarse textured and appeared relatively fresh, i.e., they were not oxide discolored. It was concluded that the subject crack in the aforementioned diaphragm resulted from the severe vibration during the event and was not submitted for further forensic examination. Two vanes from the turbine end last stage diaphragm had fractured through the weldments at the inner and outer walls and were liberated (Fig. 77). The weld fracture surfaces were coarse textured indicative of tensile overload and exhibited no evidence of oxidation. It was concluded that the weldment fractures resulted from the severe vibration and possibly impact damage during the event and were not submitted for further examination. The L-1 stage diaphragm had fractured through the end wall adjacent to the outer diameter (Fig. 78). Examination revealed a fresh appearing coarse textured fracture morphology indicative of tensile overload (Fig. 79). It was concluded that the end wall fractures resulted from the severe vibration and possibly impact damage during the event and were not submitted for further examination. Typical examples of the damage observed to diaphragms and diaphragm vanes are shown in Figs. 80 and 81.

Severe rub damage and transferred metal was present on the rotor interstage seal surfaces. The journal bearing surfaces and outboard seal surfaces exhibited extensive rub damage and transferred metal.

The fractured turbine end L-1 stage disk rim was protected with "bubble wrap", enclosed in a fabricated wooden box and finally the entire rotor was covered with "shrink wrap", as shown in Figs. 82 and 83, and shipped to the General Electric Service Center in Chicago, Illinois. Swabs of the deposits within the fractured area of the disk rim were taken prior to wrapping the disk. These swabs would be compared with swabs taken after receipt at the GE Service Center and after removal of the disk rim section to

ensure no extraneous contamination occurred during shipping or removal of the disk rim section. The swabs were forwarded to Engel Metallurgical for further forensic examination.

A protocol was developed (Protocol No. 1) detailing the steps to be followed for the removal of the fractured turbine end L-1 stage disk rim; this protocol was reviewed by all interested parties. A copy of Protocol No. 1 is presented in Appendix A. Upon receipt at the General Electric Service Center in Chicago, Illinois, the wooden box and bubble wrap protection was removed and the disk rim fracture area visually examined for shipping damage and/or contamination from shipping. No shipping damage or contamination from shipping was noted. Swabs of the deposits were obtained from the area of the fractured disk rim. GE technicians removed the remaining intact blades in the L-1 disk by driving the attachment pins out. The entire fractured disk rim area was wrapped with a polymeric backed tape and silicon sealant was applied to the outside face of the disk at the intersection of the tape and the disk as shown in Figs. 84 to 86. The disk rim was sectioned from the disk just inboard of the root attachment area by plunge cutting on a lathe from both the upstream and downstream faces of the disk. During the plunge cuts the disk was flooded with a water based coolant. The circumferentially sectioned disk rim was then radially cut at two locations approximately 180° apart using an oxyacetylene torch. After torch cutting the polymeric backed tape was removed and the fractured finger pinned blade attachments visually examined for evidence of contamination from the cutting process. A small amount of liquid and moisture was present in the vicinity of the oxyacetylene torch cut. The liquid was clear, without odor and had a neutral taste. It is believed that the liquid was water which formed from condensation of the products of combustion of the oxyacetylene gas. Swabs of the liquid and of the fractured finger pinned blade attachments where obtained after the cutting process and forwarded to Engel Metallurgical for further forensic examination. The removed sections of the fractured L-1 disk rim were wrapped in bubble wrap and boxed for shipment to Engel Metallurgical for further forensic analysis. The associated L-1 blades and attachment pins were also shipped to Engel Metallurgical for forensic examination.

Inspection of Low Pressure Turbine Rotors at General Electric Service Center, Chicago, Illinois

Magnetic particle and ultrasonic examination was performed on both the "A" and "B" low pressure turbine rotors at the General Electric Service Center in Chicago, IL. Magnetic Particle Inspection (MPI) revealed numerous indications on the internal finger pinned blade attachments of all remaining L-1 stage disk rims as shown in Figs. 87 to 91. These three L-1 disk rims were sectioned from the rotors using the same process as previously described for the fractured L-1 disk rim however, no protection from coolant was employed. The three L-1 disk rims were boxed and shipped to Engel Metallurgical for forensic examination.

Magnetic particle inspection revealed indications in the blade attachment dovetails of the generator end L-2, L-3, L-4 and L-5 stage disks of the low pressure turbine "A" rotor as shown in Figs. 92 to 99. The indications were machined/blended out by General Electric Service Center personnel prior to any investigation. Figs. 100 to 103 show examples of the indication areas after indication removal.

Generator and Exciter

The generator shaft was found to be fractured transversely just forward of the generator collector ring as shown in Figs. 104 and 105. The generator shaft end coupling was liberated from the generator shaft during the event and found on the "doghouse" enclosure floor (Fig. 106). The exciter shaft fractured transversely at three locations, adjacent to the No. 11 bearing, adjacent to the No. 12 bearing and at the Alterex collector ring as shown in Figs. 107 to 109. The fracture at the end of the exciter shaft resulted in the liberation of the Alterex collector ring which burst through the "doghouse" enclosure and bounded across the turbine deck, through a meeting room and came to rest in the control room as shown in Fig. 110. The generator rotor and stator sustained extensive rub damage as shown in Figs. 111 to 114.

Bearings and Standards

All bearings exhibited severe rub damage and transferred metal as shown in Figs. 115 to 118. Some bearings were liberated from the unit while others were found with the bottom halve rolled into/under the top half.

ANALYSIS OF INSTRUMENTED VIBRATION DATA

Instrumented data referenced in this section is presented graphically in Appendix B.

Run 1 - Initial Start-up (Rubbing on Intermediate Pressure Turbine Bearing No. 4)

The unit was started up at 10:02 AM on November 17th. The speed was ramped to 1000 RPM and held steady for approximately 12 minutes. The intermediate pressure turbine bearing No. 4 vibration levels increased to 5.5 mils peak-peak. Plant personnel thought the increased vibration level might be due to a bowed shaft or a rub in the vicinity of the No. 4 bearing. The turbine speed was decreased to 200 RPM to reduce the vibration on the intermediate pressure turbine bearing No. 4.

Run 2 - Rubbing on Intermediate Pressure Turbine

At 11:49 AM on November 17th the unit was started-up again after slow rolling at 200 RPM for approximately one hour. The speed was initially ramped to 1000 RPM. The intermediate pressure turbine bearing No. 4 vibration levels increased to approximately 4.2 mils peak-peak and then began to decrease. Turbine speed was increased to 1400 RPM. Intermediate pressure turbine bearing No. 4 vibration levels increased to 9 mils peak-peak as the speed increased. The speed was lowered back to 1000 RPM to reduce the vibration levels. The intermediate pressure turbine bearing No. 4 vibration levels decreased with speed to 5.4 mils peak-peak. The turbine speed was lowered to 200 RPM to try to eliminate the shaft bow or rub.

Run 3 - Intermediate Pressure Turbine Rub Removed

At 6:40 PM on November 17th the unit was started-up after being on turning gear for approximately 4-1/2 hours. The speed was ramped to 3000 RPM and then the speed was repeatedly varied from 3000 to 2900 to 3000 to 2900 RPM, etc. The intermediate pressure turbine bearing No. 4 vibration levels were reduced but steadily increased over time to approximately 4 mils peak to peak. The low pressure turbine "B" turbine bearing vibrations increased to 4 to 5 mils peak-peak and varied as the turbine speed was varied. At approximately 7:45 PM, the speed was increased to the normal operating speed of 3600 RPM. The intermediate pressure turbine bearing No. 4 vibration levels steadily decreased to approximately 2 mils peak-peak while the speed remained

constant. The exciter bearing No. 11 increased from 2 mils peak-peak to 4.5 mils peak-peak when the speed was increased from 2900 RPM to 3600 RPM. At approximately 8:22 PM, the unit tripped due to a generator lockout related to a new voltage regulator commissioning test. The unit was put on turning gear.

Run 4 - Initial Generator Loading (High Vibration on Exciter)

At 10:30 AM on November 18th the unit was started-up after being on turning gear for approximately 13 hours. The speed was ramped to 3600 RPM. The intermediate pressure turbine bearing No. 4 vibration levels were reduced to approximately 2 mils peak-peak. The exciter bearing No. 11 increased to approximately 6 mils peak-peak. At approximately 2:40 PM, the generator load was steadily increased to approximately 140 MW. At approximately 3:30 PM, the vibration levels increased and then reduced on the high pressure turbine bearing No. 2 and on the intermediate pressure turbine bearing No. 3. At 8:00 PM, the generator load was steadily increased to 240 MW. The intermediate pressure turbine bearing No. 4 vibration levels steadily reduced to approximately 1.5 mils peak-peak. The generator load remained at 240 MW from 9:00 PM until approximately 7:00 AM on November 19th when the load was steadily ramped to zero. At 9:15 AM on November 19th the generator load was zero. The vibrations on the exciter bearing No. 11 were very erratic. The vibration levels were reduced from 5 mils peak-peak to approximately 2 mils peak-peak when the speed was reduced from 3600 RPM to 3000 RPM. At 9:45 AM on November 19th, the vibration levels on exciter bearing No. 11 increased to 7 mils peak-peak when the speed was increased from 3600 RPM to 3750 RPM. At 10:00 AM on November 19th the turbine speed was steadily reduced to zero RPM. A balance weight was installed on the exciter coupling in an effort to reduce the exciter shaft vibration.

Shaft Vibration During Run 4 Coast Down - Shaft Lateral Natural Frequencies

The shaft vibration amplitudes were plotted versus speed during the coast down of Run 4. The rotor lateral frequencies can be determined using these plots. As shown, the exciter shaft has a lateral natural frequency near 3700 RPM which amplifies the vibration at the normal running speed of 3600 RPM. This could explain why the balance weight was required.

Run 5 - Balance Weight Added to Exciter Coupling

At 11:56 AM on November 19th, the unit was started up with a trial balance weight of 73 grams at 205° on the exciter coupling. The speed was ramped to 3100 RPM and then the speed was decreased to 2900 RPM and then increased to 3600 RPM. The speed was held at 3600 RPM for 26 minutes and then it was increased to 3750 RPM for approximately 7 minutes. The speed was lowered to 3600 RPM for approximately 4 minutes and then the speed was increased slowly. At 12:39:10 PM on November 19th the vibration levels, as measured by the vibration probes, increased dramatically at all bearing locations when the turbine speed reached 3890 RPM.

Run 5 - Zoom Plots of Final Few Seconds

At 12:38:40 PM on November 19th the speed was slowly being increased from 3800 RPM. At 12:39:10 PM the speed increased to 3890 RPM and all of the vibration probes suddenly changed. The PI® data provided in Microsoft Excel® data sheets have data recorded every second however, the actual PI® data appears to be obtained every 2 seconds (even numbers starting with zero). The data at the odd numbered seconds are interpolated values. It appears that the failure occurred between 12:39:10 and 12:39:12. The data at 12:39:11 are interpolated values between 12:39:10 and 12:39:12 and are not actual data. The vibration data were measured with shaft rider probes. The values below zero and above 15.3 mils are out of range (probe hard against the shaft or probe too far from the shaft) and are not valid.

Shaft Vibration During Final Few Seconds

In an effort to determine where the failure originated, the shaft vibration at each bearing location was plotted on a sketch of the steam turbine generator train. The data were plotted every two seconds starting before the failure at 12:39:06, the failure at 12:39:12, and finally at 12:39:20 when all of the probes were no longer functioning properly. At 12:39:10, the vibration levels were normal at a speed of 3890 RPM. At 12:39:12, the vibration levels suddenly went off scale (above 15.3 mils peak-peak) on intermediate pressure turbine bearing No. 4, low pressure turbine "A" bearing No. 6, and low pressure turbine "B" bearing No. 7. The vibration levels on the generator and the exciter were still functioning at reasonable levels which indicated that the exciter shaft

did not fail first. The unit had apparently tripped because the speed was reduced to 3817 RPM. At 12:39:14, the vibration levels were still off-scale on low pressure turbine "A" bearing No. 6 and low pressure turbine "B" bearing No. 7. The generator bearing No. 9 and exciter bearing No. 11 were now also off-scale. At 12:39:16, the speed indication was 2 RPM; however, the speed reading was no longer valid. Almost all of the vibration probes were now off-scale. At 12:39:18, the high pressure turbine bearing probes and the exciter bearing probes appeared to still be functioning. At 12:39:20, the only probe that appeared to be functioning was the high pressure turbine bearing No. 1 probe. At 12:39:22, all of the probes quit functioning.

Summary of Instrumented Vibration Data

The vibration data indicates that the event probably originated in the low pressure turbine "B" near bearing No. 7, which is near the stage L-1 blades. The bearing temperature data indicated that the maximum temperature rise also occurred on bearing No. 7.

SELECTION OF COMPONENTS FOR METALLURGICAL FORENSIC ANALYSIS

A number of components were selected for further forensic examination based on visual examinations during teardown at the plant and supplier locations, fracture characteristics, design considerations and the potential that a given failure could result in significant consequential damage to the turbine train. Damage to those components not selected for further examination was deemed to have occurred as the result of the failure of one or more of the components selected for further examination. Table 3 lists the damaged components, potential failure modes, potential failure causes, potential to be a primary failure and findings based on review of instrumented operating data and visual examinations at the plant.

Table 3
Distressed Components, Potential Failure Modes and Causes

Distressed Component	Potential Failure/Damage Modes	Potential Failure Causes	Potential as Primary Failure	Findings	Metallurgical Forensic Exam
Bearings	Babbitt Melting/Transferred Metal/Vibration	Loss of Lubrication	No	Metal Temps/Oil Temps Normal Prior to Event	
	Babbitt Melting/Transferred Metal/Vibration	Bearing Misalignment	No	Vibration Normal Prior to Event	No
	Brinelling/Transferred Metal, Vibration	Critical Speed	No	Vibration Normal Prior to Event	
LP "B" Turbine End L-0 Fractured Diaphragm Vanes	High Cycle Fatigue	Forced Excitation or Resonance	Unlikely	No Evidence of Fatigue	
	Material Defects	Material/Processing	Unlikely	No Material/Processing Anomalies	No
	Tensile Overload	High Stresses As Result of Event	No	Tensile Overload Noted	
LP "B" Turbine End L-1 Diaphragm Fractured End Wall	High Cycle Fatigue	Forced Excitation or Resonance	Unlikely	No Evidence of Fatigue	
	Material Defects	Material/Processing	Unlikely	No Material/Processing Anomalies	No
	Tensile Overload	High Stress As Result of Event	No	Tensile Overload Noted	

Distressed Component	Potential Failure/Damage Modes	Potential Failure Causes	Potential as Primary Failure	Findings	Metallurgical Forensic Exam
LP "B" Turbine End L-2 Cracked Diaphragm Inner Wall	High Cycle Fatigue	Forced Excitation or Resonance	No	No Evidence of Fatigue	No
	Material Defects	Material/Processing	No	No Material/Processing Anomalies	
	Tensile Overload	High Stress As a Result of Event	No	Tensile Overload Noted	
LP Turbine "B" Turbine End L-1 Disk Finger Pinned Blade Attachments	Stress Corrosion Cracking	Operating Stress and Environment	Yes	---	Yes
	High Cycle Fatigue	Forced Excitation or Resonance	Yes		
	Low Cycle Fatigue	Start-Stop Cycles	Unlikely		
	Embrittlement	Material Properties	Unlikely		
	Material Defects	Material/Processing	Unlikely		
	Tensile Overload	Operating Stress Exceeding UTS	No		
LP Turbine "B" Turbine End L-1 Disk Finger Pinned Blade Attachment Pins	Stress Corrosion Cracking	Operating Stress and Environment	Yes	---	Yes
	High Cycle Fatigue	Forced Excitation or Resonance	Yes		
	Low Cycle Fatigue	Start-Stop Cycles	Unlikely		
	Embrittlement	Material Properties	Unlikely		
	Material Defects	Material/Processing	Unlikely		
	Shear Overload	Operating Stress Exceeding Shear Strength	No		
LP Turbine "B" Turbine End L-1 Blades	Stress Corrosion Cracking	Operating Stress and Environment	Yes	---	Yes
	High Cycle Fatigue	Forced Excitation or Resonance	Yes		
	Low Cycle Fatigue	Start-Stop Cycles	Unlikely		
	Material Defects	Material/Processing	Unlikely		
	Tensile/Shear Overload	Operating Stress Exceeding UTS	No		

Distressed Component	Potential Failure/Damage Modes	Potential Failure Causes	Potential as Primary Failure	Findings	Metallurgical Forensic Exam
Generator Shaft	High Cycle Fatigue	Forced Excitation or Resonance	Yes	---	Yes
	Embrittlement	Material Properties	Unlikely		
	Material Defects	Material/Processing	Unlikely		
	Tensile/Shear Overload	Operating Stress	No		
Exciter Shaft	High Cycle Fatigue	Forced Excitation or Resonance	Yes	---	Yes
	Embrittlement	Material Properties	Unlikely		
	Material Defects	Material/Processing	Unlikely		
	Tensile/Shear Overload	Operating Stress	No		

METALLURGICAL FORENSIC ANALYSIS

Low Pressure Turbine "B" Fractured L-1 Disk Protocol No. 2

The two halves of the turbine end L-1 disk rim from low pressure turbine "B" that had been removed at General Electric's Service Center were received at Engel Metallurgical for forensic metallurgical examination (Figs. 119 and 120). A protocol was developed (Protocol No. 2) outlining the testing and laboratory examinations to be performed during the metallurgical forensic analysis of the fractured disk sections; the protocol was reviewed by interested parties and is presented in Appendix A.

The disk rim halves were assigned identification SID 14874 and SID 14875. Initial visual examination revealed multiple transverse cracks and fractures through the four internal finger pinned blade attachments over approximately 180° of the disk rim circumference. The finger pinned blade attachment fractures occurred at various radial heights and were oxide discolored with moderate greyish black deposits as shown in Figs. 121 to 124; the terminal ends of some fractures were not oxide discolored. There was no discernible primary initiation area(s). The blade pins were still intact in the finger pinned blade attachments inboard of the fractured sections of finger pinned blade attachments. The disk rim sections were radially sectioned into smaller subsegments to facilitate further examination and labeled as samples "A thru B" for SID 14874 and samples "A thru D" for SID 14875 as shown in Figs. 119 and 120. Table 4 identifies the subsegments removed from each disk half.

Table 4
Low Pressure Turbine "B" L-1 Disk Rim Subsegments

Disk SID	Subsegment	Testing
14874	A	Fractography, Chemical Analysis, Metallography
14874	B	Not Tested
14875	A	Fractography
14875	B	Fractography, Mechanical Testing, Metallography, SEM, EDS
14875	C	Fractography, SEM, EDS
14875	D	Metallography

Visual Examination

Subsegment "A" from SID 14874 was sectioned circumferentially between each finger pinned blade attachments and each finger was identified as "A1-A6" as shown in Fig. 125. The two middle finger pinned blade attachments in Subsegment "A" were fractured transversely. One finger root attachment fracture occurred at the ledge at the first section thickness change above the base of the attachment, extended to an adjacent pin hole and then extended diagonally outboard to the disk rim outer diameter (OD) as shown in Fig. 126. Fracture through the other finger pinned blade attachment occurred at the base of the attachment, extended radially outboard intersecting a pin hole then progressed circumferentially along the ledge at the first section thickness change above the base of the attachment and finally intersected another pin hole as shown in Fig. 127. All fracture surfaces examined exhibited coarse textured fracture morphology as shown in Figs. 128 to 135. Terminal portions of fractures exhibited morphology indicative of tensile/shear overload. No primary origin location(s) could be identified.

Subsegment "B" from SID 14875 was sectioned circumferentially between the finger pinned blade attachments and each finger was identified as "B1-B6" as shown in Fig. 136. Three internal finger pinned blade attachments in subsegment "B" were fractured transversely. One finger pinned blade attachment fracture occurred along the ledge at the first section thickness change above the base of the attachment, intersected multiple pin holes and extended diagonally to the disk rim OD as shown in Fig. 137. The second finger pinned blade attachment fracture occurred along the base of the attachment, extended radially outboard and along the ledge at the first section thickness change above the attachment base and intersected two pin holes as shown in Fig. 138. The third finger pinned blade attachment fracture occurred along the base of the attachment, extending radially to the disk rim OD on one end and on the other end extending radially outboard to the ledge at the first section thickness change as shown in Fig. 139. Examination revealed the fracture surfaces exhibited coarse textured fracture morphology as shown in Figs. 140 to 153. Terminal portions of fractures exhibited fracture morphology indicative of tensile/shear overload. No primary origin location(s) was identified.

Subsegment "C" from SID 14875 was sectioned circumferentially between the finger pinned blade attachments and each finger was identified as "C1-C6" as shown in Fig. 154. No finger pinned blade attachments were fractured however, all internal fingers exhibited circumferential/radial cracks. The cracks occurred along both the inlet and outlet sides of the finger pinned blade attachments in the ledges at changes in section thickness as well as emanating from the 9:00 and 3:00 locations around the pin holes in the finger pinned blade attachments. Three representative cracks were selected for further examination as shown in Fig. 155. Close-up photographs of the three selected cracks are shown in Figs. 156 to 165. It was noted that shallow circumferential machining grooves were present on all the side faces of the finger pinned blade attachments. In some cases cracks progressed from and along the machining grooves while at other locations they did not. These machining grooves are shown in Figs. 159, 162-163 and 165. The three representative cracks were fractured open revealing coarse textured fracture morphology similar to that observed on the previously detailed fractured finger pinned blade attachments. The fractured open crack surfaces are shown in Figs. 166 to 172.

Light general corrosion/oxidation and minor corrosion pitting were evident on finger root attachments as shown in Figs. 173 to 174.

Scanning Electron Microscopy

Representative areas on fracture surfaces from SID 14875 subsegment "B" and fractures through cracks in SID 14875 subsegment "C" were examined by scanning electron microscope and the surface deposits were qualitatively analyzed by X-Ray Energy Dispersive Spectroscopy (EDS).

Two areas were examined on SID 14875 subsegment "B4" in the as-received condition as shown in Fig. 175. This fracture occurred at the base of an internal finger pinned blade attachment. Examination revealed coarse textured intergranular fracture morphology with heavy surface deposits (Figs. 176, 177 and 179). X-Ray Energy Dispersive Spectrographic analysis of fracture surfaces revealed the presence of iron, lead, copper, tin, nickel, silicon and zinc with lesser amounts of chromium, calcium, manganese, magnesium, sulfur, aluminum and vanadium (Figs. 178 and 180). The

subject fracture was then cleaned and the three areas examined again in the scanning electron microscope (Fig. 181). The cleaning adequately removed the majority of the surface deposits. Two of the areas examined exhibited intergranular fracture morphology (Figs. 182 to 187). The third area examined had a "shiny" appearing surface and exhibited microvoid coalescence morphology indicative of tensile overload (Figs. 188 and 189).

Two areas were examined on SID 14875 subsegment C4b in the as-received condition as shown in Fig. 190. This crack occurred at the 3 o'clock position of a pin hole in the finger pinned blade attachment and was identified as crack No. 3 in Fig. 155. Examination revealed coarse textured intergranular fracture morphology with light/moderate surface deposits (Figs. 191, 192 and 194). X-Ray Energy Dispersive Spectrographic analysis of the crack surfaces revealed the presence of iron, silicon, nickel and chromium with lesser amounts of manganese, tin, sulfur, vanadium, copper, molybdenum, aluminum, calcium and chlorine (Figs. 193 and 195).

Seven areas were examined on SID 14875 subsegment C4d in the as-received condition as shown in Figs. 196 and 197. This crack occurred along the ledge at the first section thickness change above the base of the finger pinned blade attachment, intersected a pin hole and was identified as crack No. 2 in Fig. 155. Examination revealed coarse textured intergranular fracture morphology with moderate to heavy surface deposits (Figs. 198 and 199, 201 and 202, 204 and 205, 207 and 208, 210 and 211, 213 and 214, and 216 and 217). X-Ray Energy Dispersive Spectrographic analysis of the crack surface revealed the presence of iron, nickel, chromium, lead and silicon with lesser amounts of tin, calcium, sodium, manganese, sulfur, copper, aluminum, chlorine, zinc, vanadium and phosphorus (Figs. 200, 203, 206, 209, 212, 215 and 218). The subject fracture was cleaned and four areas examined again in the Scanning Electron Microscope as shown in Figs. 219 and 220. The cleaning adequately removed the majority of the surface deposits. Examination of the four areas revealed an intergranular fracture morphology (Figs. 221 and 222 and 224 and 225). X-Ray Energy Dispersive Spectrographic analysis in one area revealed the presence of iron, nickel, chromium with lesser amounts of silicon, manganese and sulfur (Fig. 223).

Chemical Analysis

Quantitative chemical analysis of a sample removed from the fractured disk rim identified the composition of the low pressure turbine rotor as meeting the requirements of ASTM A470, Grade C low alloy steel (Table 5).

Mechanical Testing

Mechanical testing was conducted to determine mechanical properties of LP rotor material. Mechanical test coupons were removed from the side faces of the disk rim as shown in Figs. 226 and 227. Tensile testing was performed on radially oriented 0.250" specimens per ASTM E8. Material specification ASTM A470 requires 0.500" diameter tensile test specimens however, material availability and configuration limited the specimen diameter to 0.250". Results of the room temperature ultimate tensile strength, 0.2% yield strength, elongation and reduction in area met the requirements for ASTM A470 Class 7 and are presented in Table 6. Room temperature Charpy V-notch impact testing was performed on radially oriented specimens; the notch was oriented tangentially. Room temperature impact test results ranged from 92 to 94 ft·lbs, which conformed to ASTM A470 Class 7 requirement of 40 ft·lbs minimum (Table 7). Low temperature Charpy impact tests were performed to ensure compliance with material specification ASTM A470 $FATT_{50}$ transition temperature requirements. Generation of a full $FATT_{50}$ transition temperature curve was not performed. Low temperature Charpy impact testing indicated that the disk rim material tested exhibited upper shelf Charpy impact strength at 30°F and -30°F (Table 8). ASTM A470 Class 7 requires a $FATT_{50}$ transition temperature of 50°F maximum.

Table 5
Chemical Composition (wt. %) of Low Pressure Turbine Rotor "B"

Element	Sample 1	ASTM Specification A470, Grade C
Fe	Remainder	Remainder
C	0.22	0.28 max.
Mn	0.32	0.20 - 0.60
P	0.006	0.012 max.

Element	Sample 1	ASTM Specification A470, Grade C
S	0.009	0.012 max.
Si	0.08	0.10 max.
Cu	0.04	NR
Ni	3.41	3.25 - 4.00
Cr	1.68	1.25 - 2.00
Mo	0.33	0.25 - 0.60
Al	<0.01	0.015 max.
V	0.129	0.05 - 0.15
Ti	<0.005	--
Cb	<0.005	--
B	<0.0005	--

Table 6
Low Pressure Turbine "B" Rotor Tensile Test Results

	0.2% Yield Strength (ksi)	Ultimate Tensile Strength (ksi)	Elongation (%)	Reduction in Area (%)
Sample 1	116.8	132.1	22.0	69.6
Sample 2	119.3	133.4	22.0	69.1
ASTM A470 Class 7	100 min	120-135	17 min	50 min

Table 7
Low Pressure Turbine "B" Rotor Room Temperature Charpy Impact Test Results

	Test Temperature (°F)	Impact Energy (ft·lbs)
Sample 1	68	93
Sample 2	68	94
Sample 3	68	92
ASTM A470, Class 7	RT	40 min

Table 8
Low Pressure Turbine "B" Rotor Low Temperature Charpy Impact Test Results

	Test Temperature (°F)	Impact Energy (ft·lbs)
Sample 1	-30	86
Sample 2	-30	92
Sample 3	-30	91
Sample 4	30	89
Sample 5	30	91
Sample 6	30	93

Metallography

SID 14875 subsegment "D2" was sectioned transversely through a crack which extended along the ledge at the second change in section thickness radially outboard of the base of the finger pinned blade attachment as shown in Figs. 228 and 229. In the as-polished condition the crack exhibited a jagged crack path with a significant amount of secondary crack branching as shown in Figs. 230 to 233. Areas of oxidation were evident at a number of locations along the crack front as well as within the secondary branched cracks. Examination of the crack path in the etched condition confirmed that the crack path was intergranular and progressed along the prior austenite grain boundaries as shown in Fig. 234. Corrosion pitting up to 0.006" deep was evident on machined surfaces of finger pinned blade attachments (Figs. 235 to 238). The microstructure of the finger pinned blade attachment, at and away from the crack, consisted of tempered martensite and is typical of properly quenched and tempered ASTM A470 Grade C, Class 7 low alloy steel (Figs. 239 and 240).

SID 14875 subsegment "D3" was sectioned to remove a crack which extended along the ledge of the first change in section thickness radially outboard of base of finger pinned blade attachment as shown in Figs. 241 to 242. The metallographic sample was mounted in a planar direction. In the as-polished condition the crack exhibited a jagged crack path with a significant amount of secondary crack branching as shown in Figs. 243 to 245. Areas of oxidation were evident at a number of locations along the crack front and in the secondary branched cracks. The microstructure of the finger pinned blade attachment, at and away from cracks, consisted of tempered martensite

and is typical of properly quenched and tempered ASTM A470 Grade C, Class 7 low alloy steel (Figs. 246 and 247).

SID 14875 subsegment "D5" was sectioned to remove a crack which extended along the ledge at the first change in section thickness radially outboard of the base of the finger pinned blade attachment as shown in Figs. 248 and 249. One metallographic sample was mounted in a planar direction and another was mounted in a transverse direction relative to the crack. In the as-polished condition the transverse sample exhibited an irregular jagged crack path with significant secondary crack branching (Figs. 250 and 251). Examination of the crack path in the etched condition confirmed that the crack path was intergranular and progressed along the prior austenite grain boundaries (Figs. 252 and 253). Microstructure of finger pinned blade attachment, at and away from cracks, consisted of tempered martensite and is typical of properly quenched and tempered ASTM A470 Grade C, Class 7 low alloy steel (Figs. 254 and 255). Examination of the planar sample in the as-polished condition also revealed an irregular jagged crack path with significant secondary crack branching (Figs. 256 to 257). The microstructure of the finger pinned blade attachment, at and away from cracks, consisted of tempered martensite and is typical of properly quenched and tempered ASTM A470 Grade C, Class 7 low alloy steel (Figs. 258 and 259).

SID 14875 subsegment No. B4" was sectioned transversely through a fracture at the base of a finger pinned blade attachment as shown in Figs. 260 to 262. Examination of the fracture in the as-polished condition revealed an irregular jagged fracture path with secondary crack branching (Figs. 263 and 264). The microstructure of the finger pinned blade attachment, at and away from fracture, consisted of tempered martensite and is typical of properly quenched and tempered ASTM A470 Grade C, Class 7 low alloy steel (Figs. 265 and 266).

SID 14874 subsegment "A4" was sectioned transversely through a crack at the base of a finger pinned blade attachment as shown in Figs. 267 and 268. Examination of the crack in the as-polished condition revealed an irregular jagged crack path with secondary crack branching (Figs. 269 and 270). Microstructure of finger pinned blade attachment, at and away from fracture, consisted of tempered martensite and is typical

of properly quenched and tempered ASTM A470 Grade C, Class 7 low alloy steel (Figs. 271 to 272).

Summary of Protocol No. 2 Forensic Examination

The fracture morphology of the fractures and cracks and evidence of significant crack branching are indicative of caustic stress corrosion cracking of low alloy steels operating in the precipitate transition zone of low pressure steam turbines. The chemical species responsible for the caustic cracking is suspected to be sodium hydroxide (NaOH) although the presence of sodium was only detected within one area on one of the fracture surfaces analyzed; it is not unusual for sodium to be absent on the fracture surfaces of caustic stress corrosion cracked low alloy steels in steam turbine environments. Terminal ends of some fractures were due to tensile/shear overload.

Analysis indicated the presence of base metal oxides on the fracture and crack surfaces along with deposits of material believed to be from the leaded brass labyrinth seals and chemical elements in the inlet steam. The presence of circumferential machining grooves, generated during original manufacture of the rotor, on the side faces of the finger pinned blade attachments, although undesirable, are not considered to have been significant factors contributory to the initiation of the stress corrosion fractures and cracks. The tensile properties and Charpy impact strength of the disk rim material conformed to the requirements of ASTM A470, Class 7 low alloy steel. The chemical composition of the disk rim material conformed to the requirements of ASTM A470 Grade C low alloy steel. The microstructure of the disk rim material was typical of properly heat treated ASTM Grade C, Class 7 low alloy steel. There were no apparent material or processing anomalies contributory to cracking.

METALLURGICAL FORENSIC ANALYSIS

Low Pressure Turbine "B" Blades from Fractured L-1 Disk - Protocol No. 4

The low pressure turbine "B" turbine end L-1 blades were received at Engel Metallurgical for forensic analysis and included the blades recovered at the plant site as well as those removed from the L-1 disk at the GE Service Center in Chicago, Illinois. Many of the blades recovered at the site were still attached to the fractured finger pinned blade attachments with the pins intact.

A protocol was developed (Protocol No. 4) outlining the testing and laboratory examinations to be performed during the metallurgical forensic analysis of the blades from the fractured disk of the low pressure turbine "B"; the protocol was reviewed by the interested parties and is presented in Appendix A.

The blades exhibited severe impact damage and secondary damage resulting in extensive deformation as shown in Figs. 273 to 277. Many blades were fractured through the airfoils at various locations above the root platform as shown in Figs. 278 to 280. Visual examination revealed that these fractures were due to tensile/shear overload. One blade was fractured through the airfoil just above the root platform and exhibited "progressive" features on the fracture surface (Figs. 281 to 285). The fracture was slanted relative to the radial axis of the blade. Scanning electron microscope examination of the fracture revealed microvoid coalescence characteristic of tensile/shear overload (Figs. 286 to 289).

Chemical Analysis

Quantitative chemical analysis of a sample removed from a blade root identified the chemical composition of the blade as meeting the requirements of ASTM A276, Grade 403 stainless steel (Table 9).

Hardness Testing

Direct Rockwell C hardness testing was performed on finger pinned attachments of five different blades. The results are presented in Table 10. The measured hardness ranged

from HRC 22.9 to HRC 24.9 and was typical of properly quenched and tempered 403 stainless steel used in steam turbine blading applications.

Table 9
Chemical Composition (wt. %) of a Low Pressure Turbine Rotor "B" Blade

Element	Sample 1	ASTM Specification A276, Grade 403
Fe	Remainder	Remainder
C	0.14	0.15, max.
Mn	0.47	1.00, max.
P	0.016	0.040, max.
S	<0.005	0.030, max.
Si	0.37	0.50, max.
Cu	0.10	--
Ni	0.35	--
Cr	11.8	11.5 - 13.0
Mo	0.13	--
V	0.034	--
Cb	0.068	--

Table 10
Hardness Testing of LP Turbine "B" Turbine End L-1 Stage Blades

	Hardness, HRC (avg.)
SID 14893, Pc "A3"	23.7
SID 14895, Pc "A3"	22.9
SID 14897, Pc "A3"	23.4
SID 14914, Pc "A3"	24.0
SID 14936, Pc "A4"	24.9

Metallography

Examination of a planar section through a finger pinned attachment of a representative blade, SID 14914, Pc "A3", revealed a microstructure consisting of tempered martensite typical of properly quenched and tempered ASTM A276, Grade 403 stainless steel (Figs. 290 to -291). There were no apparent material or processing anomalies.

Summary of Protocol No. 4 Forensic Examination

Fracture morphology of fractures through airfoils of low pressure turbine "B" turbine end L-1 blades was indicative of tensile/shear overload. There was no evidence of fatigue. The chemical composition of blades conformed to ASTM A276, Grade 403 stainless steel. Hardness of blades was typical of properly quenched and tempered 403 stainless steel used in steam turbine blading applications. The microstructure of the blades was typical of properly quenched and tempered ASTM A276, Grade 403 stainless steel. There were no apparent material or processing anomalies.

METALLURGICAL FORENSIC ANALYSIS

Low Pressure Turbine "B" Blade Pins from Fractured L-1 Disk - Protocol No. 3

The low pressure turbine "B" turbine end L-1 blade pins were received at Engel Metallurgical for forensic analysis and included the blade pins which remained attached to the blades recovered at the plant site as well as the blade pins removed from the L-1 disk at the GE Service Center in Chicago, IL (Figs. 292 to 294).

A protocol was developed (Protocol No. 3) outlining the testing and laboratory examinations to be performed during the metallurgical forensic analysis of the blade pins from the fractured L-1 stage disk of the low pressure turbine "B"; the protocol was reviewed by the interested parties and is presented in Appendix A.

Visual examination of the blade pins revealed varying degrees of yielding along the length of the blade pins (Figs. 295-298). Blade pins associated with fractured and liberated finger pinned blade attachments were sheared at the blade/disk attachments. Surfaces of pins exhibited wear damage, likely due to removal from blade/disk and general corrosion. Scanning electron microscope examination of a representative pin revealed scattered light corrosion pitting (Figs. 299 to 300). X-Ray Energy Dispersive Spectroscopy conducted on the surface of blade pin SID 14897 Pc "C" revealed the presence of iron, chromium and manganese with lesser amounts of lead, silicon, copper, tin, nickel, calcium and sulfur (Figs. 301 to 304). Iron, chromium and manganese are present in the pin base material while copper, lead, nickel and tin are believed to be from the leaded brass labyrinth seal wear debris and the silicon, calcium and sulfur are believed to be chemical elements from the inlet steam.

Chemical Analysis

Quantitative chemical analysis of a sample removed from a blade pin identified the chemical composition of the pin as meeting the requirements of ASTM A193, Grade B16 low alloy steel (Table 11).

Table 11
Chemical Composition (wt. %) of a Low Pressure Turbine Rotor "B" Blade Pin

	Sample 1	ASTM Specification A193, Grade B16
Fe	Remainder	Remainder
C	0.44	0.36 - 0.47
Mn	0.53	0.45 - 0.70
P	0.010	0.035, max.
S	<0.005	0.04, max.
Si	0.32	0.15 - 0.35
Cu	0.05	--
Ni	0.04	--
Cr	1.01	0.80 - 1.15
Mo	0.54	0.50 - 0.65
Al	<0.01	0.015, max.
V	0.266	0.25 - 0.35
Ti	<0.005	--
Cb	<0.005	--
B	0.0007	--

Hardness Testing

Direct Rockwell C hardness testing was performed on the surface of six different blade pins. The results are presented in Table 12. Hardness ranged from HRC 36.8 to HRC 40.8. This material can be heat treated to a wide range of strength levels and the required strength level is not known.

Table 12
Hardness Testing of LP Turbine "B" Turbine End L-1 Stage Blade Pins

	Hardness, HRC (*)
SID 14887, Pc "A"	40.3
SID 14914, Pc "B"	36.8
SID 14914, Pc "C"	39.5
SID 14914, Pc "D"	40.2

	Hardness, HRC (*)
SID 14893, Pc "B"	39.4
SID 14893, Pc "C"	38.1
SID 14893, Pc "D"	40.1
SID 14895, Pc "B"	40.5
SID 14895, Pc "C"	40.3
SID 14895, Pc "D"	39.7
SID 14897, Pc "B"	36.9
SID 14897, Pc "C"	40.8
SID 14897, Pc "D"	40.3
SID 14936, Pc "B"	37.2
SID 14936, Pc "C"	37.6

***** Corrected per ASTM E18-08b, Table A6.1

Metallography

Examination of a transverse section through a blade pin, SID 14914, Pc "B", revealed a microstructure consisting of tempered martensite typical of properly quenched and tempered ASTM A193, Grade B16 low alloy steel (Figs. 305 to 306). There were no apparent material or processing anomalies.

Summary of Protocol No. 3 Forensic Examination

Fracture morphology of blade pin fractures associated with fractured and liberated finger pinned blade attachments were indicative of shear overload which occurred at the blade/disk attachments. The chemical composition of blade pins was similar to ASTM A193, Grade B16 low alloy steel. Hardness of pins ranged from HRC 36.8 to HRC 40.8; pin hardness requirement is not known. Microstructure of blade pins was typical of quenched and tempered ASTM A193, Grade B16 low alloy steel. There were no apparent material or processing anomalies.

METALLURGICAL FORENSIC ANALYSIS

Fractured Generator Shaft - Protocol No. 5

The generator shaft fractured transversely just forward of the generator collector ring (Figs. 307 to 311). The aft end generator shaft fracture and the generator side fracture, which was removed from the generator shaft at the GE Service Center, were shipped to Engel Metallurgical for forensic examination. The aft coupling on the generator shaft was liberated during the turbine event and sent to Engel Metallurgical for forensic analysis (Fig. 312).

A protocol was developed (Protocol No. 5) outlining the testing and laboratory examinations to be performed during the metallurgical forensic analysis of the fractured generator shaft; the protocol was reviewed by the interested parties and is presented in Appendix A.

Visual examination of the generator shaft fracture surfaces revealed a greyish discolored coarse textured fracture morphology (Figs. 313 to 321). The forward end fracture was sectioned to remove two subsegments to facilitate further examination in the scanning electron microscope as shown in Fig. 322. Scanning electron microscope examination of fracture surfaces revealed fracture morphology consisted of microvoid coalescence indicative of tensile/shear overload (Figs. 323 to 330).

Chemical Analysis

Quantitative chemical analysis of a sample removed from the forward end of the generator shaft fracture identified the chemical composition of the generator shaft as meeting the requirements of ASTM A469, Grade 6, 7 and 8 low alloy steel (Table 13).

Table 13
Chemical Composition (wt. %) of Generator Shaft

Element	Sample 1	ASTM Specification A469, Grade 6, 7 and 8
Fe	Remainder	Remainder
C	0.21	0.28, max.
Mn	0.30	0.60, max.

Element	Sample 1	ASTM Specification A469, Grade 6, 7 and 8
P	0.006	0.015, max.
S	0.012	0.015, max.
Si	0.04	0.30, max.
Cu	0.06	--
Ni	3.36	3.25 - 4.00
Cr	1.68	1.25 - 2.00
Mo	0.34	0.30-0.60
Al	<0.01	--
V	0.085	0.05 - 0.15
Ti	<0.005	--
Cb	<0.005	--
B	<0.0005	--

Mechanical Testing

Mechanical testing was performed to determine mechanical properties of the generator shaft material. Two coupons for machining tensile specimens were removed from the forward end of the generator shaft fracture as shown in Fig. 331. Tensile testing was performed on longitudinally oriented 0.500" specimens per ASTM E8. Results of the room temperature ultimate tensile strength, 0.2% yield strength, elongation and reduction in area met the requirements for ASTM A469 Grade 7 and are presented in Table 14. Hardness testing was performed on a subsegment cut from the forward end of the generator shaft fracture as shown in Fig. 332. Brinell hardness was 250 HBW; there are no specification hardness requirements.

Table 14
Generator Shaft Tensile Test Results

	0.2% Yield Strength (ksi)	Ultimate Tensile Strength (ksi)	Elongation (%)	Reduction in Area (%)
Sample 1	110.1	114.0	18.5	72.9
Sample 2	111.1	115.9	17.9	72.1
ASTM A469 Grade 7	90 min	110 min	17 min	50 min

Metallography

Metallographic examination of transverse and longitudinal sections through the generator shaft in the vicinity of fracture revealed a microstructure consisting of bainite with dispersed carbides (Figs. 333 to 336) typical of properly heat treated ASTM A469 Grade 7 low alloy steel. There were no apparent material or processing anomalies.

Summary of Protocol No. 5 Forensic Examination

Fracture morphology of the generator shaft fracture was indicative of tensile/shear overload. Chemical composition of the generator shaft conformed to requirements of ASTM A469, Grade 6, 7 and 8 low alloy steel. Tensile properties of the generator shaft conformed to the requirements of ASTM A469, Grade 7 low alloy steel. The microstructure of the generator shaft was typical of properly heat treated ASTM A469, Grade 7 low alloy steel. There were not apparent material or processing anomalies.

METALLURGICAL FORENSIC ANALYSIS

Fractured Exciter Shaft - Protocol No. 6

The exciter shaft fractured transversely at three locations, adjacent to the No. 11 bearing, adjacent to the No. 12 bearing and at the Alterex collector ring as shown in Figs. 337 to 340. The exciter shaft was shipped to Engel Metallurgical for forensic analysis.

A protocol was developed (Protocol No. 6) outlining the testing and laboratory examinations to be performed during the metallurgical forensic analysis of the fractured exciter shaft; the protocol was reviewed by the interested parties and is presented in Appendix A.

Visual examination of the fracture surface of the transverse fracture adjacent to the No. 11 bearing revealed a coarse textured morphology typical of tensile/shear overload (Figs. 341 to 343). Examination of the fracture surface of the transverse fracture adjacent to the No. 12 bearing revealed a coarse textured morphology typical of tensile/shear overload (Figs. 344 to 348). Examination of the fracture surface of the transverse fracture adjacent to the Alterex collector ring revealed a coarse textured morphology typical of tensile/shear overload (Figs. 349 to 351).

A subsegment was removed from the exciter shaft fracture adjacent to the No. 11 bearing for examination by scanning electron microscopy as shown in Figs. 352 to 353. Scanning electron microscope examination of fracture revealed microvoid coalescence indicative of tensile/shear overload (Figs. 354 to 358). A subsegment was removed from the exciter shaft fracture adjacent to the No. 12 bearing for examination by scanning electron microscopy as shown in Figs. 359 to 360. Scanning electron microscope examination of fracture revealed microvoid coalescence indicative of tensile/shear overload as shown in Figs. 361 to 364 and Figs. 366 to 367; some areas of the fracture exhibited rub damage. X-Ray Energy Spectrographic analysis of the fracture surface revealed the presence of base metal oxides and small amounts of aluminum and silicon (Fig. 365). A subsegment was removed from the exciter shaft fracture adjacent to the Alterex collector ring for examination by scanning electron microscopy as shown in

Figs. 368 to 369. Scanning electron microscope examination of fracture revealed microvoid coalescence indicative of tensile/shear overload (Figs. 370 to 374); some areas of fracture exhibited rub damage.

Chemical Analysis

Quantitative chemical analysis of a sample removed from the exciter shaft fracture identified the chemical composition of the exciter shaft as meeting the requirements of ASTM A469, Grade 6, 7 and 8 low alloy steel (Table 15).

Table 15
Chemical Composition (wt. %) of Exciter Shaft

Element	Sample 1	ASTM Specification A469, Grade 6, 7 and 8
Fe	Remainder	Remainder
C	0.19	0.28, max.
Mn	0.35	0.60, max.
P	0.005	0.015, max.
S	0.010	0.015, max.
Si	0.07	0.30, max.
Cu	0.07	--
Ni	3.29	3.25 - 4.00
Cr	1.57	1.25 - 2.00
Mo	0.38	0.30 - 0.60
Al	<0.01	--
V	0.113	0.05 - 0.15
Ti	<0.005	--
Cb	<0.005	--
B	<0.0005	--

Mechanical Testing

Mechanical testing was performed to determine mechanical properties of the exciter shaft material. Two coupons for machining tensile specimens were removed from the

exciter shaft. Tensile testing was performed on longitudinally oriented 0.500" specimens per ASTM E8. Results of the room temperature ultimate tensile strength, 0.2% yield strength, elongation and reduction in area met the requirements for ASTM A469 Grade 7 and are presented in Table 16. Hardness of exciter shaft was 268 HBW; there are no hardness requirements in ASTM A469.

Table 16
Exciter Shaft Tensile Test Results

	0.2% Yield Strength (ksi)	Ultimate Tensile Strength (ksi)	Elongation (%)	Reduction in Area (%)
Sample 1	93.6	121.7	21.5	71.5
Sample 2	94.2	121.9	22.1	70.2
ASTM A469 Grade 7	90 min	110 min	17 min	50 min

Metallography

Metallographic examination of transverse and longitudinal sections through exciter shaft in vicinity of fracture revealed a microstructure consisting of martensite typical of properly heat treated ASTM A469 Grade 7 low alloy steel (Figs. 375 to 378). There were no apparent material or processing anomalies.

Summary of Protocol No. 6 Forensic Examination

The fracture morphology of all three transverse fractures through the exciter shaft was indicative of tensile shear overload. The chemical composition of the exciter shaft conformed to the requirements of ASTM A469, Grade 6, 7 and 8 low alloy steel. Tensile properties of the exciter shaft conformed to the requirements for ASTM A469, Grade 7 low alloy steel. The microstructure of the exciter shaft was typical of properly heat treated ASTM A469, Grade 7 low alloy steel. There were no apparent material or processing anomalies.

METALLURGICAL FORENSIC ANALYSIS

Cracked Low Pressure Turbines "A" and "B" L-1 Disk Rims - Protocol No. 7

The turbine end and generator end L-1 disk rims from low pressure turbine "A" and the generator end L-1 disk rim from low pressure turbine "B" exhibited numerous linear indications in the finger pinned blade attachments during magnetic particle inspection at the General Electric Service Center in Chicago, Illinois. These indications would not have been visible unless the blades were first removed from the disk. The disk rim sections of all the L-1 disks were removed and shipped to Engel Metallurgical for forensic analysis (Figs. 379 to 381).

A protocol was developed (Protocol No. 7) outlining the testing and laboratory examinations to be performed during the metallurgical forensic analysis of the cracked finger pinned blade attachments in the generator end L-1 disk of low pressure turbine "B" and both the turbine end and generator end L-1 disks of low pressure turbine "A"; the protocol was reviewed by the interested parties and is presented in Appendix A.

One half of each disk rim section received from each L-1 disk was sectioned transversely into smaller subsegments and then these subsegments were further circumferentially sectioned between the blade attachment fingers to facilitate examination. Visual examination of blade attachment fingers revealed a multitude of circumferential and radial cracks along the ledges at the changes in section thickness and at the blade pin holes as shown in Figs. 382 to 396. It was noted that shallow circumferential machining grooves were present on all the side faces of the finger pinned blade attachments. In some cases cracks progressed from and along the machining grooves while in other locations they did not. These machining grooves are shown in Figs. 382 to 389 and 393 to 396. Cracks from each disk were removed from the disk subsegments and fractured open for examination. Visual examination of fractures through all cracks revealed dark oxide discolored coarse textured intergranular fracture morphology with varying amounts of surface deposits (Figs. 397 to 417). Scanning electron microscope examination of crack surfaces confirmed intergranular fracture morphology (Figs. 418 and 419, 422 to 424, and 428 and 429). X-Ray Energy Dispersive Spectroscopy identified the presence of base metal oxides and small

quantities of silicon on the crack surfaces (Figs. 420 and 421, 425 and 427, and 430 and 431); one area also contained trace amounts of copper and aluminum.

Chemical Analysis

Quantitative chemical analysis of a sample removed from a cracked disk rim from the turbine end of low pressure turbine "A" identified the composition of the low pressure turbine rotor as meeting the requirements of ASTM A470, Grade C low alloy steel (Table 17).

Table 17
Chemical Composition (wt. %) of Low Pressure Turbine Rotor "A"

Element	Sample 1	ASTM Specification A470, Grade C
Fe	Remainder	Remainder
C	0.21	0.28, max.
Mn	0.34	0.20 - 0.60
P	0.005	0.012, max.
S	0.009	0.012, max.
Si	0.04	0.10, max.
Cu	0.03	NR
Ni	3.42	3.25,-,4.00
Cr	1.65	1.25,-,2.00
Mo	0.33	0.25,-,0.60
Al	<0.01	0.015, max.
V	0.102	0.05,-,0.15
Ti	<0.005	--
Cb	<0.005	--
B	<0.0005	--

Mechanical Testing

Mechanical test coupons were removed from the turbine end L-1 disk rim subsegment "A1" from low pressure turbine "A". Tensile testing was performed on radially oriented

0.250" specimens per ASTM E8. Material specification ASTM A470 requires 0.500" diameter tensile test specimens however, material availability and configuration limited the test specimen diameter to 0.250". Results of the room temperature ultimate tensile strength, 0.2% yield strength, elongation and reduction in area met the requirements for ASTM A470 Class 7 and are presented in Table 18. Room temperature Charpy V-notch impact testing was performed on radially oriented specimens with the notch oriented tangentially. Room temperature impact test results ranged from 105-110 ft-lbs which conformed to ASTM A470 Class 7 requirement of 40 ft-lbs minimum (Table 19).

Table 18
Low Pressure Turbine "A" Rotor Tensile Test Results

	0.2% Yield Strength (ksi)	Ultimate Tensile Strength (ksi)	Elongation (%)	Reduction in Area (%)
Sample 1	108.6	123.0	22.0	73.6
Sample 2	109.1	122.8	22.0	73.8
ASTM A470 Class 7	100 min	120-135	17 min	50 min

Table 19
Low Pressure Turbine "A" Rotor Room Temperature Charpy Impact Test Results

	Test Temperature (°F)	Impact Energy (ft·lbs)
Sample 1	70	105
Sample 2	70	110
Sample 3	70	109
ASTM A470, Class 7	RT	40 min

Metallography

Metallographic specimens were prepared from cracked areas of finger pinned blade attachment subsegments of the turbine end and generator end L-1 disk rims of the low pressure turbine "A" and the generator end of the low pressure turbine "B" as shown in Figs. 432, 441 and 451. Examination of the cracks in the as-polished condition revealed irregular and jagged intergranular crack paths with secondary crack branching (Figs. 433 to 438, 442 to 448 and 452 to 462). The microstructure of samples at and

away from cracks in all finger pinned blade attachments examined consisted of tempered martensite and is typical of properly quenched and tempered ASTM A470 Grade C, Class 7 low alloy steel (Figs. 439 and 440, 449 and 450, and 463 and 464).

Summary of Protocol No. 7 Forensic Examination

The fracture morphology and the branched nature of the cracks in the finger pinned blade attachments from both low pressure turbine "A" L-1 stage disks and the low pressure turbine "B" generator end L-1 disk are indicative of caustic stress corrosion cracking of low alloy steels operating in the precipitate transition zone of low pressure steam turbines. The characteristics of these cracks were identical to those observed in the low pressure "B" turbine end L-1 disk finger pinned blade attachments fractures. The chemical species responsible for the caustic cracking is suspected to be sodium hydroxide (NaOH) although the presence of sodium was not detected on any of the crack surfaces examined; it is not unusual for sodium to be absent from the fracture surfaces of caustic stress corrosion cracked low alloy steels in steam turbine environments. The crack surfaces exhibited base metal oxides and trace amounts of silicon from the inlet steam. The presence of circumferential machining grooves, generated during original manufacture of the rotor, on the side faces of the finger pinned blade attachments, although undesirable, are not considered to have been a significant factor contributory to stress corrosion cracking. The chemical composition of the low pressure turbine "A" L-1 disk rim material conformed to the requirements of ASTM A470 Grade C low alloy steel. The tensile properties and Charpy impact strength of the disk rim material from the low pressure turbine "A" conformed to the requirements of ASTM A470, Class 7 low alloy steel. The microstructure of the disk rim material from low pressure turbine "A" was typical of properly heat treated ASTM Grade C, Class 7 low alloy steel. There were no apparent material or processing anomalies contributory to cracking.

METALLURGICAL FORENSIC ANALYSIS

Deposit Analysis - Protocol No. 10

A number of deposit samples were obtained during the investigation at the plant site and at supplier facilities. A protocol was developed (Protocol No. 10) outlining the testing and laboratory examinations to be performed during the energy dispersive spectrographic analyses of the deposit samples; the protocol was reviewed by the interested parties and is presented in Appendix A.

Deposits from High Pressure and Intermediate Pressure Turbines

Deposits were collected at the plant site and at the Alstom Repair Facility from the high pressure and intermediate pressure turbines. These deposits were collected from the rotating blades and from inside the casing. The samples collected and their details are presented in Table 20. The results of X-Ray Energy Dispersive Spectrographic analyses of the deposits are presented in Table 21. The deposits contained base metal oxides, wear debris from seal materials and chemical elements present in the inlet steam.

Table 20
Samples Collected from HP and IP Turbines for Chemical Analysis

Identification	Deposit Type	Location
L349136 (SID 15000)	Residue on carbon stub	HP 2nd Stage Blade
L349137 (SID 15004)	Residue on carbon stub	HP 6th Stage Blade
L349138 (SID 15007)	Residue on carbon stub	HP Casing Nozzle Bore
L349141 (SID 14994)	Residue on carbon stud	IP GE 1st Stage Blade
L349143 (SID 14834)	Residue on carbon stub	IP TE 6th Stage Blade

Table 21
EDS Analyses Results of Deposit Samples from HP and IP Turbines

Identification	EDS Result
L349136 (SID 15000) loc A	Fe, Cr, Mn, Si, Sn, Ni, Mo, V, Al
L349136 (SID 15000) loc B	Fe, Cr, Cu, Sn, Mn, Si, Zn, Al, Ca, Ni, V, Mo
L349137 (SID 15004)	Fe, Cr, Mn, Al, Ca, Si, Cu, Mo, Ni, V

Identification	EDS Result
L349138 (SID 15007)	Fe, Cr, Mn, Ca, Cu, Mo, Si, V, Ni, Al
L349141 (SID 14994)	Fe, Cr, Mo, Mn, Si
L349143 (SID 14834)	Fe, Cr, Cu, Mn, Ni, Mo, Zn, Si, V, Ca, Al

Deposits from Fractured Finger Pinned Blade Attachments from Low Pressure Turbine "B" Turbine End L-1 Disk

Deposits were collected at the plant site and the GE Service Center from the low pressure turbine "B" L-1 disk rim. The deposits were collected from the fractured finger pinned blade attachments before shipping the rotor from the plant, upon receipt of the rotor at the GE Service Center, before sectioning at the GE Service Center and after sectioning at the GE Service Center. The samples collected and their details are presented in Table 22. The results of X-Ray Energy Dispersive Spectroscopic analyses of the deposits are presented in Table 23.

Results from samples removed from the finger pinned blade attachments prior to shipment from the plant and upon arrival at the GE Service Center indicates essentially the same elements present on all samples. Slight differences in analyses are likely due to the normal variation observed in deposit chemistry from one area to another. There was no element present in the sample removed from the finger pinned blade attachment upon arrival at the GE Service Center that was not also present in the sample removed prior to shipment from the plant.

Comparison of results from samples removed prior to sectioning the low pressure turbine "B" L-1 disk rim and after sectioning indicated essentially the same elements present in all samples with the exception that the sample after sectioning contained small amounts of titanium, sulfur and vanadium. It is believed that the differences are likely due to the normal variation observed in deposit chemistry from one area to another.

At the GE Service Center the low pressure turbine "B" L-1 disk rim was removed from the turbine disk by circumferentially machining the disk just below the finger pinned

blade attachments and then cut radially using an oxyacetylene torch. Prior to machining and torch cutting the entire disk rim was completely sealed with adhesive tape and sealant to prevent coolant from coming in contact with fracture surfaces. After sectioning the disk rim it was noticed that a very small amount of liquid was present in the finger pinned blade attachment areas. Samples of the liquid were captured on a cotton swap. Analysis of the swap indicated that all elements present in the liquid were also present on the finger pinned blade attachments prior to sectioning indicating that the liquid observed in the finger pinned blade attachment areas was likely condensation associated with the oxyacetylene torch cutting.

Table 22
Samples Collected from Fractured LP Turbine "B" L-1 Disk
Finger Pinned Blade Attachments for Chemical Analysis

Identification	Deposit Type	Location
SID 14837	Cotton swab	Side of Finger at Marked Location No. 7 at Plant
SID 14839	Cotton swab	Finger Fracture Surface at Marked Location No. 7 at Plant
SID 15034	Cotton swab	Finger before Sectioning at GE Service Center
SID 14937	Cotton swab	Water from Finger After Sectioning at GE Service Center
SID 14938	Cotton swab	Finger Fracture Surface After Sectioning at GE Service Center

Table 23
EDS Analyses Results of Deposit Samples from LP "B" Turbine L-1 Disk Rim

Identification	EDS Result
SID 14837	Pb, Cu, Fe, Sn, Zn, Ni, Si, Ca, Na, Mo, Al, Cr, Mg, Mn, Cl
SID 14839	Pb, Cu, Fe, Sn, Zn, Si, Ni, Ca, Al, Cr
SID 15034	Pb, Cu, Fe, Sn, Zn, Si, Ni, Ca, Cr, Al, Cl, Mn
SID 14937	Pb, Cu, Fe, Sn, Si, Zn, Ni, Ca, Al
SID 14938	Fe, Al, Pb, Si, Cu, Ni, Sn, Cr, Zn, Ca, S, Mn, Ti, V

Summary of Protocol No. 10 Deposit Analysis

Deposits from the rotating blades and inner casings of both the high pressure and intermediate pressure turbines were found to contain base metal oxides, wear debris from seal materials and chemical elements from the inlet steam. Deposit analyses of samples obtained from the fractured finger pinned blade attachments from the low pressure turbine "B" L-1 disk prior to shipment from the plant site and upon arrival at the GE Service Center indicates that no contamination occurred in the area of the subject finger pinned blade attachments during shipping. Deposit analyses of samples obtained from the fractured finger pinned blade attachments from the low pressure turbine "B" L-1 disk prior to and after machining and torch cutting of subject disk rim indicates that no contamination of the fractured finger pinned blade attachments occurred during machining or torch cutting of the L-1 disk rim.

IDENTIFICATION OF PRIMARY FAILURE

Forensic analyses revealed that the fractures and cracks in the finger pinned blade attachments in the L-1 disks of the low pressure turbines "A" and "B" resulted from a time dependent material damage mechanism. The specific time dependent damage mechanism was identified as stress corrosion cracking. The generator shaft fracture and the three fractures through the exciter shaft were identified as being due to tensile/shear overload and each occurred instantaneously, although not necessarily at the same time. The L-1 stage blade fractures from the fractured L-1 stage disk were due to tensile/shear overload and each occurred instantaneously but once again not necessarily at the same instant. The blade pin fractures from the fractured L-1 stage disk were due to shear overload and also would have occurred instantaneously but not all at the same instant. The fractures of the aforementioned components that were subjected to metallurgical forensic analysis were identified as being primary or secondary as detailed below and summarized in Table 24; the distress to the bearings and diaphragms has previously been deemed secondary as outlined in an earlier section of this document.

- Low Pressure Turbine "B" Turbine End L-1 Blades - The blade fractures occurred in the airfoils; no root fractures were observed. The blade airfoil fractures were due to tensile/shear overload indicating that the fractured sections of the airfoils were subjected to static stresses above their ultimate tensile strength. There was no evidence of fatigue. Static stress in the blade airfoils is a function of centrifugal loading, due to rotational speed, and bending due to steam loading. At the time of the November 19th incident the steam flow was very low and therefore the steam bending loads were negligible. Steam turbine blades are designed so that the static stress in the airfoil and the root is well below the yield strength and ultimate tensile strength during normal operation and overspeed test conditions. The fractured L-1 blades would have experienced higher centrifugal loading during overspeed testing in 1999 (3972 RPM), 2002 (3960 RPM) and 2005 (3945 RPM) compared to that experienced during the overspeed testing on November 19, 2011. Therefore, it is concluded that the airfoil fractures were secondary and occurred due to the combined effect of centrifugal loading due to rotational speed and very high bending loads due to impact with surrounding components and

liberated L-1 blades and finger pinned blade attachments during the November 19, 2011 event.

- Low Pressure Turbine "B" Turbine End L-1 Attachment Pins - The blade attachment pin fractures were due to shear overload indicating that the static stress exceeded the pin material shear strength. There was no evidence of fatigue. Three pins attach each blade to the finger pinned blade attachment on the L-1 stage disk. The pins pass through the blade fingers and finger pinned blade attachments at three radial locations below the disk outer diameter. Many of the liberated blades were still attached to the fractured finger pinned blade attachments by the blade pins; the blade pins shearing only at the intersection with the unfractured finger pinned blade attachments. Similarly, many of the blade pins were found intact in the finger pinned blade attachments where the finger pinned blade attachments had fractured at a radially outboard location. In order for a blade pin on a given blade to shear it must deform, meaning that there must be movement of the pin and hence blade in an outboard direction. Since there are multiple pins in each blade with multiple attachments points this means that one pin cannot deform at one attachment point unless all the blade pins associated with the blade deform to the same degree. The evidence indicates that this did not occur. The static stresses on the blade pins is a function of centrifugal loading due to rotational speed and circumferential/axial bending due to steam loading on the blades. The blade pins are designed so that the static stress is well below the yield strength and ultimate tensile strength during normal operation and overspeed test conditions. The sheared L-1 blade pins would have experienced higher centrifugal loading during overspeed testing in 1999 (3972 RPM), 2002 (3960 RPM) and 2005 (3945 RPM) compared to that experienced during the overspeed testing on November 19, 2011. Therefore it is concluded that the shearing of the L-1 blade pins was secondary and occurred after the finger pinned blade attachments fractured which resulted in static stress above the shear strength of the pins where they passed through unfractured finger pinned blade attachments.

- Low Pressure Turbine "B" Turbine End L-1 Finger Pinned Blade Attachments - The fractures and cracks through the finger pinned blade attachments in the L-1 stage disks were due to tensile overload which progressed from pre-existing stress corrosion cracks. There was no evidence of fatigue. Some of the stress corrosion cracks had progressed through the entire cross section of a given finger

pinned blade attachment. Stress corrosion cracking is a time dependent damage mechanism. Considerable time, measured in years, is required for cracks to initiate and propagate to the degree observed on the subject failure. The static stress in the finger pinned blade attachments is a function of centrifugal loading due to rotational speed and axial/circumferential bending due to steam loading on the L-1 stage blades. The fracture of the finger pinned blade attachments resulted in liberation of associated blades, blade pins and said attachments. The liberated sections of the L-1 stage disk contacted the remaining L-1 stage blades and L-0 stage diaphragm vanes resulting in extensive impact damage and fractures. Additionally, the liberated disk sections resulted in a large imbalance which would create severe vibration throughout the turbine train accompanied by large deflections of the rotors and shafts. It is concluded that the presence of the stress corrosion cracks in the finger pinned blade attachments of fractured L-1 stage disk had reduced the load carrying capability to a degree that centrifugal loads during the overspeed test exceeded the load carrying capability of the compromised finger pinned blade attachments. The fractures in the finger pinned blade attachments are deemed to be the primary failure.

- Generator Shaft - The generator shaft fracture was due to tensile/shear overload indicating that the static stress exceeded the ultimate tensile strength of the shaft material. There was no evidence of fatigue. The static stress on the generator shaft in the vicinity of the generator collector ring is generally very low and is a function of centrifugal loading due to rotational speed, bending due to shaft misalignment and torsion. For the generator shaft to have fractured in tensile/shear overload would require very large deflections which are simply impossible during operation with the bearings intact and the shaft balanced. Based on the observations above and the fact that vibration levels were normal up to the time of the incident, it is concluded that the shaft fracture was secondary and occurred due to large amplitude vibration and associated deflection associated with the imbalance due to the fracturing of the low pressure turbine "B" turbine end L-1 stage disk rim.

- Exciter Shaft - The three exciter shaft fractures were due to tensile/shear overload indicating that the static stress exceeded the ultimate tensile strength of the shaft material at all three fracture locations. There was no evidence of fatigue. The static stress on the exciter shaft adjacent to the No. 11 bearing, adjacent to the No. 12 bearing and at the Alterex collector ring is generally very low and is a

function of centrifugal loading due to rotational speed, bending due to shaft misalignment and torsion. For the exciter shaft to have fractured in tensile/shear overload would require very large deflections which are simply impossible during operation with the bearings intact and the shaft balanced. Based on the observations above and the fact that vibration levels were normal up to the time of the incident, it is concluded that the exciter shaft fractures were secondary and occurred due to large amplitude vibration and associated deflection associated with the imbalance resulting from the fracture of the low pressure turbine "B" turbine end L-1 stage disk rim.

Table 24
Distressed Components, Potential Failure Modes and Causes

Distressed Component	Potential Failure Modes	Potential Failure Causes	Potential Primary Failure	Findings	Primary or Secondary
Bearings	Babbitt Melting/Transferred Metal/Vibration	Loss of Lubrication	No	Metal Temps/Oil Temps Normal Prior to Event	
	Babbitt Melting/Transferred Metal/Vibration	Bearing Misalignment	No	Vibration Normal Prior to Event	Secondary
	Brinelling/Transfer Metal, Vibration	Critical Speed	No	Vibration Normal Prior to Event	
LP "B" Turbine End L-0 Fractured Diaphragm Vanes	High Cycle Fatigue	Forced Excitation or Resonance	Unlikely	No Evidence of Fatigue	
	Material Defects	Material/Processing	Unlikely	No Material/Processing Anomalies	Secondary
	Tensile Overload	High Stresses As Result of Event	No	Tensile Overload Noted	
LP "B" Turbine End L-1 Diaphragm Fractured End Wall	High Cycle Fatigue	Forced Excitation or Resonance	Unlikely	No Evidence of Fatigue	
	Material Defects	Material/Processing	Unlikely	No Material/Processing Anomalies	Secondary
	Tensile Overload	High Stress As Result of Event	No	Tensile Overload Noted	
LP "B" Turbine End L-2 Cracked Diaphragm Inner Wall	High Cycle Fatigue	Forced Excitation or Resonance	No	No Evidence of Fatigue	
	Material Defects	Material/Processing	No	No Material/Processing Anomalies	Secondary
	Tensile Overload	High Stress As a Result of Event	No	Tensile Overload Noted	

Distressed Component	Potential Failure Modes	Potential Failure Causes	Potential Primary Failure	Findings	Primary or Secondary
LP Turbine "B" Turbine End L-1 Disk Finger Pinned Blade Attachments	Stress Corrosion Cracking	Operating Stress and Environment	Yes	Stress Corrosion Present	Primary
	High Cycle Fatigue	Forced Excitation or Resonance	Yes	No Evidence of Fatigue	
	Low Cycle Fatigue	Start-Stop Cycles	Unlikely	No Evidence of Fatigue	
	Embrittlement	Material Properties	Unlikely	No Evidence of Embrittlement	
	Material Defects	Material/Processing	Unlikely	No Material Defects	
	Tensile Overload	Operating Stress Exceeding UTS	No	Yes-Terminal Ends of SCC Cracks	
LP Turbine "B" Turbine End L-1 Disk Finger Pinned Blade Attachment Pins	Stress Corrosion Cracking	Operating Stress and Environment	Yes	No Evidence of SCC	Secondary
	High Cycle Fatigue	Forced Excitation or Resonance	Yes	No Evidence of Fatigue	
	Low Cycle Fatigue	Start-Stop Cycles	Unlikely	No Evidence of Fatigue	
	Embrittlement	Material Properties	Unlikely	No Evidence of Embrittlement	
	Material Defects	Material/Processing	Unlikely	No Material Defects	
	Shear Overload	Operating Stress Exceeding Shear Strength	No	Yes	
LP Turbine "B" Turbine End L-1 Blades	Stress Corrosion Cracking	Operating Stress and Environment	Yes	No Evidence of SCC	Secondary
	High Cycle Fatigue	Forced Excitation or Resonance	Yes	No Evidence of Fatigue	
	Low Cycle Fatigue	Start-Stop Cycles	Unlikely	No Evidence of Fatigue	
	Material Defects	Material/Processing	Unlikely	No Material Defects	
	Tensile/Shear Overload	Operating Stress Exceeding UTS	No	Yes	
Generator Shaft	High Cycle Fatigue	Forced Excitation or Resonance	Yes	No Evidence of SCC	Secondary
	Embrittlement	Material Properties	Unlikely	No Evidence of Embrittlement	
	Material Defects	Material/Processing	Unlikely	No Material Defects	
	Tensile/Shear Overload	Operating Stress Exceeding UTS	No	Yes	

Distressed Component	Potential Failure Modes	Potential Failure Causes	Potential Primary Failure	Findings	Primary or Secondary
Exciter Shaft	High Cycle Fatigue	Forced Excitation or Resonance	Yes	No Evidence of SCC	Secondary
	Embrittlement	Material Properties	Unlikely	No Evidence of Embrittlement	
	Material Defects	Material/Processing	Unlikely	No Material Defects	
	Tensile/Shear Overload	Operating Stress Exceeding UTS	No	Yes	

FUNDAMENTALS OF STRESS CORROSION
STEAM TURBINE ROTOR MATERIALS

Stress corrosion cracking is a phenomenon whereby a material can crack/fracture at a stress well below its yield strength or with an applied stress intensity acting on a crack well below the typical fracture toughness of the material. The applied stress and corrosion reactions combine synergistically resulting in a time dependent failure. Stress corrosion cracking requires three components to be active: a susceptible material, tensile stress and a specific environment. The stress corrosion cracking phenomenon is very complex and not completely understood. Several mechanisms have been proposed and some have gained wider acceptance than others. Gaining complete understanding is difficult because mechanisms vary with material type and conditions and the mechanisms active in one may not be active in another system. One generally accepted mechanism for stress corrosion cracking can be simplified as anodic dissolution of the crack tip and passivation of the crack walls. An applied stress initiates the process by locally rupturing the passive film on a metal surface. The bare metal that is revealed is then subject to anodic dissolution, which extends the crack further. An environmental condition allows the crack walls to repassivate. Film formed at the crack tip then ruptures allowing the cycle to continue and the crack to propagate.

During the final stages of energy extraction in the low pressure turbine, the steam pressure and temperature are reduced so that the steam becomes wet. This region in the low pressure turbine was originally referred to as the Wilson Line. However, continuing work has shown that the Wilson Line is not a defined region in the turbine and now the region is typically referred to as the Phase Transition Zone (PTZ). The region is typically in the last few rows of blades in the turbine, that is, rows L-0, L-1 and under certain conditions the L-2. The moisture present is known to contribute to corrosion issues that are not applicable to the other parts of the turbine including stress corrosion cracking.

Much of the research work on low pressure steam turbine components was initiated following a catastrophic failure at the Hinkley Point Nuclear Plant in England in 1969. An off-line operational test was performed at speeds exceeding the design speeds. A

catastrophic failure occurred in which the rotor shaft fractured in five places and three disks were liberated from the unit. Investigation of the Hinkley accident concluded that the cause of the failure was the propagation to critical size of a stress corrosion crack in a keyway. The material used was a 3%Cr-0.5%Mo low alloy steel. No specific causative chemical species was identified but sodium hydroxide (NaOH) was suspected because it had been used for pH control of feedwater for an extended period.

After the Hinkley Point failure, inspections of other low pressure steam turbines in the United Kingdom revealed stress corrosion cracks in keyways of 50 other turbines. Subsequently, similar stress corrosion cracks were found in keyways, on bore surfaces and on blade attachment surfaces of disks on low pressure steam turbines in the US and throughout the world. As a result of the Hinkley Point failure and widespread reports of stress corrosion with low pressure steam turbines, a number of laboratory research programs were initiated to identify factors responsible for stress corrosion cracking in low pressure steam turbine disk materials. Analyses of experience and of previous laboratory studies conducted in several countries showed that stress corrosion cracking of low pressure steam turbine disk steels can occur in high purity water as well as a number of more corrosive environments such as concentrated hydroxides. It has been established that stress corrosion crack growth is dependent upon the presence of liquid water, disk yield strength, disk temperature, tensile stress level and the aggressiveness of the environment including oxygen concentration, concentrations of ionic species and pH. Also a limited amount of data indicates that tight crevices between mating surfaces significantly increases the susceptibility of disks to stress corrosion cracking.

Stress corrosion cracking consists of an initiation phase and a propagation phase. The majority of laboratory testing has been conducted on stress corrosion crack propagation. The following briefly describes the influences of materials, environment and applied stress on the stress corrosion behavior of steam turbine rotor/disk materials.

Environmental Influences

As moisture forms in the low pressure steam turbine impurities tend to partition from the gas to the liquid and increase to the order of hundreds of parts per billion (ppb) in the

early condensates to tens of ppb near the outlet, where the moisture contents are higher. The thermodynamics and kinetics of the impurity partitioning are not completely understood. The concentration of these impurities or additives during condensation of steam is difficult to control. Steam turbine materials can be particularly susceptible to stress corrosion cracking in various wet steam environments, including sodium hydroxide, chlorides, sulfides, sulfates, carbon dioxide and other acids. Stress corrosion cracking has been observed in disk/rim attachments, the disk web and rotor keyways, all caused by cyclic evaporation and concentration of impurities. Steam turbine rotor materials can be particularly susceptible to stress corrosion cracking in various wet steam environments, including sodium hydroxide. This form of stress corrosion cracking is also known as caustic cracking. Stress corrosion cracking of low alloy steels in sodium hydroxide environments is typically intergranular.

Although steam turbine chemistry is carefully controlled, it is possible for impurities to be carried over from the boiler water. Each of the impurities can have a detrimental effect on the rotor materials. In most cases, these impurities are not observed in isolation. Several impurities will exist in combination and will vary by location in the turbine. The particular combination of species might lead to interaction of corrosion mechanisms though these are difficult to isolate in the laboratory.

Temperature and pressure vary throughout a turbine as the steam expands and energy is transferred to the blades. Temperature can change from over 400°F to below 200°F in the LP. If the unit power is decreased for off load cycling on evenings and weekends the temperature might be decreased to approximately 160°F. During shutdown the temperature is decreased to ambient. The reduction in temperature leads to increased wetness and might allow more impurities to concentrate.

The role of oxygen has been debated among experts in the field of steam turbine corrosion. Initial work demonstrated that turbines in boiling water nuclear reactors were more susceptible to cracking than in pressurized water reactors implying that oxygen played a key role in the stress corrosion cracking mechanism. Some researchers have shown that oxygen has little or no effect on initiation or growth of stress corrosion cracks. Arguments have also been made that oxygenated treatments of water in fossil

power plants lead to no detrimental effects on turbines. Although inlet steam can contain more than 100 ppb oxygen, condensates in the PTZ have been shown to contain no measureable oxygen.

Material Behavior

Although stress corrosion cracking consists of an initiation phase and a propagation phase the majority of laboratory testing has been conducted on crack propagation. Laboratory testing is typically conducted in a static test environment while it is common knowledge that stress corrosion can occur under a variety of service conditions or upset conditions and the change in environmental conditions can have a significant effect on stress corrosion behavior. The long times needed for testing and the lack of consistency in experimental techniques used by different researchers can lead to further difficulties. Because there are no universally accepted techniques for determination of stress corrosion cracking resistance designers usually adopt the most conservative approach.

Crack initiation testing has always been plagued by the inability of laboratories and researchers to settle on a standard definition for crack initiation. Some consider initiation to be the formation of an "engineering crack", of approximately 1/16" depth, while others take the position that initiation occurs when there is a disruption in the surface layer of the specimen. With today's rapidly improving ability to observe surface degradation in-situ at very high magnifications it is unlikely that the debate will conclude anytime soon. Therefore, stress corrosion crack initiation data is usually viewed in a qualitative sense. Laboratory testing has shown that four factors have significant effects on stress corrosion crack initiation in 3.5%NiCrMoV turbine steels. These are steel yield strength, tensile stress level, the presence of tight crevices and the K_{ISCC} values of the materials. In general, susceptibility of LP steam turbine disks to crack initiation increases with increasing steel yield strength (Fig. 476). Crack initiation is much more likely to occur in the presence of high tensile stresses on creviced surfaces as are present with disk keyways, bores and blade attachment slots (Figs. 477 and 478). Crack initiation has been found to be independent of disk steel composition, the presence of manganese sulfide or other inclusions and pitting although it has been observed that cracks can be initiated at pits formed on steel surfaces at inclusions if the value of K_I at a pit exceeds K_{ISCC}.

Stress corrosion crack growth rate is dependent on stress intensity. At very low stress intensities the stress corrosion crack growth rates are too slow to measure. As the stress intensity exceeds 1.5-3 ksi·in$^{1/2}$, the observed crack growth rates rise to a plateau value which is not further increased even as the stress intensities are raised to extremely large values. This means that over a very broad range of stress intensities there is no effect of stress intensity on the stress corrosion crack growth rate as shown in Fig. 479. The influence of yield strength on the stress corrosion crack growth rate of steam turbine rotor steel 3.5NiCrMoV is illustrated in Figs. 480 and 481 for two different temperatures, 100°C and 160°C. It is obvious that two different yield strength ranges may be recognized: one below 1100 MPa where the effect of yield strength on the stress corrosion crack growth rate is moderate and another above 1100 MPa where increasing yield strengths results in extremely strong increases of stress corrosion crack growth.

The influence of temperature on the growth rates of intergranular stress corrosion cracks in "clean" 3.5NiCrMoV steam turbine rotor steel is shown in Fig. 482. The curve clearly shows the increase in stress corrosion crack growth rate with increasing temperature.

One approach to improving turbine design is to consider the threshold stress or stress intensity necessary to initiate stress corrosion cracking. Data is available for NiCrMoV steels in nominally pure water (Fig. 483). Design operating stresses above the σ_{scc} curve risks stress corrosion cracking in service. Developed cracks or natural crack like defects resulting in stress intensities greater than K_{Iscc} will result in stress corrosion crack propagation.

FINITE ELEMENT ANALYSIS OF LOW PRESSURE TURBINE L-1 DISK FINGER PINNED BLADE ATTACHMENTS

As part of the subject root cause analysis a Finite Element Analysis was undertaken to determine the location (s) and magnitude of tensile stresses present at the finger pinned blade attachments under normal operation and during overspeed test conditions. A solid model was created using Solidworks™ software. The model was created in several sections (parts) which were assembled to form a disk-blade-pin assembly. Finite Element Analysis (FEA) computations were performed using Solidworks™ Simulation Professional as a linear elastic analysis.

Construction of the Solid Model

A transverse section of the turbine end L-1 disk rim containing the finger pinned blade attachments from the low pressure turbine "B" and an L-1 blade from the low pressure turbine "A" were provided to Thielsch Engineering to facilitate construction of the solid model (Fig. 484). Using information from these components and dimensional measurements provided by Engel Metallurgical, the blade and disk finger pinned blade attachments areas were modeled as shown in Figs. 485 to 488. The blade weight was measured to be 10.567 lbs. and the length was measured to be 20.9"; the airfoil twist was not included in the model.

The interlocking of the blade root fingers and the disk finger pinned blade attachments were based upon the components submitted and the measurements of Engel Metallurgical but, were idealized so that blade spacing and distances were easily matched. The finger pinned blade attachment ledge radii were initially modeled as being uniformly 0.060" at all locations and the curvature at the bottom of the finger attachments was smoothly transitioned between each finger. This geometry is referred to as Case 1. A second analysis was undertaken using the actual minimum measured radii at each ledge location as measured by Engle Metallurgical and a larger radius without a smooth transition at the base of the finger pinned blade attachments. This geometry is referred to as Case 2. The geometry of both Cases is presented in Fig. 489.

Simulation Boundary Conditions

The individual solid models of the L-1 disk and L-1 blades were combined as shown in Figs. 490 and 491. Boundary and loading conditions were as follows:

1. Circular symmetry conditions were used to reduce computation time and only those features that were deemed important were modeled.
2. The disk was restrained on the OD surface and on the cut faces to allow sliding.
3. The tapered section up to the disk rim was not constrained.

The model incorporated separation between the blade fingers and disk finger pinned blade attachments as shown in Fig. 492. The global contact condition for the assembly was "bonded". This condition shares nodes between parts so that they act as one unit. Separate contact sets were specified for the split half-holes on the blade fingers with respect to the pins. At these locations the mating surfaces of the outer blade fingers and the pins were specified as "no penetration" as shown in Fig. 493. This condition allows the pins and blades to move independently of each other by adding additional contact-type nodes between the components at these surfaces.

Centrifugal loading was analyzed with a frequency of rotation of 3600 RPM (60Hz) applied to the axis of rotation. One additional analysis was conducted at 4100 RPM to simulate overspeed test condition. Loading due to steam bending was not considered to simplify the analysis. Stresses from steam bending are typically 10% or less of the stresses due to centrifugal loading. Steam bending results in both circumferential and axial stresses in the finger pinned blade attachments and are therefore not simply additive to the radial stresses generated due to centrifugal loading. Thermal strains were not considered because the temperature differentials through the thickness of the finger pinned blade attachments, along the radial length of the finger pinned blade attachments and circumferentially around a given finger pinned blade attachment are minimal and therefore the stresses due to any thermal gradients would be minimal. Finally, residual stresses were not considered because they are unknown. The components were assumed to be isotropic with an elastic modulus of 29.5×10^6 psi. The yield strength of the rotor material was measured as part of the forensic analysis at

Engel Metallurgical. Typical mesh quality is indicated in Fig. **Error! Reference source not found.**494. The mesh was formed using parabolic tetrahedral elements (10 nodes).

State of Stress Basics (excerpt from Solidworks™ Simulation manual)

The state of stresses at a point is completely defined by normal (SX, SY, SZ) and shear stress (TXY, TYZ, …) components in reference to an orthogonal coordinate system XYZ. In general, the values of the stress components change if the coordinate system is rotated as shown in Fig. 495. At a certain orientation (X'Y'Z'), all shear stresses vanish and the state of stresses is completely defined by three normal stress (P1, P2 and P3 and also named as s_1, s_2, and s_3) components. These three normal stress components are referred to as principal stresses and the corresponding reference axes (X'Y'Z') are referred to as principal axes. The principal stresses are numbered conventionally in descending order of magnitude, $s_1 \geq s_2 \geq s_3$. So the 1st Principal stress (s_1) is defined as the one stress of the three principal stresses that is most positive. Generally, the first principal stress winds up being the maximum tensile stress and is therefore the stress that initiates and propagates cracks.

The von Mises stress criterion is based on the von Mises-Hencky theory, also known as the Shear-Energy Theory or the Maximum Distortion Energy Theory. In terms of the principal stresses s_1, s_2, and s_3, the von Mises stress, $s_{vonMises}$, is expressed as:

$$s_{vonMises} = \{[(s_1 - s_2)^2 + (s_2 - s_3)^2 + (s_1 - s_3)^2]/2\}^{(1/2)}$$

The theory states that a ductile material starts to yield at a location when the von Mises stress becomes equal to the stress limit. In most cases, the yield strength is used as the stress limit.

$$s_{vonMises} \geq s_{limit}$$

Yield strength is a temperature-dependent property. This specified value of the yield strength should consider the temperature of the component. Therefore when performing linear elastic analysis, if the stresses exceed the yield strength, then the actual values of the stress at the node are unknown and the only known information is

qualitative. Elastic-plastic analysis is used to calculate stresses above the yield strength.

Results of Analysis

The results of analysis, with a frequency of rotation of 3600 rpm applied to the axis of rotation, of the first principle stresses and von Mises stresses for the disk finger pinned blade attachments under the aforementioned loading conditions is presented in Figs. 496 and 497, respectively. It is noted that the local stresses are higher about the pin holes and along the ledges of the finger attachments where there is a change in geometry. Stresses are nearly symmetric about the centerline of the six fingers with the higher stresses being on the outward faces. Also the local stresses are slightly higher at the first bank of pins, then decrease slightly as the diameter increases.

The differences between the 1st principal stresses for Case 1 and Case 2 are shown in Figs. 498 and 499. The nodes at similar locations were probed and their values indicate that the smaller radii produced slightly higher local stresses as expected. For Case 1, using uniform ledge radii of 0.060", the probed local stresses were:

1. At pin holes - 107 to177 ksi
2. At ledges - 56 to 64 ksi
3. At base of fingers - 52 to 85 ksi

For Case 2, using ledge radii of 0.020" and 0.033", the probed stresses were:

1. At pin holes - 93 to 169 ksi
2. At ledges - 53 to 71 ksi
3. At base of fingers - 51 to 86 ksi

As previously mentioned, the stresses reported above are local stresses with the bulk stresses being considerably lower. The bulk stresses were between 10 ksi to 30 ksi and varied with radial location along each finger pinned blade attachment.

Analysis of stresses resulting from a frequency of rotation of 4100 rpm applied to the axis of rotation, simulating an overspeed test condition, revealed that the localized stresses at pin holes, ledges and at the base of the attachment fingers increased and the area over which these high stresses were present also increased as shown in Fig. 500. However, the bulk stresses at all locations remained near or below 50% of the material yield strength.

MAINTENANCE AND OUTAGE RECORDS

The maintenance and outage reports were made available by Xcel Energy. A summary of the outage details follows:

1989 Major Outage

The unit came off-line on February 10, 1989. A complete inspection of the steam turbine generator train was performed including four control valves, three main stop valves and two combined reheat intercept valves.

Three control valve seats were found to have vertical cracks, at the seat area, through the hard surface material extending into the parent material. The damaged valve seats were replaced.

The right side high pressure turbine inlet flange was leaking upon disassembly. Both inlet flange bolts were removed and ultrasonically tested. No defects were found. New gaskets were installed at reassembly.

The high pressure turbine outer and inner casings were removed and blasted. No repairs were needed.

The high pressure turbine diaphragms were removed and blasted. It was noted that the first five stages showed a considerable amount of erosion considering that the unit had only been running for 18 months. The fourth stage diaphragm exhibited impact damage along the vane trailing edges. The fourth stage diaphragm was repaired. The other stages were not repaired. New spill strips were installed on all stages of the high pressure turbine. The high pressure turbine rotor was removed, cleaned and blasted. Minor pitting was found in the radius between the 7^{th} stage wheel and the packing box area. The pitting was blended out, metal removal of approximately 0.010-0.012", and the area polished.

The reheat intermediate pressure turbine rotor was removed, blasted and inspected. Only minor impact damage to blade trailing edges was noted. The intermediate

pressure turbine inner casing was removed and blasted. No conditions of note were identified.

The low pressure turbine "A" casing was removed and inspected. No indications were noted. All diaphragms were blasted and non-destructively inspected. A few minor indications were noted on the leading and trailing edges of the diaphragm vanes. A few of these indications were repaired.

The low pressure turbine "A" rotor was removed, blasted and non-destructively inspected. L-1 stage blade tie wire end sleeves were found loose and few were missing. Missing ones were replaced and loose ones were re-soldered where they pass thru the blades. Last stage and L-1 stage blades exhibited water droplet erosion along leading edges. The last stage and L-1 stage blade pins were ultrasonically inspected with no reported indications.

The low pressure turbine "B" outer casing hood was removed and inspected. No indications were noted. All diaphragms were removed, blasted and non-destructively inspected. Only minor repairs were required except for the L-5 stage generator end double flow diaphragm which exhibited major impact damage to the leading and trailing edges of the diaphragm. This diaphragm was sent off site for repair. The low pressure turbine "B" rotor was removed, blasted and non-destructively inspected with no indications noted. Tie wires on the L-1 blades were found loose and were re-soldered. Last stage and L-1 stage blades exhibited water droplet erosion along leading edges.

All bearings were inspected and found acceptable: no repairs had to be performed. The generator and exciter were inspected with nothing major noted. The bearings on the generator and exciter shaft were found in acceptable conditions.

The unit rolled off turning gear on March 26th, 1989. After running for about 30 minutes the No. 4 bearing vibration went to 9.7 mils at 1720 RPM. The unit was brought down to 1000 RPM and left for approximately one hour. When brought back up the No. 4 bearing exhibited vibration of 6 mils at 3000 RPM. The unit developed a rub resulting in high vibration after an oil trip test. The unit was again brought off line so a balance shot

could be added to the Alterex coupling. After running for approximately 24 hours the unit was brought off line for additional balance shots at the No. 1 bearing (5.6 oz. at 70°), the No. 2 bearing (5.6 oz. at 250°), the No. 7 bearing (8 oz. at 110°) and at the No. 8 bearing (8 oz. at 290°). The unit ran for approximately one day and was again brought off line to add balance shots to the generator. Weights were added in each end of the generator field of 16.75 oz. on the collector end and 16.78 oz. on the turbine end at the 200° mark on both ends.

1990 Minor Outage

The unit was taken off line and put on turning gear in May 1990 to investigate the source of a noise in the number two control valve at or near full load. The noise was reported as an intermittent metallic rapping emanating from the number two valve area of the valve chest. There was a concern that the noise might be due to a loose object that could have passed beyond the valve and into the turbine. The No. 2 valve was removed from the valve chest and inspected with nothing of note identified. The inside of the steam chest was inspected visually and no marking or damage was noted that would indicate a loose object. The valve was re-assembled and the unit started back up without incident.

1991 Minor Outage

The unit was taken offline in March 1991 for a maintenance outage. The work was limited to inspection of the front standard and repairing a steam leak at the No. 4 control valve.

The front standard cover was removed and a complete inspection was performed per the General Electric Procedure. Nothing of importance was noted.

The No. 4 control valve was removed and it was discovered that the gasket had been leaking. A new gasket was installed in the No. 4 control valve and the valve body torqued to specification requirements.

The unit was started and a steam leak was noted at the steam chest at the No. 1 control valve. The unit was shut down and the remaining control valve removed. The No. 1

control valve was found to have a bad gasket. The gasket was replaced and the valve body re-torqued to specification requirements. The unit was started back up. The date of start-up was not reported.

1993 Major Outage

The unit came off line on March 19th 1993. A complete inspection of the steam turbine generator train was performed including the four control valves and three stop valves.

Visual examination revealed that two control valve seats, No. 1 and No. 4, were cracked. The two valve seats were replaced.

The inner and outer high pressure turbine casings were removed and blasted. No notable indications were reported and no repairs were required. The high pressure turbine diaphragms were removed and blasted. The first stage nozzle was shipped off site for major repair and the 2nd thru 6th stage diaphragms were sent off site for minor repair. The high pressure turbine shaft packing and diaphragm packing was replaced with Quabbin retractable packing. The high pressure turbine rotor was removed, blasted and inspected. Moderate solid particle erosion was evident on the 2nd and 3rd stage blade leading edges.

The reheat intermediate pressure turbine rotor was removed and sandblasted. A crack in one 13th stage rotating blade cover on the generator end was noted. This cover was removed and a new cover installed. Impact damage was noted on numerous stage blading with significant solid particle erosion damage observed on the 8th stage generator end blading. The eroded areas were polished off. The reheat intermediate pressure turbine inner and outer casing were removed and blasted. Non-destructive inspection revealed no issues of note. The reheat intermediate pressure turbine 8th stage diaphragms were sent off site for a major repair. The 9th stage, turbine and generator end, 10th stage turbine end, 12th stage turbine end and 13th stage turbine end diaphragms were sent off site for minor repairs.

The low pressure turbine "A" outer hood and inner cylinder were removed, blasted and inspected. No issues were identified. All diaphragms were removed and blasted. Many

diaphragms required vane straightening and the last stage diaphragm required weld repair of eight cracked vanes. The low pressure turbine "A" rotor was removed, blasted and non-destructively inspected. The tenons on a center blade in a five blade generator end L-1 blade group was found cracked. The cover on this blade group was bent and sections worn away from rubbing. The five blades were replaced and a new cover installed. Additional covers were found to be lifted on the L-1 generator end blade row requiring another blade to be replaced along with two additional covers. Fifty last stage dovetail pins, six on the turbine end and forty-four on the generator end were identrified as cracked by ultrasonic inspection. The pins were drilled out and new pins installed.

The low pressure turbine "B" outer hood and inner cylinder were removed, blasted and inspected. There were no indications of note. All diaphragms were removed and blasted. Many diaphragms required straightening of vanes and a few required minor weld repair for impact damage. The low pressure turbine "B" rotor was removed, blasted and non-destructively inspected. Thirteen last stage dovetail pins on the generator end were replaced and four last stage dovetail pins on the turbine end were replaced. The reason for pin replacement was not reported.

The unit came off turning gear on April 29th 1993. The unit tripped on May 2nd due to high vibration and a rub was encountered on the way down. High vibration was encountered again on the way back up and eventually on May 3rd it was decided to put a balance shot on both ends of both low pressure turbine rotors. The unit was brought back up to speed without incident. The overspeed test was conducted at 4080 RPM.

1996 Major Outage

The unit came off line on February 16, 1996. The primary purpose of the outage was to perform inspections in support of the investigation into the low pressure turbine L-1 blade tie wire cracking.

Both low pressure turbine rotors were disassembled and groups of five L-1 blades were removed from each end of both rotors. Blade tie wires were removed and then the rotors were dust blasted and non-destructively inspected around the tie wire holes. The blade tenons were also ultrasonically inspected. No tie wire cracking was discovered.

Significant impact damage on the trailing edges of three generator end L-1 blade trailing edges were noted during the inspection. Two of the three blades were replaced with new General Electric double boss blades. Moderate axial rub damage to L-3 blade covers was observed. The axial rub damage is believed to have occurred due to a short rotor from a fast cool down.

The unit started up on March 16, 1996 without incident. The overspeed trip test was conducted at 3986 RPM.

1999 Major Outage

The unit was removed from service on February 26, 1999. All turbine sections, valves and lube oil pumps were disassembled and inspected. All low pressure turbine L-1 stage blades were replaced with a new designed blade. The generator stator and field were rewound. The Alterex was disassembled and inspected.

The high pressure turbine rotor was disassembled, blasted and non-destructively inspected. Non-destructive inspection included bore visual examination, bore magnetic particle testing, radial beam boresonic testing, angle beam boresonic testing, periphery ultrasonic testing, axial ultrasonic testing and periphery magnetic particle testing. Bore surface examination revealed a few very small indications. A light stoning to a depth of approximately 0.015" removed all the indications. Although these indications had not been reported at the time of manufacturing, it was concluded that they were likely present as-manufactured and that current inspection methods are simply much more sensitive. The indications did not exhibit crack like features. Axial ultrasonic testing performed from the ends of the rotor revealed no indications. Periphery magnetic particle testing performed on the external surfaces of the rotor in both radial and axial directions revealed no indications. The first stage notch blades exhibited lifting in the range of 0.010” to 0.200". The second stage diaphragm exhibited moderate partition erosion and a major weld repair was performed. Minor repairs were performed to the 3rd thru 7th stage diaphragms.

The reheat intermediate pressure turbine rotor was disassembled, blasted and non-destructively inspected. Non-destructive inspection included bore visual examination,

bore magnetic particle testing, radial beam boresonic testing, angle beam boresonic testing, periphery ultrasonic testing, axial ultrasonic testing, dovetail ultrasonic testing and periphery magnetic particle testing. Bore surface examination revealed a few very small indications. A light stoning to a depth of approximately 0.016" removed all the indications. Although these indications had not been reported at the time of manufacturing, it was concluded that they were likely present as-manufactured and that current inspection methods are simply much more sensitive. The indications did not exhibit crack like features. Axial ultrasonic testing performed from the ends of the rotor revealed no indications. An ultrasonic test of the accessible wheel dovetail hooks on stages 1, 2 and 3 of both turbine and generator ends of the rotor disclosed source type indications in all stages except the turbine end third stage. None of the indications showed evidence of continuity in the circumferential direction and there was no loss of the reference reflections. It was concluded that the indications did not warrant blade removal for further investigation. Periphery magnetic particle testing performed on the external surfaces of the rotor in both radial and axial directions revealed no indications. The turbine and generator end eighth stage blades exhibited heavy erosion to the leading edges, tenons and cover foxholes. The turbine end and generator end eighth stage diaphragms exhibited light partition erosion and minor repairs were performed.

The low pressure turbine "A" rotor was disassembled, blasted and non-destructively inspected. Non-destructive inspection included bore visual examination, bore magnetic particle testing, radial beam boresonic testing, angle beam boresonic testing, periphery ultrasonic testing, axial ultrasonic testing, dovetail ultrasonic testing and periphery magnetic particle testing. Bore surface examination revealed no indications. Axial ultrasonic testing performed from the ends of the rotor revealed no indications. An ultrasonic test of the accessible wheel dovetail hooks was performed on stages L-2 and L-3 of both the turbine and generators ends of the rotor. Point source type indications were detected in both L-2 stages. None of the indications showed evidence of continuity in the circumferential direction and there was no loss of the reference reflections. It was concluded that these indications did not warrant blade removal for further investigation. Periphery magnetic particle testing performed on the external surfaces of the rotor in both radial and axial directions revealed no indications. The L-1 blades were replaced with a new designed General Electric continuously coupled blade. The last stage turbine

and generator end blade tenon covers were found to be moderately eroded. Ultrasonic inspection identified thirty-three last stage pins cracked on the turbine end. Ultrasonic inspection identified one hundred and seventy last stage pins cracked on the generator end. All cracked pins were replaced. The cause of cracks was not reported.

The low pressure turbine "B" rotor was disassembled, blasted and non-destructively inspected. Non-destructive inspection included bore visual examination, bore magnetic particle testing, radial beam boresonic testing, angle beam boresonic testing, periphery ultrasonic testing, axial ultrasonic testing, dovetail ultrasonic testing and periphery magnetic particle testing. Bore surface examination revealed no indications. Axial ultrasonic testing performed from the ends of the rotor revealed no indications. An ultrasonic test of the accessible wheel dovetail hooks was performed on stages L-2 and L-3 of both the turbine and generators ends of the rotor. Point source type indications were detected in both L-2 stages. None of the indications showed evidence of continuity in the circumferential direction and there was no loss of the reference reflections. It was concluded that these indications did not warrant blade removal for further investigation. Periphery magnetic particle testing performed on the external surfaces of the rotor in both radial and axial directions revealed no indications. The L-1 blades were replaced with a new designed General Electric continuously coupled blade. The last stage turbine and generator end blade tenon covers were found to be moderately eroded. Ultrasonic inspection identified one last stage pin cracked on the turbine end. Ultrasonic inspection identified fifty-five last stage pins cracked on the generator end. All cracked pins were replaced. The cause of cracks was not reported.

Bearings No. 5, No. 7, No. 8, No. 9, No. 10, No. 11 and No. 12 were re-babitted due to slight bottom wiping and excess clearance. Remaining bearings were found acceptable or required only minor repairs.

General Electric had been contracted to perform the boresonic inspection of the four turbine rotors and the generator field. They were also responsible for replacement of the Low Pressure Turbine L-1 blades, inspection of the finger pinned blade attachments in the L-1, modification of the low pressure turbine L-1 diaphragms and replacement of the low pressure turbine last stage diaphragm spill strips and holders. The General Electric

workscope was specified in an Xcel Energy purchase order which detailed the tasks to be performed by reference to a L-1 Bucket Upgrade Proposal 401T1132B prepared and issued by General Electric. The General Electric outage report does not indicate that the L-1 finger pinned blade attachment magnetic particle inspection was planned for or performed. As part of the subject root cause analysis, Xcel Energy requested documentary evidence that the L-1 finger pinned blade attachment MPI inspection was performed but, to date General Electric has not found any such document. Other non-destructive inspections were performed by Northern States Power M&SP personnel and MQS Inspection, Inc. The outage report from Northern States Power M&SP states that General Electric performed the "LP Blade Finger Inspection on L-1 Rows". A table in the aforementioned report also indicates that the L-1 disks in both low pressure turbines were inspected by VT and MT and no indications were noted. It is unclear whether the results in the table are for the L-1 finger pinned blade attachments or other areas of the L-1 disk. The table also appears to contain non-destructive test results of all entities involved in the outage. The MQS Inspection, Inc. outage report makes no mention of the low pressure turbine L-1 finger pinned blade attachment magnetic particle inspection. It is inconclusive whether the magnetic particle inspection of the L-1 stage finger pinned blade attachments was performed during the subject outage.

The unit was started up on April 18, 1999 with minimal rub induced vibration. A balance shot was made in the Alterex coupling to reduce No. 11 bearing vibration. The overspeed test was performed at 3972 RPM. The highest vibration was 4 mils at the No. 9 bearing. The unit was returned to service on April 19th, 1999.

2002 Minor Inspection Outage

The unit was shut down on March 9, 2002 for a scheduled maintenance inspection. The turbine workscope included inspection of the No. 1, No. 2 and No. 6 journal bearings, CV linkage work, low pressure turbine hood expansion bellows replacement, and low pressure turbine hood spray and steam seal system modifications. The generator workscope included generator HIT SCID testing, generator electrical testing and generator and exciter visual inspections.

Visual examination of the low pressure turbine last stage blades revealed heavy water droplet erosion on the continuously coupled tenons to a depth of approximately 1/16". A visual inspection of the low pressure turbine L-1 blades was conducted by borescope through the access ports on the inner casing. Light water droplet erosion was noted on the continuously coupled blade cover tenons.

The No. 1 journal bearing, No. 2 journal bearing and No. 6 journal bearing were disassembled and inspected. No conditions of note were reported. No repairs were performed on the bearings other than the replacement of a thermocouple on the No. 2 journal bearing.

The unit was returned to service on April 14, 2002. No issues were reported with the start-up. The overspeed trip test was performed at 3960 RPM.

2005 Major Inspection Outage

The unit was shut down on October 7, 2005 for a scheduled major maintenance inspection. The turbine workscope included inspection of the high pressure turbine, the reheat intermediate pressure turbine, both low pressure turbines, main stop valves, control valves, combined reheat valves, miscellaneous front standard components and the lube oil system pumps and motors. The generator workscope included complete disassembly of the generator and exciter, generator HIT SCID testing and generator and exciter electrical testing.

The reheat intermediate pressure turbine eighth stage blades on both the turbine end and the generator end were replaced. Both the turbine end and generator end last stage blade covers were replaced on both low pressure turbines. Journal bearings No. 2, No. 5, No. 6 and No. 7 were repaired. Minor repairs were performed on the high pressure turbine 1st stage nozzles and various diaphragms in the reheat intermediate pressure turbine and both low pressure turbines. ReGenco performed a fracture mechanics based condition assessment of the generator rotor, high pressure turbine rotor, reheat intermediate pressure turbine rotor and both low pressure turbine rotors. Wesdyne performed linear phased array ultrasonic inspection of the tangential entry

dovetail roots on the generator end and turbine end L-2 and L-3 disks on both low pressure turbines.

The unit was started back up during the week of December 5, 2005. The overspeed test was conducted at 3945 RPM. No further details on the startup were available.

2008 Minor Inspection Outage

The unit was taken off line on October 2, 2008 for a scheduled outage to conduct major plant controls upgrade and minor turbine and generator work.

The last stage blading was found to be in generally good condition with only light deposits and evidence of water droplet erosion of the Stellite strips. There was some separation noted between the last stage covers and the blade tips. The separation was believed to be due to poor installation when the covers were replaced during the 2005 outage.

The generator was partially disassembled for repair of a stator winding leak.

The No. 6 and No. 7 journal bearings were inspected and found to be in good condition other than a small amount of electrolysis damage to both bearings. The No. 9 bearing was inspected and found to be in good condition.

The unit was started up sometime in December, exact date was not reported. No problems were noted during startup. The overspeed trip test was performed at 3868 RPM.

2010 Forced Outage

The unit was forced offline on September 13, 2010 due to an air gearbox heater failure. During the forced outage the lube oil became significantly contaminated with water due to a leaking turbine steam seal supply block valve. The water contaminated lube oil was inadvertently circulated throughout the lube oil system. This resulted in essentially zero resistance to ground readings on the insulated generator and exciter bearings. The

No. 10 generator bearing and both exciter bearings were cleaned, dried and reassembled.

The work was completed on September 25, 2010 but the start-up was delayed until November 4, 2010 due to boiler problems. Details of the start-up were not available.

2011 Major Outage-Steam Turbine Generator Upgrade

The unit was taken offline on September 15, 2011. The workscope for the outage included the following items.

- Installed a new 1043MVA generator step-up transformer in place of the existing 1000MVA GSU.
- A new high pressure turbine rotor and complete inner cylinder including diaphragms was installed. A new reheat intermediate pressure turbine rotor and diaphragms were installed. The material supply and the installation of these components were contracted to Alstom Power, Inc. The new turbine sections improve the efficiency, increase the power rating of the turbine train, improves the resistance to long term wear and extends the maintenance outage intervals.
- The existing Alterex exciter was disassembled and sent off site for rewinding. The rotor was rewound by utilizing the existing copper coils.
- The Alterex stator was rewound using new copper coils by General Electric in Chicago.
- Replaced the existing analog automatic voltage regulator system with a digital system. This component controls the voltage that is used to excite the field of the generator.
- Retrofit of the main Iso-Phase bus to allow for forced cooling of the Bus by using a cooling system that is cooled by the auxiliary cooling water system to maintain the Bus below design temperature.
- Replaced the existing water cooled rectifier with a redesigned water cooled rectifier to eliminate risk of leaks. The rectifier converts the AC voltage from the AVR into DC voltage that excites the field in the generator.

REVIEW OF WATER CHEMISTRY DATA

Details of Unit 3 System

The steam flow and operating parameters for Unit No. 3 are shown in the heat balance diagram in Fig. 502. Sherco Unit 3 utilizes a drum boiler with nominal boiler pressure of 2520 psi and 1000°F. The steam is reheated and enters the intermediate pressure turbine at 589 psi and 1000°F. Attemperation is provided to the steam prior to entering the intermediate pressure turbine using boiler feed water. Steam from the intermediate pressure turbine enters the low pressure turbines through crossovers. Exhaust from the low pressure turbines enters the condensers after which make-up water is added using boiler feed water. The condensed steam then flows to the condenser pump discharge and into full flow condensate polishers incorporating 50% redundancy. The polishers are operated full time to optimize feedwater quality and polisher element life. The fluid then passes through a number of feedwater heaters and the boiler economizer before re-entering the boiler evaporator section.

Boiler Water Treatment

Xcel Energy plant personnel indicated that the boiler water treatment from commissioning until 2000 was All Volatile Treatment-Reducing (AVT-R) using a combination of ammonia hydroxide and hydrazine for pH control and oxygen scavenging, respectively. In 2000 the boiler water treatment was changed to All Volatile Treatment-Oxidizing (AVT-O). Ammonia hydroxide was continued for pH control however, hydrazine usage was eliminated. Personnel reported that phosphate and/or caustic boiler treatments were never used in Unit 3 at any time during its operation. The Sherco plant follows EPRI cycle chemistry guidelines for All-Volatile Treatment-Oxidizing (Ref. 10).

Water/Steam Chemistry Monitoring

Sherco Unit 3 had an on-line water chemistry monitoring system in place since the unit began operation in 1987. The system provided real time information directly to the control room. The data was not electronically archived from 1987 to 2000. In the year 2000, the on-line monitoring system was incrementally linked to the PI® electronic archival system. The instrumentation monitoring condensate pump discharge sodium

content and cation conductivity, boiler water cation conductivity and economizer inlet cation conductivity was linked to the PI® system in mid-November 2000. Seven months later, in mid-June of 2001, instrumentation for continuous monitoring of boiler water sodium content was linked to the PI® system. Grab samples from the Unit 3 boiler have been obtained since the start-up of the unit in 1987. These grab samples are analyzed on-site for sodium by atomic emission spectroscopy. Samples were taken at approximately 2 week intervals. Unit 3 water quality operating limits are shown in Table 22.

Table 22
Water Quality Panel Operating Limits

Condensate Pump Discharge

Parameter	OT	AVT
pH	9.00 - 9.30	9.00 - 9.30
Cation Conductivity (CC), µS/cm	≤ 0.20	≤ 0.30
Dissolved Oxygen (DO), ppb	≤ 20	≤ 10
Sodium (Na), ppb	≤ 3	≤ 3

Polisher Effluent

Parameter	OT	AVT
pH	9.2 - 9.5	9.0 - 9.5
Cation Conductivity (CC), µS/cm	< 0.15	≤ 0.30
Dissolved Oxygen (DO), ppb	30 - 50	≤ 10
Silica (SiO_2), ppb	≤ 10	≤ 10
Sodium (Na), ppb	≤ 3	≤ 3

Economizer Inlet

Parameter	OT	AVT
pH	9.3 - 9.5	9.3 - 9.5
Cation Conductivity (CC), µS/cm	≤ 0.15	≤ 0.20
Dissolved Oxygen (DO), ppb	30 - 50	≤7
Sodium (Na), ppb	≤ 3	≤ 3

Boiler Downcomer

Parameter	OT	AVT
pH	9.0 - 9.40	9.0 – 9.50
**Cation Conductivity (CC), µS/cm	≤ 0.42	See Curve
* Dissolved Oxygen (DO), ppb	< 8	≤7
**Sodium (Na), ppm	See Curve	See Curve
**Silica (SiO_2), ppm	See Curve	See Curve

Main Steam

Parameter	OT	AVT
pH	9.0 – 9.5	9.0 - 9.5
Cation Conductivity (CC), µS/cm	≤ 0.30	≤ 0.30
Silica (SiO_2), ppb	< 5	< 5
Sodium (Na), ppb	<3	<3

Importance of Water Chemistry Controls

The risk of chemistry related turbine damage is greatest within the so-called phase transition zone where corrosion of low pressure blades and disks results in substantial availability losses with commensurate cost impacts on the generating units. Within the phase transition zone the impurities, oxides and ions in the superheated steam act as centers for the heterogeneous nucleation of the first drops of moisture condensate. These drops concentrate the impurities which are known to be electrically charged. It is important to note that there is no oxygen within these droplets even for units operating on oxygenated treatment. These droplets can impinge on the turbine surfaces and give rise to liquid films on the surfaces. The concentration of impurities in the liquid film is at least ten times higher than in droplets and the pH can drop down to below 7. These liquid films are important because they provide the dynamic environment for the phase transition zone corrosion mechanisms. Research has shown that unit cycle chemistry has a major effect on the properties of the liquid films. When the turbine shuts down and if no protective environment is provided, the deposits become moist once the surfaces cools down causing passivity breakdown and the formation of pits. Repetition of the operating/shutdown environments eventually leads to microcracks. Only when the turbine is operating is the steady state loading sufficient to drive the microcracks into stress corrosion cracks.

EPRI Guidelines

The EPRI guidelines were developed " based upon an understanding of the effects of impurities on cycle component materials under stress and heat transfer conditions, and recently developed knowledge of chemical transport from the sources of the impurities throughout the water and steam cycle." Further, "These guidelines suggest target values and action levels for both drum and once-through units for all key cycle contaminants and, for drum units, as a continuum over a broad range of operating pressures."

During the development of the initial EPRI Cycle Chemistry Guidelines, a review of the sensitivities of cycle components to water steam purity determined that limiting the concentration of ionic contaminants throughout the cycle to levels consistent with the levels in the steam tolerable by the turbine, adequately protected the boiler and other cycle components. The basic rule was that the concentration of a molecular impurity in superheated steam should not exceed its solubility anywhere in the turbine. The solubility was considered to be lowest just before the saturation line. The target values for sodium and chloride were derived from the limits for sodium hydroxide and sodium chloride respectively.

The process to derive boiler water contaminant limits for sodium, chloride, sulfate and silica started with the allowed turbine steam composition (based on the solubility limits). By considering mechanical and vaporous carryover, the allowable impurity concentrations in boiler water was determined. Both mechanical and vaporous carryover are pressure dependent and therefore the target values for boiler water ionic contaminants are also pressure dependent.

In Revision 1 of the subject EPRI Guidelines document the steam limits for sodium, chloride and sulfate were reduced from 3 ppb to 2 ppb. In addition EPRI moved away from the approach of using the ray diagram and deriving boiler water limits from steam solubilities using mechanical and vaporous carryover. Revision 1 now uses method of portioning of impurities, salts and oxides into steam to set the boiler water limits.

The Boiler water sample point monitors drum boiler water chemistry to minimize deposition and corrosion in the boiler tubes. This sample point allows for control of

boiler water chemistry through blowdown and chemical feed and is a primary control point for steam chemistry. Downcomer boiler drum samples are used for boiler water analysis.

The economizer inlet sample point allows the direct measurement of the total contaminant ingress to the boiler. The condensate pump discharge sample point monitors magnitude of contaminants introduced by condenser leakage, magnitude of contaminants introduced by the makeup treatment system and the carryover of contaminants and treatment chemicals in the steam.

The EPRI Guidelines contain action levels for control parameters at critical sample points. The four action levels were established based on the following criteria:

- **Normal**. Values are consistent with long term system reliability. A safety margin has been provided to avoid concentration of contaminants at surfaces and under deposits.
- **Action Level 1**. There is a potential for the accumulation of contaminants and
- **Action Level 2**. The accumulation of impurities and corrosion will occur. Return values to normal levels within 24 hours.
- **Action Level 3**. Experience indicates that rapid corrosion could occur, which can be avoided by shutdown of the unit within 4 hours.

Review of Sherco Unit 3 Boiler Water Sodium Content

Analysis of boiler water grab samples obtained at approximately 2 week intervals from 1987 thru the event of November 19, 2011 revealed that the sodium content of all samples tested was well under the EPRI guideline limits as shown in Fig. 503. The highest recorded sodium content during this span was 192 ppb. In mid-June of 2001 online monitoring instrumentation of boiler water sodium content linked to the PI® archival database was in place. Boiler water sodium content as-recorded by the online monitoring instrumentation from June 2001 through March 2002 was much higher than the boiler water sodium content as measured from the grab samples analyzed by Atomic Emission Spectroscopy as shown in Fig. 504. After a study by plant personnel it was determined that the on-line monitoring measurements were erroneous due to an incorrect signal range. It was determined that the online monitoring instrumentation signal range needed to be "synchronized" with the measured boiler water sodium

content from the grab samples. Between March 2002 and April 2002 the online monitoring instrumentation was synchronized and when the unit was started-up in April of 2002 the boiler water sodium content reported by the online monitoring instrumentation was in line with the boiler water sodium content as measured from the grab samples analyzed by Atomic Emission Spectroscopy as shown in Fig. 505. From April 2002 through November 2011 the boiler water sodium content as reported by the online monitoring instrumentation was within EPRI guidelines. The data from the online monitoring instrumentation is presented in Appendix C.

Review of Boiler Water Cation Conductivity Data

Boiler water cation conductivity data is available from the online monitoring system from November 2000 through November 2011. From April 2002 through November 2011 the boiler water cation conductivity as reported by the online monitoring instrumentation was within EPRI guidelines. The data from the online monitoring instrumentation is presented in Appendix C.

Review of Cation Conductivity and Sodium Content at the Condensate Pump Discharge

Condensate pump discharge cation conductivity and sodium content data is available from the online monitoring system from November 2000 through November 2011. From April 2002 through November 2011 the cation conductivity and sodium content at the condensate pump discharge as reported by the online monitoring instrumentation was within EPRI guidelines. The data from the online monitoring instrumentation is presented in Appendix C.

Review of Cation Conductivity at the Economizer Inlet

Economizer Inlet cation conductivity data is available from the online monitoring system from November 2000 through November 2011. From April 2002 through November 2011 the cation conductivity at the economizer inlet as reported by the online monitoring instrumentation was within EPRI guidelines. The data from the online monitoring instrumentation is presented in Appendix C.

INDUSTRY EXPERIENCE

In 1980 EPRI undertook an industry wide survey of nuclear and fossil fueled plants related to stress corrosion cracking. The survey included one decommissioned plant and 33 of 72 operating US Nuclear plants. The 33 plants had a total of 79 low pressure turbines. Cracking was found in 70 disks from 36 low pressure turbine rotors; 35 disks had keyway cracks, 5 disks had bore surface cracks, 7 disks had face cracks and 30 disks had rim attachment cracks. All the units containing cracks were manufactured by Westinghouse Electric. Cracks were predominantly intergranular and branched and it was generally agreed that the operative mechanism was stress corrosion cracking. The survey only included 34 US fossil fueled plants with 45 low pressure turbines-18 made by Westinghouse, 19 by General Electric and 8 by Allis-Chalmers. Disk cracking was reported in 49 disks in 31 turbines of 22 plants. 31 disks had web face cracks (29 of these were Westinghouse manufactured), 16 disks had rim attachment cracks (14 of these were manufactured by General Electric Co.), one disk had a bore crack (manufactured by Allis-Chalmers) and one disk had a keyway crack (manufactured by Allis-Chalmers). Cracking occurred in 22 of 24 rotors used in plants with once-through boilers and 9 of 21 rotors in plants with drum boilers. Since this 1980 survey, inspection of General Electric turbines used in nuclear plants in the U.S. and in other countries has revealed disk keyway crack indications in approximately 60 disks.

In 1990 EPRI organized a workshop to gather and consolidate pertinent industry experience regarding the problem of SCC in fossil turbine disks. General Electric reported that 1049 disks in 85 of the older fossil turbines of GE design had been inspected. Of these 36 disks were reported to have ultrasonic indications in the keyways. 12 of these disks were removed and analyzed and SCC was confirmed in 6 of the disks. Westinghouse also provided a summary of their disk cracking experience at the workshop. Of a total of 220 fossil disks inspected no cracking of any type was reported in these disks.

In 1997 EPRI organized yet another stress corrosion workshop, this time to address the issue of disk rim attachment cracking which had increased dramatically in both nuclear and fossil low pressure turbines since the first survey in 1980. The survey included all

109 currently operating nuclear units in the United States. Low pressure turbine rotor rim attachment cracking was reported in 41 of these units. The cracking mechanism reported was predominantly stress corrosion cracking with a few instances of corrosion-fatigue and one incident of high cycle fatigue. The survey database contained primarily General Electric and Westinghouse manufactured turbines. Rim cracking was reported in nuclear units with operating times ranging from 33,000 to 140,000 hours. In General Electric manufactured turbines cracking was most severe in the L-2 and L-3 rows which had circumferential entry straddle mount blade attachments; temperatures at these rows are in the range of 220°F to 260°F. No cracking was reported in the L-0 and L-1 rows of the GE turbines which have a finger and pin attachment design. In Westinghouse turbines cracking was primarily in the L-0 to L-4 rows which had axial- entry blade attachments; temperatures at these rows are in the range of 120-260°F. Compared with results of the 1980 survey where rim attachment cracking was reported only in certain rows of Westinghouse turbines, the 1995 data shows a significant shift in the number of cracks by row number to downstream rows and significant rate of cracking in General Electric rotors, not reported up to 1980. The survey included 757 fossil units from 33 utilities. The incidence of cracking was ten times higher in supercritical units with once through boilers than in subcritical units. The cracking mechanism reported was predominantly stress corrosion cracking with a few instances of corrosion-fatigue. Data on unit operating time was insufficient however, the number of units with rim-attachment cracks by in-service dates indicated that the largest fraction of units with rim cracks went into service between 1966 and 1975 (approximately 100,000 to 200,000 operating hours). Compared with nuclear units, the apparently longer time for initiation of cracking in fossil units is related to steam conditions (wetness and temperature) during operation, which are typically drier for fossil units. For GE turbines no rim cracking was reported in subcritical units; in supercritical units cracking was reported to be most severe in the L-1 and L-2 rows; temperatures in these rows are approximately in the 160-200°F range. Cracking in GE designs was also reported at various locations (pin holes, base radius and ledges) in the multi-finger pinned type of attachment used in the L-0 and L-1 rows of four units.

LP Finger Attachment Cracking - Navajo Generating Station

The Navajo Generation Station has three tandem compound double flow General Electric Model 3 low pressure turbines each rated at 805 MW. Each unit is fueled by coal and operates at supercritical conditions. The three units went into operation between the years 1974 and 1976. Extensive stress corrosion cracking was found in Unit 1 low pressure "B" L-1 finger pinned blade attachments during an April 1995 bucket replacement. Forensic analysis identified the cracks as being intergranular and the primary chemical compound responsible for stress corrosion cracking as being sodium hydroxide (caustic) although the presence of sodium on the crack surfaces was not found in detectable quantities. In 1996 the other two units were inspected and stress corrosion cracking was found in all low pressure L-1 finger pinned blade attachments. The most severe cracking occurred in Fingers 3, 4 and 5. There was no cracking in Fingers 1 and 6, the outer sides of the disk. Some cracks were observed in the upper land pinholes. The material of the LP turbine rotors was identified as ASTM A470, Class 7 with measured yield strengths of between 95-114 ksi. The initial report concluded that steam chemistry, polisher operation and high centrifugal stress contributed to the stress corrosion cracking.

NGS queried seven other user group owners of similar units and found that three had experienced stress corrosion cracking in the low pressure turbine finger pinned blade attachments. The names of the seven owners were not identified.

No other reports of cracking in General Electric finger pinned blade attachments have been uncovered in the open literature.

Installed Base of GE Steam Turbines That May Have Similar Low Pressure Turbine L-1 Root Attachment Design

An installation list of steam turbine generator trains manufactured by General Electric with 33.5" last stage blades and operating in plants with drum type boilers is presented in Fig. 506. It is reported that the low pressure turbine L-1 stages on these units may have finger pinned blade attachments similar to those of Sherco 3 unit. Only one unit in the installation list has an in-service date later than Sherco Unit 3. No information regarding operating conditions, operating time, heat balance, low pressure turbine L-1

blade attachment design, low pressure turbine rotor material of construction, inspection records or maintenance records for the units listed in Fig. 506 were available for review. The initiation time for caustic stress corrosion cracks to form on the blade attachments on any one of the units listed in Fig. 506 is dependent on the following variables:

- Operating Stress - The operating stress is primarily a function of blade attachment geometry and certain operating conditions. No information on blade attachment geometry and insufficient operating information for the units in Fig. 506 is available to provide any insight into the susceptibility of these units to caustic stress corrosion cracking in comparison to Sherco Unit 3. The effect of static stress on stress corrosion crack susceptibility is shown in Fig. 483.

- Environment - The risk of caustic stress corrosion cracking is greatest within the phase transition zone where impurities, such as sodium, can concentrate. Insufficient information is available for the units in Fig. 506 to determine the location of the phase transition zone in these units. The risk of caustic cracking increases with sodium content in the boiler water and steam. No boiler water or steam chemistry data for the units shown in Fig. 506 is available for comparison with the water chemistry of the Sherco Unit 3. The number of shutdowns and perhaps part load operation may result in further concentration of sodium compounds within the blade attachments that could increase the susceptibility to caustic stress corrosion cracking. Shutdown and part load operation details for the units shown in Fig. 506 is not available for comparison to Sherco Unit 3. Further details on impact of steam chemistry on stress corrosion cracking is available in earlier sections of this report.

- Materials of Construction - As previously mentioned, there is little difference in the caustic stress corrosion susceptibility of common steam turbine LP rotor materials. Nevertheless, there can be significant variation between heats especially with regards to initiation time. This variation can be as large as 200%.

The preceding discussion was concerned with variables affecting stress corrosion crack initiation within steam turbine blade attachments. However, the presence of cracks is not sufficient to result in a failure of the steam turbine blade attachments. Failure will

only occur when the stress corrosion cracking has progressed in a manner which reduces the load carrying capability of the attachments to a degree that the attachments can no longer withstand the stresses generated during operation and the attachments fracture resulting in liberation of attachments, blade pins and blades. The time required for cracking to progress to the extent necessary for failure is dependent on crack distribution, crack orientation, crack propagation rates, crack propagation direction and crack linkage. It is not possible to predict crack distribution, crack orientation and crack linkage. Significant scatter with regards to blade attachment failure time would be expected even with identical attachment geometry and operating conditions. As an example, it is noted that the low pressure turbine "B" turbine end L-1 stage finger pinned blade attachments on the Sherco 3 unit fractured over about half the circumference of the L-1 stage disk but remained intact, although cracked, in the other half of the disk. Further, no failures of the finger pinned blade attachments occurred in the remaining L-1 stage disks in low pressure turbines "A" and "B" on Sherco Unit 3 although extensive stress corrosion cracking was evident in these attachments.

OTHER RELEVANT DOCUMENTS

General Electric US Patent 7,387,494

In June 2008 General Electric was granted a patent from the US Patent Office titled "Finger Dovetail Attachment Between a Turbine Rotor Wheel and Bucket for Stress Reduction; the patent application was originally filed in April 2005. The invention is for finger pinned blade attachments in steam turbine disks such as that in the low pressure turbine L-1 disks in the Sherco Unit 3 steam turbine generator. Specifically the invention involves providing generous transition fillet radii between finger sections of different section thickness and generous fillets at bottom of the finger slots. According to the patent abstract the purpose is "…to reduce stress concentrations and to avoid stress corrosion cracking in steam turbine applications." A copy of the patent is presented in Appendix D.

General Electric TIL 1121-3A and 1121-3AR

In May 1992, General Electric issued a Technical Information Letter 1121-3A detailing a newly developed magnetic particle inspection procedure for non-destructive inspection of finger pinned blade attachments in steam turbine disks. The TIL states "This procedure describes the use of wet fluorescent magnetic particle inspection (MPI) to detect stress corrosion cracking (SCC) on steam turbine wheels with finger dovetails." The TIL recommends that the magnetic particle inspection should be performed whenever the blades are removed. The TIL indicates that "…abnormal operation or unusual operating events that cause concern for long term reliability of the unit may be reason to consider removal of buckets, before normal replacement, for MPI of dovetail area." The TIL does not define what an abnormal operating condition or unusual operating events are.

In February 1993 General Electric issued Technical Information Letter 1121-3AR1. This revision of the original TIL 1121-3A addressed an improvement in the magnetic particle inspection method. It also provided some definition of "abnormal operation or unusual events". Specifically TIL 1121-3AR states "Abnormal events or operational anomalies are any out-of-the-ordinary occurrences, during operation or maintenance, which may increase the risk of stress corrosion and/or fatigue cracking, such as but not limited to

the following: a) caustic or chemical ingestion or contamination, b) carryover from boiler, c) leaking condenser heater tube, d) overspeeds and e) water ingestion. The subject Root Cause Analysis did not reveal any "out-of-the-ordinary" operational events during operation or maintenance that would have required the inspection to be performed.

Both Technical Information Letters and their respective cover letters are presented in Appendix E.

General Electric TIL 1277-2

In December 1999, General Electric issued a Technical Information Letter 1277-2, titled "Inspection of Low Pressure Rotor Wheel Dovetails on Steam Turbines with Fossil Fueled Once-Through Boilers", informing users of the need to inspect low pressure rotor wheel dovetails on steam turbines to detect possible Stress Corrosion Cracking. The TIL indicates that stress corrosion cracking had been found over the past several years in low pressure rotor dovetails, both tangential and pinned finger type, of fossil steam turbine units with once through boilers. The document indicated that most cases involved L-1 and L-2 stages.

Technical Information Letter 1277-2 is presented in Appendix E.

General Electric Energy Product Brochure

A General Electric product brochure titled Steam Turbine 34.5-Inch Low-Pressure Section Upgrade, dated 2006 contains a brief section regarding stress corrosion cracking. The brochure mentions that "The incidence of SCC in the low pressure sections of units operating with once through boilers has been much higher than in units with drum type designs. However, there has been a rise in SCC indications on drum type units. SCC is a time dependent phenomenon with some cracks developing in supercritical units after approximately 25 years. The crack initiation period on drum type units may simply be longer than for once-through boilers, all other factors being equal."

IDENTIFICATION OF CAUSAL FACTORS

Three major categories were investigated as potential causal factors responsible for the stress corrosion cracking and fractures of the low pressure turbine L-1 stage disk finger pinned blade attachments. The categories were design, operation and maintenance. The design factors investigated included the suitability of the rotor material for the intended application and the static design stresses in the finger pinned blade attachments at normal operating condition. Operational factors investigated were the influence of part load operation and boiler water chemistry. Finally, past maintenance practices were scrutinized for potential influences.

Design

Steam turbine rotor materials are generally specified per ASTM A470. Some proprietary grades are used by European and Japanese manufacturers. Low alloy steels with varying amounts of chromium, nickel, molybdenum and vanadium account for the vast majority of steam turbine rotors manufactured. On rare occasions stainless steel and iron-based superalloys are used for very demanding operating conditions and/or environments. The low pressure turbine rotor material is selected based on a myriad of mechanical and physical properties including stress corrosion resistance. The stress corrosion resistance of the low alloy steels available per ASTM A470 do not vary significantly. Although the subject low pressure turbine rotor material is the highest strength alloy available per ASTM A470 and yield strength does influence stress corrosion crack initiation and propagation, it is not deemed sufficiently high enough to have been a significant factor contributory to cracking.

Finite Element Analysis indicates that localized steady stresses in the finger pinned blade attachments at the pin holes, ledges and at the base of the fingers is very high and approaches or exceeds the yield strength of the rotor material. At these calculated tensile stress levels the subject alloy has been shown to be susceptible to stress corrosion cracking even in "pure water" environments (Fig. 501). The susceptibility of the design to stress corrosion cracking is supported by OEM Technical Information Letter 1121-3A and a patent granted to the OEM for an improved finger pinned blade

attachment design to reduce the localized stresses and increase the resistance to stress corrosion cracking.

The design of the subject low pressure turbine L-1 disk finger pinned blade attachments is concluded to be susceptible to stress corrosion cracking under normal operating conditions and is considered a primary causal factor for the subject fracture of the Unit 3 finger pinned blade attachments in the low pressure "B" turbine end L-1 disk and cracking in Unit 3 finger pinned blade attachments in the low pressure "B" generator end and low pressure "A" generator and turbine end L-1 disks.

Operation

Unit 3 has since its initial start-up operated at varying power levels depending on grid demands and cycled offline rarely and then only for planned and forced outages. The power is varied by decreasing or increasing inlet steam flow. The result of operating at part load, compared to full load, would be a decrease in stage pressure and stage temperature although the decrease in stage temperature would likely be small compared to the decrease in stage pressure. During part load operation the "Wilson line" or "precipitate transition zone" would move ever so slightly upstream and the L-1 stage would become "wetter". The net effect could be a small increase in the concentration of certain chemical species within the finger pinned blade attachments in a manner similar to that experienced during a shutdown. There are no OEM limitations on part load operation. There are no technical papers in the open literature or any industry guidelines indicating that part load operation adversely affects corrosion and/or stress corrosion susceptibility of low pressure steam turbine disks. It is therefore concluded that part load operation was not a significant factor contributory to stress corrosion cracking of the Unit 3 finger pinned blade attachments of the low pressure turbine L-1 disks.

The influence of steam chemistry is difficult to assess for enclosed crevices such as the finger pinned blade attachment region. The bulk steam chemistry is not necessarily relevant or reflective of the chemistry within the blade attachment area of the L-1 disk and contaminant chemical species can become concentrated over time due to wet/dry excursions associated with shutdowns and start-ups. For this reason a conservative

design philosophy with regards to operating stresses is imperative to insure that stress corrosion cracking is not encountered when steam turbines are operated with industry steam chemistry guidelines. A review of water chemistry data from Sherco Unit 3 revealed that the boiler water sodium content had conformed to EPRI guidelines from commissioning through November 19, 2011. It is concluded that the steam chemistry was not a significant factor contributory to stress corrosion cracking of the LP L-1 disk finger pinned blade attachments.

Maintenance

A review of Unit 3 STG maintenance records revealed no repairs or modifications to the turbine that would have affected the stress corrosion cracking susceptibility of the low pressure turbine L-1 disk finger pinned blade attachments.

CONCLUSIONS

The Unit 3 Steam Turbine Generator event of November 2011 was precipitated by the fracture of multiple finger pinned blade attachments in the Low Pressure Turbine "B" turbine end L-1 stage disk rim. The fractures resulted in liberation of portions of the finger pinned blade attachments and associated L-1 blades. The loss of mass, due to the liberation of disk sections and blades, created a significant imbalance at the affected stage resulting in high amplitude vibration throughout the steam turbine generator train. This vibration was responsible for the fracture of the generator shaft, fractures of the exciter shaft at three locations and extensive additional damage to the steam turbine generator train and other plant equipment.

The fractures of the finger pinned blade attachments in the low pressure turbine L-1 turbine end disk were due to the presence of pre-existing caustic stress corrosion cracks at the pin holes, ledges and at the base of the finger pinned blade attachments. The chemical species responsible for stress corrosion cracking could not be positively identified but sodium hydroxide (NaOH) is suspected. Although the exact age of the stress corrosion cracks could not be determined, it is likely that they initiated a few years ago. The propagation and "linking-up" of the stress corrosion cracks during subsequent operation incrementally reduced the load carrying capability of the finger pinned blade attachments. By November 2011 the load carrying capability of the finger pinned blade attachments had been reduced to the point that they could no longer sustain the centrifugal stresses generated during the planned overspeed test and fractured due to tensile overload. Investigation also revealed numerous similar stress corrosion cracks in the finger pinned blade attachments of the LP "B" generator end L-1 disk and the generator and turbine end L-1 disks of the LP "A" turbine.

The primary causal factor responsible for the stress corrosion cracking of the LP "B" L-1 disk was the high static stresses generated during normal operation at the pin holes, ledges and at the base of the fingers of the finger pinned blade attachments in the low pressure turbine L-1 stage disks. These stresses in the finger pinned blade attachments are solely a function of the original design and operation at design conditions.

The water chemistry of Unit 3 conformed to EPRI guidelines and was not a significant factor contributory to the stress corrosion cracking observed in the finger pinned blade attachments of the L-1 stage disks. There was no evidence of abnormal operating conditions that would have affected the stress corrosion susceptibility of the L-1 disks. There was no evidence of abnormal operating conditions or maintenance practices that would have contributed to the stress corrosion susceptibility of the finger pinned blade attachments in the L-1 disks.

The material of the low pressure turbine rotors conformed to the mechanical and chemical requirements of ASTM A470 Grade C, Class 7 low alloy steel. There was no apparent material or processing anomalies observed in the disk sections examined.

REFERENCES

1. GEZ 5691C, "Protection of Turbine and Generator Components During Shipping and Prior to Start-up", General Electric Company, Schenectady, NY

2. GE Power Generation Steam Turbine Inspection Report FSR No. : 401T0799, dated July 7, 1993.

3. Information from Schottler, D.

4. Alstom Thermodynamic Design Review Report STD0012619, dated December 21, 2009.

5. Holdsworth, S.R., et al., "Laboratory Stress Corrosion Cracking Experience in Steam Turbine Disc Steels", *Proceedings: Steam Turbine Stress Corrosion Workshop*, TR-108982, Electric Power Research Institute, Palo Alto, CA , September 1997.

6. Bachelet, E., et al., *High Temperature Materials for Power Engineering 1990, Part I*, Kluwer Academic Publishers, 1990.

7. Speidel, M.O. and Magdowski, R., "Major Influences on the Growth Rates of Stress Corrosion Cracks in Steam Turbine Rotor and Blade Materials", *Proceedings: Steam Turbine Stress Corrosion Workshop*, TR-108982, Electric Power Research Institute, Palo Alto, CA , September 1997.

8. Magdowski, R. and Speidel, M.O., "Environmental Assessment and Life Time Prediction of Low Alloy Steam Turbine Rotor Steels", *Proceedings of Seventh International Symposium on Environmental Degradation of Materials in Nuclear Power Systems-Water Reactors*, Breckenridge, 1995.

9. Jonas, O., "Steam Turbine Corrosion", Materials Performance, February 1985a.

10. GEK 72281c, "Steam Purity Recommendations for Utility Steam Turbines", GE Energy, Revision April 2004.

11. Cycle Chemistry Guidelines for Fossil Plants: All-volatile Treatment, Revision 1, Electric Power Research Institute, November 2002.

12. *Steam Turbine Disc Cracking Experience, Volume 7: Metallurgical Analysis of Cracked Discs From 10 U.S. Power Plants*, EPRI NP-2429-LD, Project 1398-5, Final Report, Electric Power Research Institute, Pala Alto, CA, June 1982.

13. *Guidelines for Predicting the Life of Steam Turbine Disks Exhibiting Stress Corrosion Cracking*, EPRI NP-6444, Project 1929-16, 2518-1, Final Report, Electric Power Research Institute, Palo Alto, CA, July 1989.

14. *Low-Pressure Steam Turbine Corrosion Mechanisms and Interactions: State of Knowledge 2010*, 1020671, Final Report, Electric Power Research Institute, Palo Alto, CA, July 2010.

15. *Relationship Between Turbine Rotor and Disk Metallurgical Characteristics and*

Stress Corrosion Cracking Behavior, EPRI-4695M, Project 1929-6, Final Report, Electric Power Research Institute, Palo Alto, CA, September 1986.

16. *Metallurgical Analysis of Rim Cracking in a LP Steam Turbine Disc*, EPRI NP-1532, Project 1398-1, Final Report, Electric Power Research Institute, Palo Alto, CA, September 1980.

17. Lyle, F.F., "Stress Corrosion Crack Initiation in Steam Turbine Steels", *Proceedings: Steam Turbine Stress Corrosion Workshop*, EPRI TR-108982, Baltimore, MD, 1997.

18. Yehle, et al., "Finger Dovetail Attachment Between a Turbine Rotor Wheel and Bucket for Stress Reduction", United States Patent 7,387,494, June 17, 2008.

19. Technical Information Letter 1277-2, General Electric Energy Services, December 2, 1999.

20. Technical Information Letter 1121-3, General Electric Power Generation Product Service, May 15, 1992.

21. Technical Information Letter 1121-3AR, General Electric Power Generation Parts & Product Service, February 1, 1993.

22. Kavney, K., Lesiuk, J., and Wright, J., "Steam Turbine 34.5-Inch Low-Pressure Section Upgrade", General Electric Energy, 2006.

23. Nowak, E., "Low Pressure Turbine Stress Corrosion Cracking Investigation at the Navajo Generating Station", *Proceedings: Steam Turbine Stress Corrosion Workshop*, EPRI TR-108982, Baltimore, MD, 1997.

24. Rosario, D., Wells, C., Licina, G. and Viswanathan, R., "Stress Corrosion Cracking of Steam Turbine Rotors", *Proceedings: Steam Turbine Stress Corrosion Workshop*, EPRI TR-108982, Baltimore, MD, 1997.

25. Jonas, O. and Machemer, L., "Steam Turbine Corrosion and Deposit Problems and Solutions", *Proceedings of the 37th Turbomachinery Symposium*, Houston, TX, 2008.

26. Denk. J., "Effect of Transient Loading Conditions on Stress Corrosion Crack Initiation"", *Proceedings: Workshop on Corrosion of Steam Turbine Blading and Disks in the Phase transition Zone*, EPRI TR-111340, Palo Alto, CA, 1998.

27. Atlas of Stress-Corrosion and Corrosion Fatigue Curves, Ed. By A. J. McEvily, Jr., ASM International, Materials Park, Ohio, 1990.

28. *Stress Corrosion Characterization of Turbine Rotor Materials*, EPRI NP-4622, Project 1929-S Final Report, Electric Power Research Institute, Palo Alto, CA, 1986.

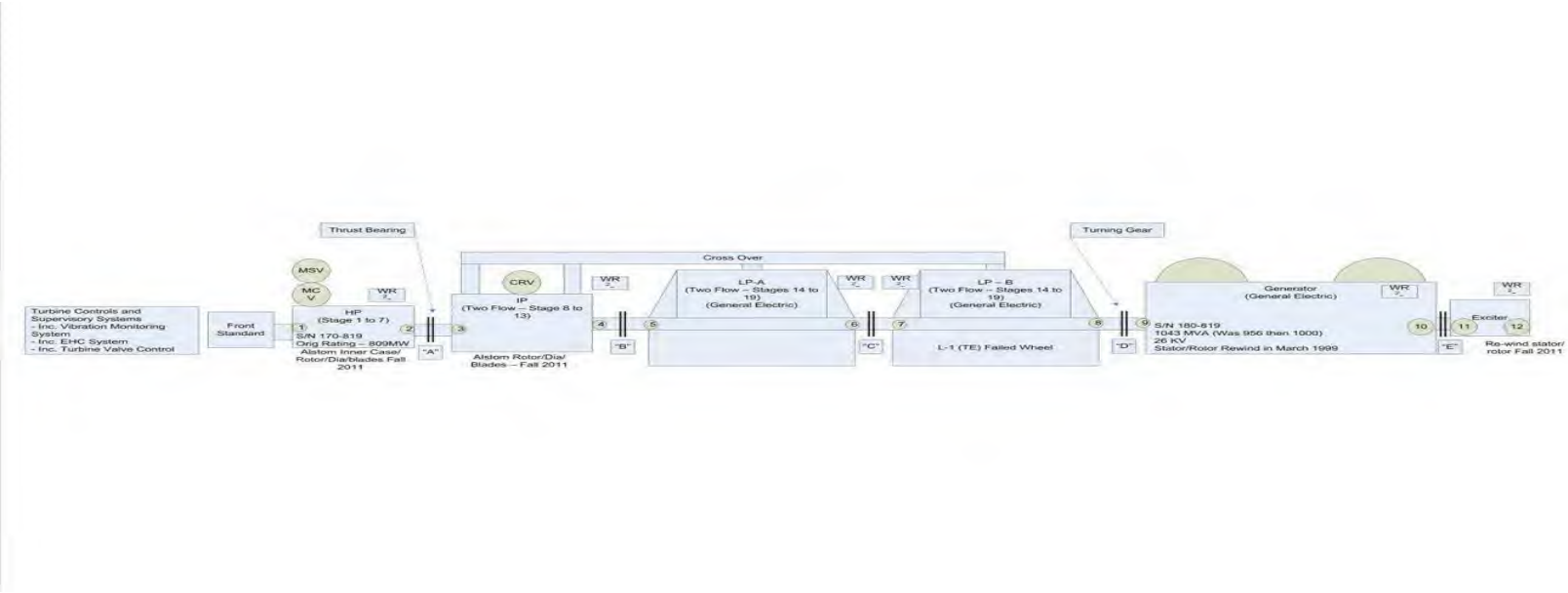

Fig. 1. Pictorial of Unit No. 3 Steam Turbine Generator after Fall 2011 retrofit. Bearing locations identified by small circles with numbers ranging from 1 thru 12.

Fig. 2. Photograph of Sherco Unit 3 steam turbine generator after the event of November 19, 2011

Fig. 3. Photograph of Sherco Unit 3 steam turbine generator after the event of November 19, 2011.

Fig. 4. Photograph of Sherco Unit 3 steam turbine generator after the event of November 19, 2011.

Fig. 5 Photograph of high pressure end of Sherco Unit 3 steam turbine generator after the event of November 19, 2011.

Fig. 6. Photograph of high pressure end of Sherco Unit 3 steam turbine generator after event of November 19, 2011.

Fig. 7. Photograph of Sherco Unit 3 steam turbine generator at exciter end after event of November 19, 2011.

Fig. 8. Photograph of exciter "Doghouse" from Sherco Unit 3 steam turbine generator after event of November 19, 2011.

Fig. 9. Photograph of damaged coupling cover between the low pressure turbines of Sherco Unit 3 steam turbine generator after event of November 19, 2011.

Fig. 10. Photograph of an outer casing fastener from the Sherco Unit 3 steam turbine generator after the event of November 19, 2011.

Fig. 11. Photograph of the Sherco 3 high pressure turbine.

Fig. 12. Photograph of high pressure turbine rotor from Sherco Unit 3 at the Alstom Power, Inc., repair facility in Richmond, VA.

Fig. 13. Close-up photograph of high pressure turbine rotor shown in Fig. 12.

Fig. 14. Close-up photograph of high pressure turbine rotor shown in Fig. 13 showing moderate/heavy rub damage on blade integral shrouds.

Fig. 15. Close-up of high pressure rotor shown in Fig. 12 showing rub damage (arrows) on blade integral shrouds.

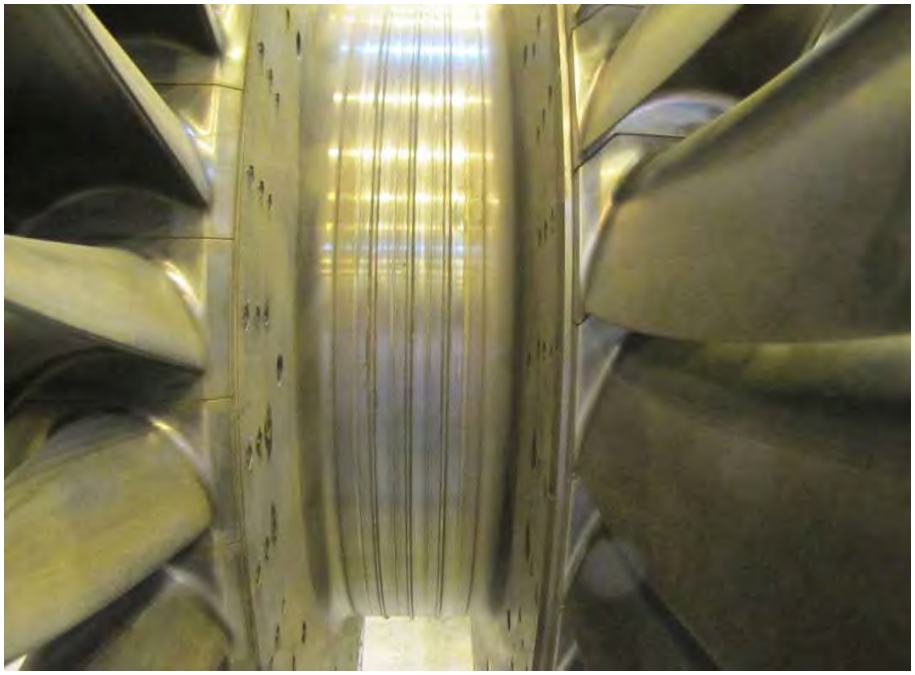

Fig. 16. Photograph of high pressure rotor shown in Fig. 12 showing light rub damage to interstage seal areas.

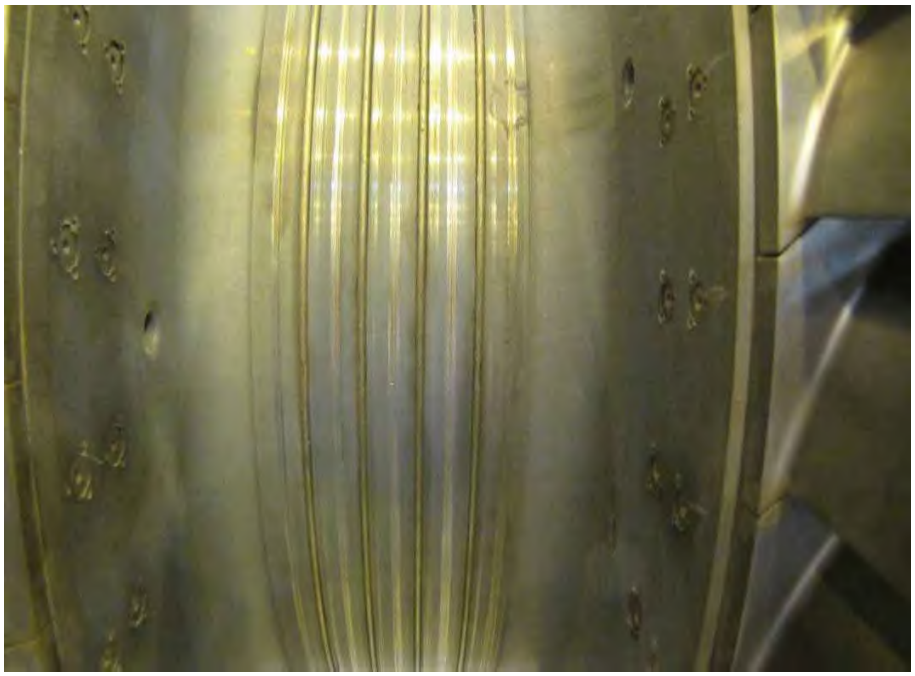

Fig. 17. Photograph of high pressure rotor shown in Fig. 12 showing rub damage to interstage seal areas.

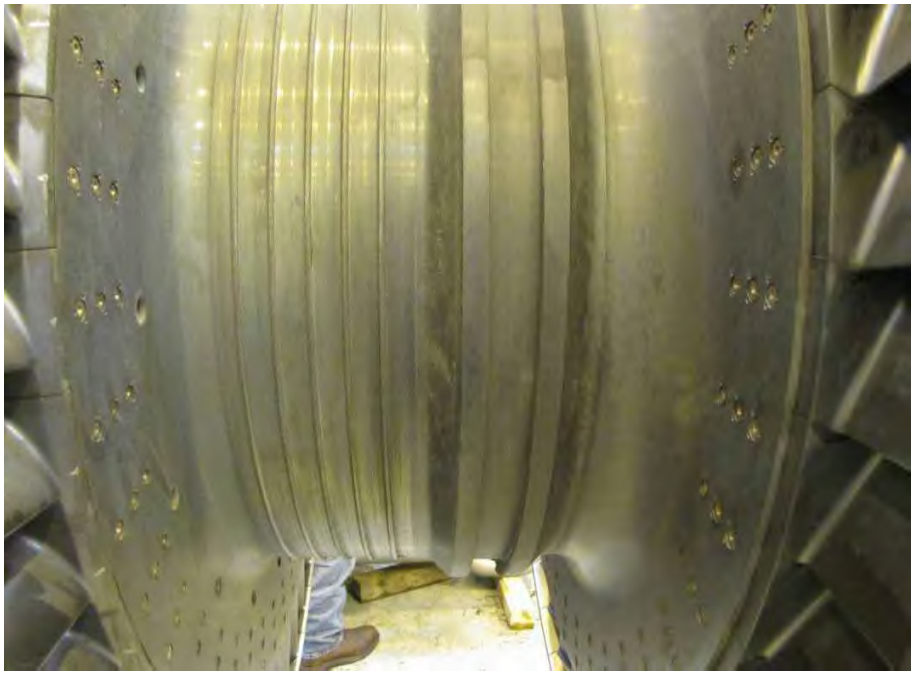

Fig. 18. Photograph of high pressure rotor shown in Fig. 12 showing rub damage to interstage seal areas.

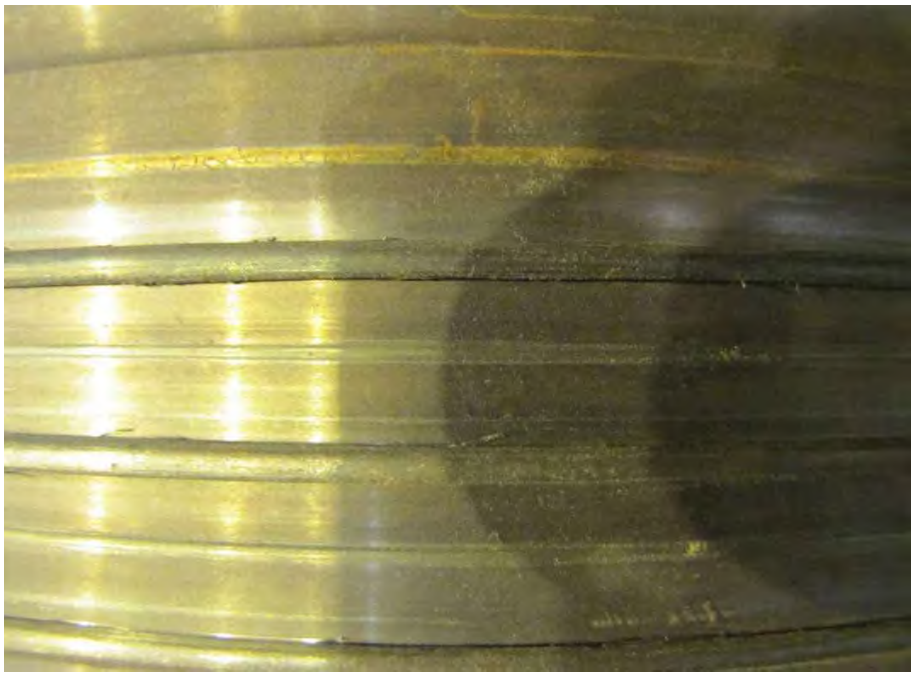

Fig. 19. Photograph of high pressure rotor shown in Fig. 12 showing rub damage to interstage seal areas.

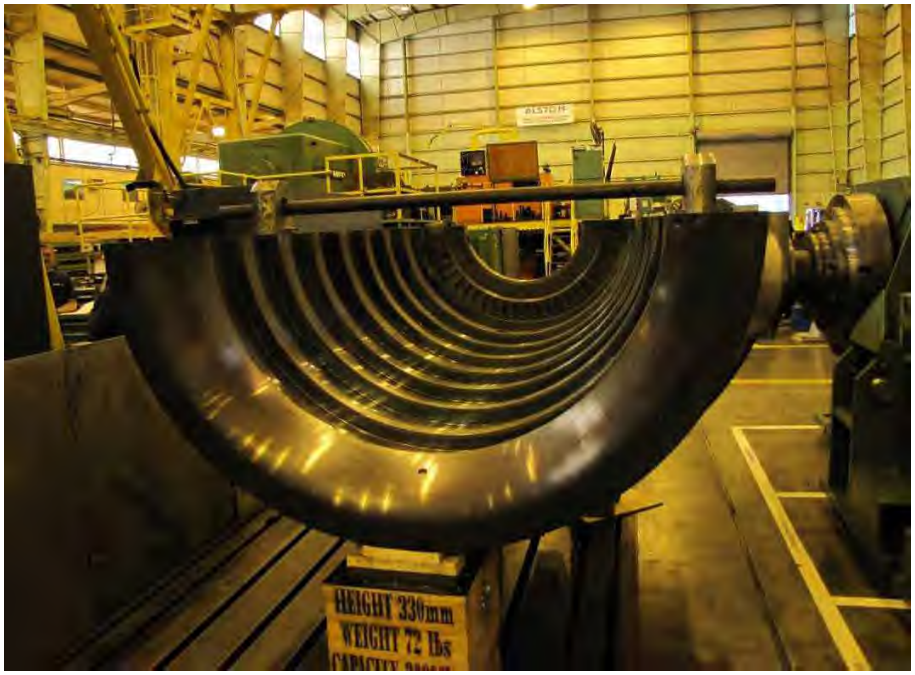

Fig. 20. Photograph of high pressure turbine inner casing at the Alstom Power, Inc. repair facility in Richmond, VA.

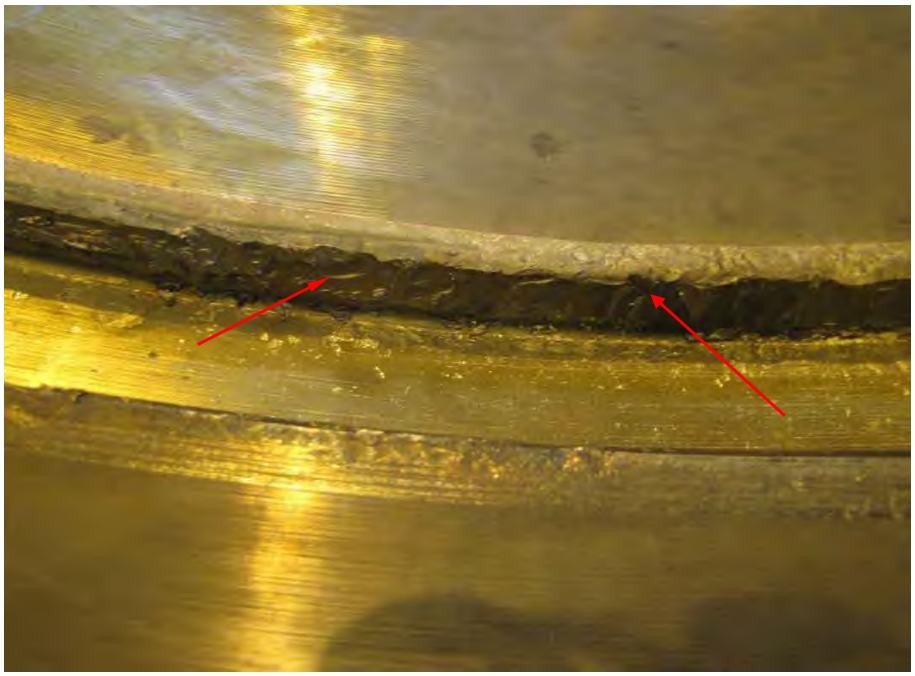

Fig. 21. Close-up of high pressure turbine inner casing shown in Fig. 20 showing extent of galling (arrows) at inlet gland seal fit area.

Fig. 22. Close-up of high pressure turbine inner casing shown in Fig. 20 showing fractured section of the inlet gland seal fit.

Fig. 23. Photograph of high pressure turbine inlet gland casing showing fractured casing material (arrow) attached to outer surface.

Fig. 24. Close-up photograph of fractured casing material shown in Fig. 23.

Fig. 25. Photograph of high pressure turbine inlet gland bolts.

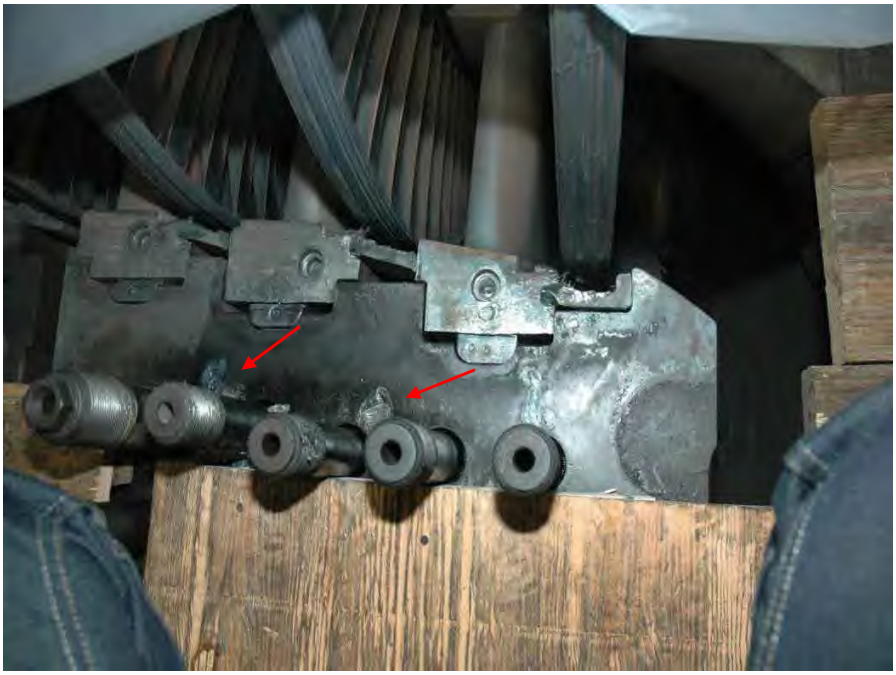

Fig. 26. Close-up of intermediate pressure turbine inner casing showing evidence of melting (arrows) on horizontal split.

Fig. 27. Close-up of melted areas on intermediate pressure turbine inner casing, shown in Fig. 26, after removal of rotor and diaphragms.

Fig. 28. Close-up of melting on intermediate pressure turbine inner casing shown in Fig. 27

.

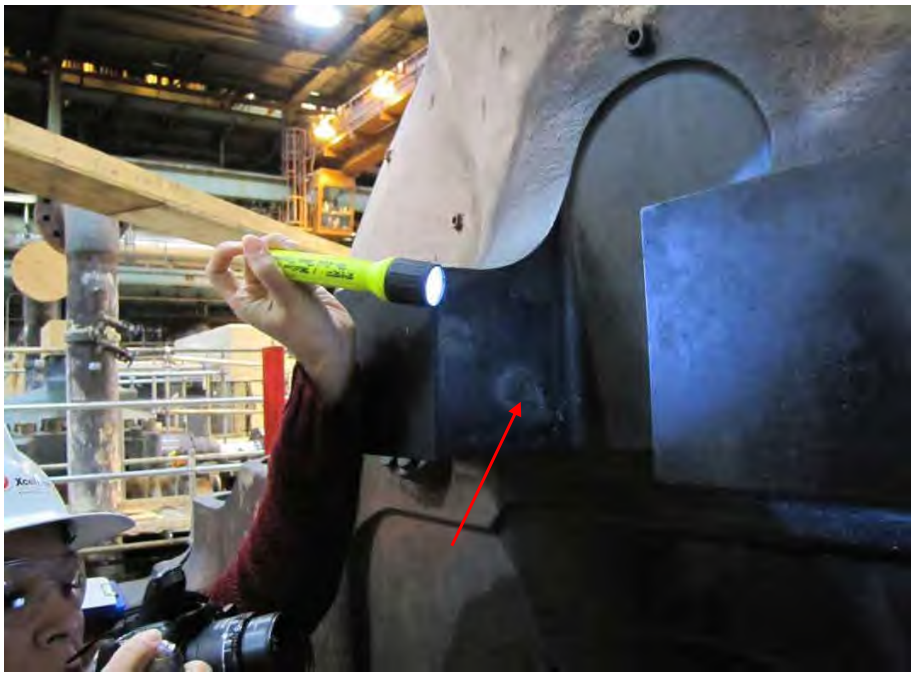

Fig. 29. Photograph of melted area (arrow) on alignment lug of outer casing from intermediate pressure turbine.

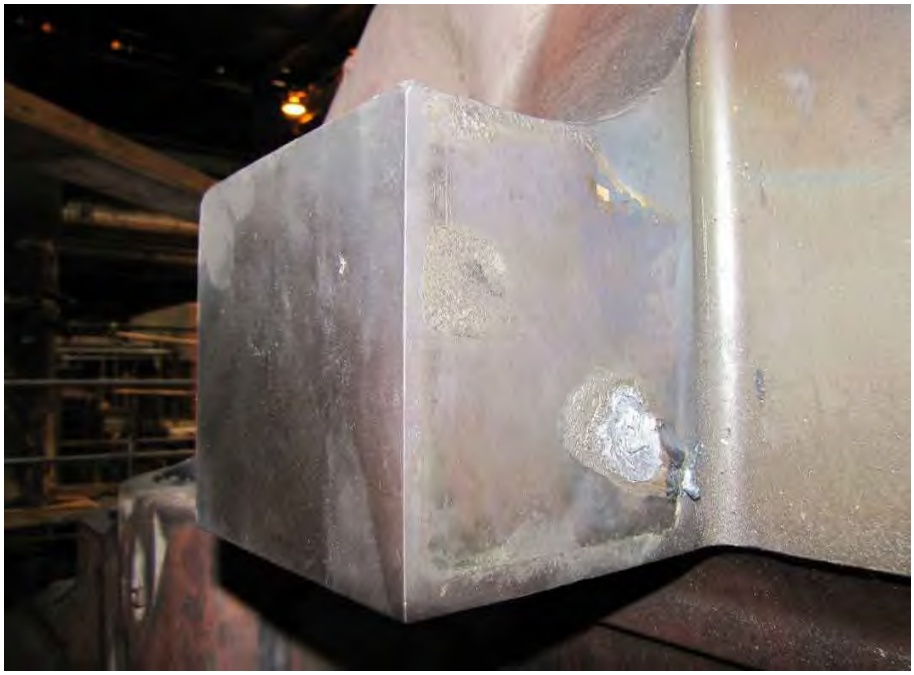

Fig. 30. Close-up of melted area on alignment lug on intermediate pressure turbine outer casing shown in Fig. 29.

Fig. 31. Photograph of reheat intermediate pressure turbine rotor from the Sherco 3 steam turbine generator train at the Alstom Power, Inc. repair facility.

Fig. 32. Close-up of intermediate pressure turbine rotor shown in Fig. 31 showing moderate to heavy rub damage on blade integral shrouds.

Fig. 33 Close-up of intermediate pressure turbine rotor shown in Fig. 31 showing moderate to heavy rub damage on blade integral shrouds.

Fig. 34. Close-up photograph of intermediate pressure turbine rotor shown in Fig. 31 showing rub damage seal surfaces.

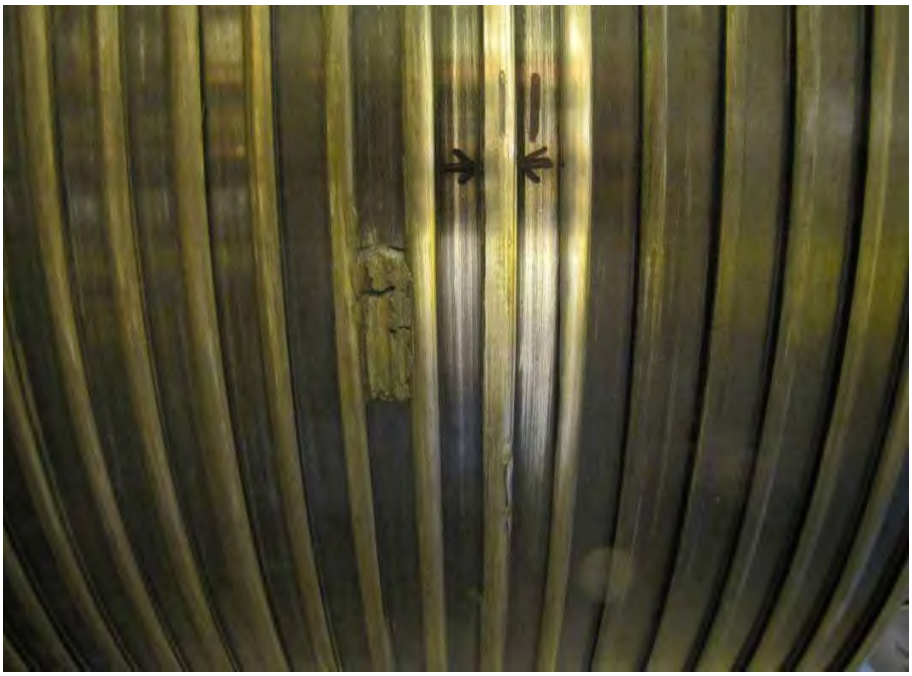

Fig. 35. Close-up photograph of Intermediate Pressure Turbine showing rub damage on seal surface.

Fig. 36. Close-up photograph of intermediate pressure turbine showing rub damage on seal surface.

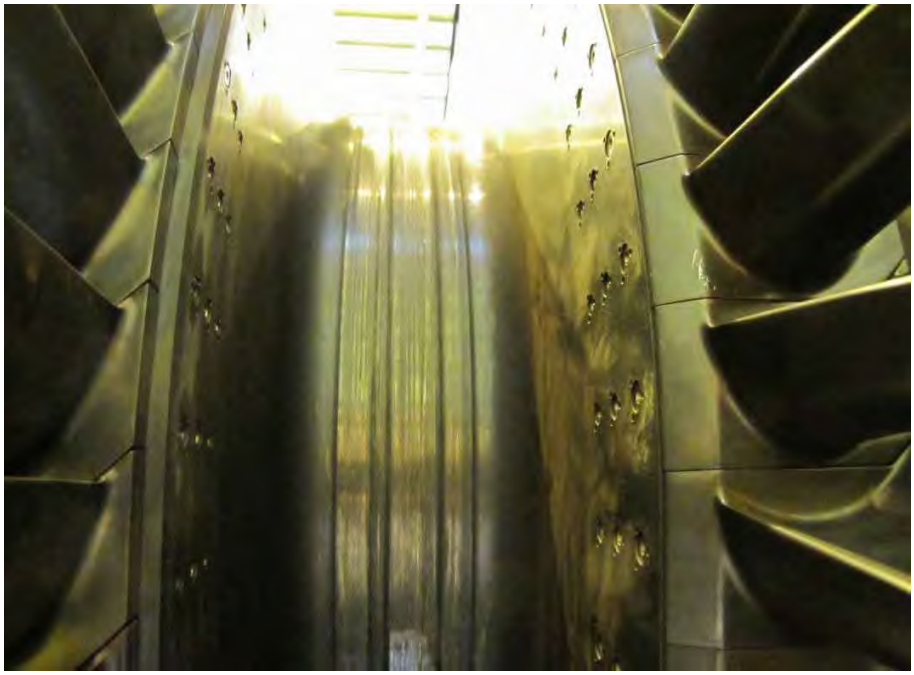

Fig. 37. Close-up photograph of intermediate pressure turbine rotor showing light rub damage on interstage seal surfaces.

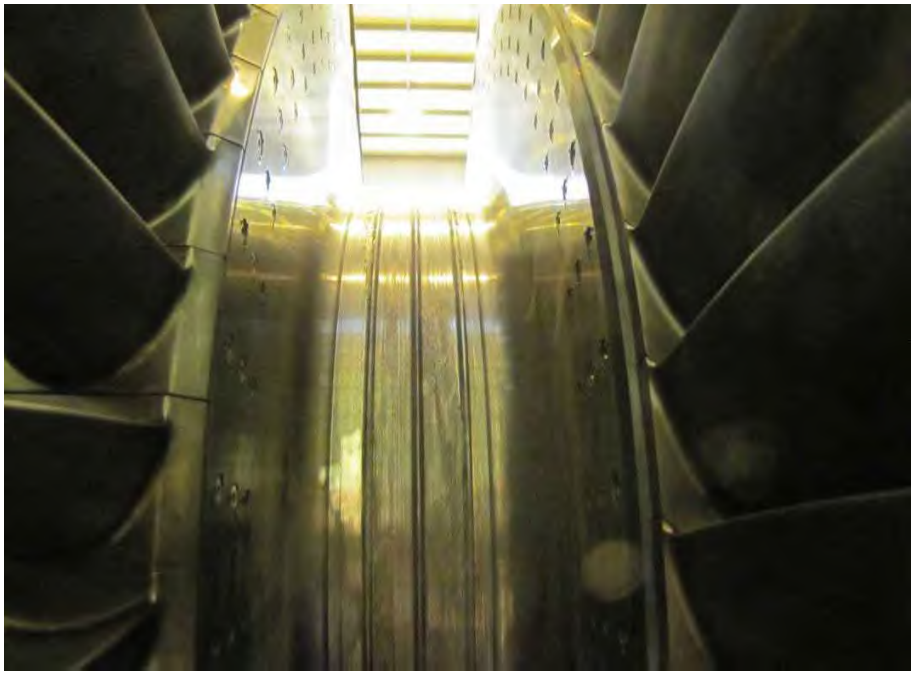

Fig. 38. Close-up photograph of intermediate pressure turbine rotor showing light rub damage on interstage seal surfaces.

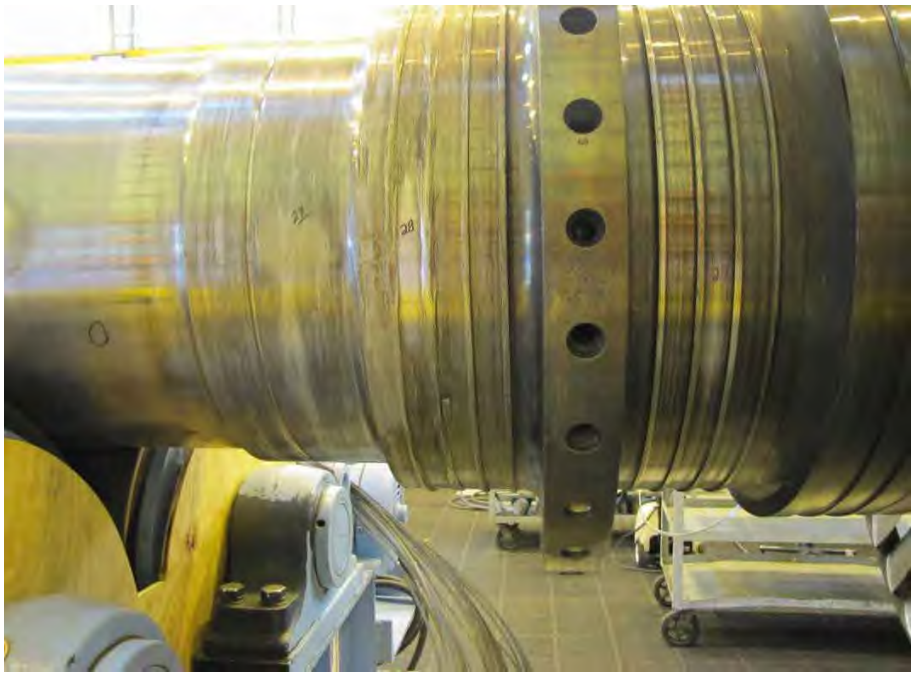

Fig. 39. Close-up photograph of intermediate pressure turbine rotor showing light to moderate rub damage on seal surfaces.

Fig. 40. Photograph of intermediate pressure turbine rotor generator end coupling.

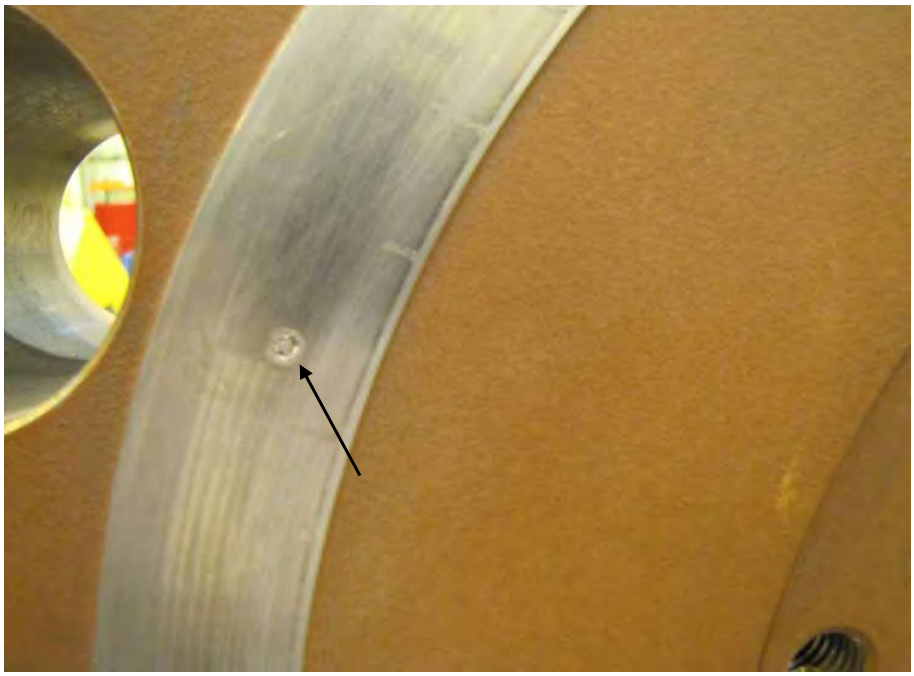

Fig. 41. Close-up photograph of intermediate pressure turbine rotor generator end coupling showing evidence of melting (arrow) on machined face.

Fig. 42. Photograph of intermediate pressure turbine rotor turbine end coupling.

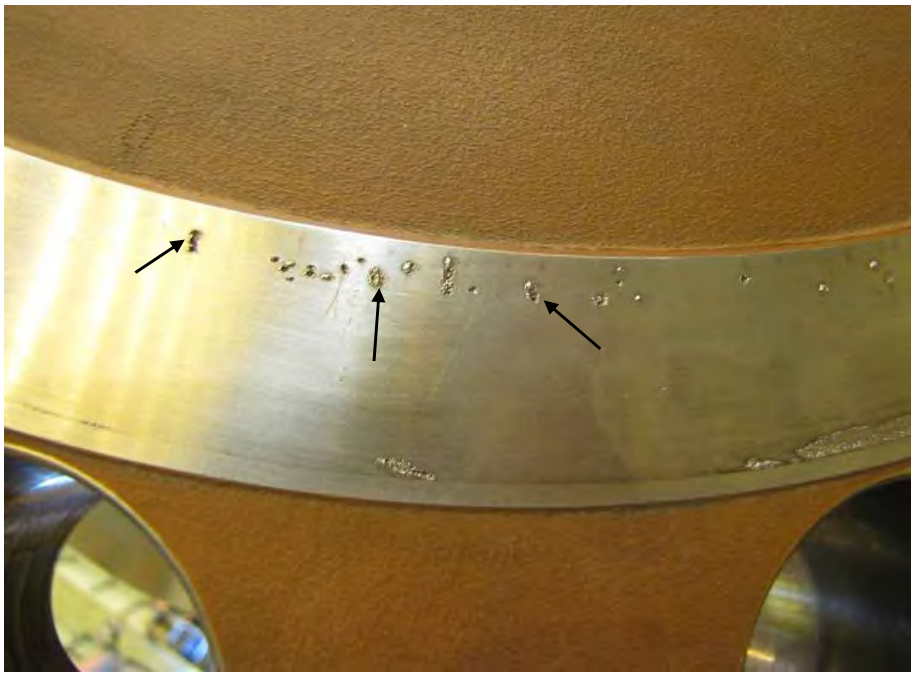

Fig. 43. Close-up photograph of intermediate pressure turbine rotor turbine end coupling showing evidence of melting (arrows) on machined face.

Fig. 44. Photograph of low pressure turbine rotor "A" in stands at site.

Fig. 45. Photograph of low pressure turbine rotor "A" shown in Fig. 44.

Fig. 46 Photograph of low pressure turbine rotor "A" shown in Fig. 44.

Fig. 47. Photograph of generator end of low pressure turbine "A" rotor shown in Fig. 44..

Fig. 48. Generator end of low pressure turbine "A" showing extent of rub damage on L-3, L-4 and L-5 blade covers and tenons.

Fig. 49. Generator end of low pressure turbine "A" showing extent of rub damage on L-2 blade covers and tenons.

Fig. 50. Low pressure turbine "A" turbine end showing extent of rub damage on L-4 and L-5 blade covers and tenons.

Fig. 51. Close-up of low pressure turbine "A" turbine end L-3 stage blade covers showing extent of rub damage.

Fig 52. Close-up of low pressure turbine "A" showing rub damage to trailing edges of turbine end L-5 and L-4 blades and leading edges of generator end L-5 stage blades.

Fig. 53 Close-up of generator end L-4 diaphragm from low pressure turbine "A" showing rub damage to vanes.

Fig. 54. Close-up of generator end L-4 upper half diaphragm from low pressure turbine "A" showing rub damage to vanes.

Fig. 55. Photograph of low pressure turbine rotor "B" in casing showing section of disk rim which fractured (arrows) through finger root attachments.

Fig. 56. Photograph of low pressure turbine "B" Rotor showing section of turbine end L-1 stage disk rim which fractured (arrows) through finger root attachments.

Fig. 57. Close-up of fractured turbine end L-1 stage disk of the low pressure turbine "B" rotor shown in Fig. 55.

Fig. 58. Close-up of fractured disk section of turbine end L-1 stage on low Pressure turbine "B" rotor shown in Fig. 55.

Fig. 59. Close-up of fractured turbine end L-1 stage disk section of low pressure turbine "B" rotor shown in Fig. 55.

Fig. 60. Photograph of turbine end L-1 stage blades from low pressure turbine "B" rotor showing extent of damage.

Fig. 61. Close-up photograph of turbine end L-1 stage blades from low pressure turbine "B" rotor shown in Fig. 55.

Fig. 62. Photograph of liberated turbine end L-1 blades from the low pressure turbine "B" rotor which section of fractured inner finger root attachment from disk rim.

Fig. 63. Close-up photograph of turbine end of low pressure turbine "B" showing extent of damage to last stage blades.

Fig. 64. Photograph of turbine end last stages blades from low pressure turbine "B" showing missing blade spacers.

Fig. 65. Photograph of turbine end last stage blades from low pressure turbine "B".

Fig. 66. Photograph of turbine end of low pressure turbine "B" rotor showing damage to L-2, L-3 and L-4 stage blade covers.

Fig. 67. Photograph of turbine end of low pressure turbine "B" rotor showing missing covers on L-2 and L-3 stage blades.

Fig. 68. Photograph of turbine end L-3 stage blading on low pressure turbine "B" rotor showing damage to covers and missing covers.

Fig. 69. Photograph of generator end of low pressure turbine "B" rotor.

Fig. 70. Photograph of generator end of low pressure turbine "B" showing damage to shrouds on L-1, L-2 and L-3 stages.

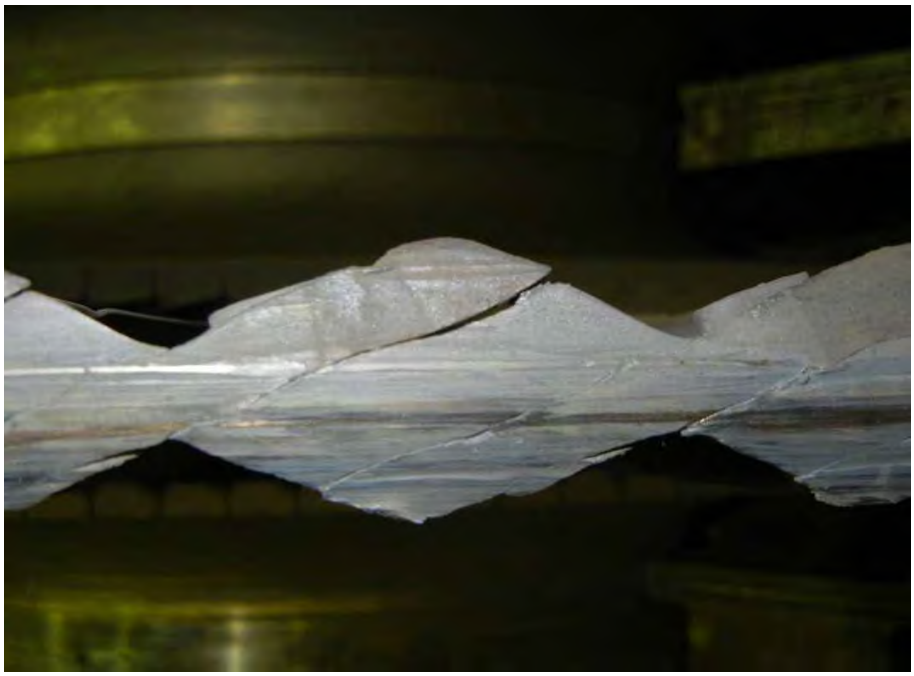

Fig. 71. Close-up photograph of low pressure turbine "B" generator end L-1 blade tips and spacers showing severe rub damage.

Fig. 72. Close-up photograph of low pressure turbine "B" generator end L-1 blade tips and spacers showing severe rub damage.

Fig. 73. Photograph of low pressure turbine "B" generator end last stage blades.

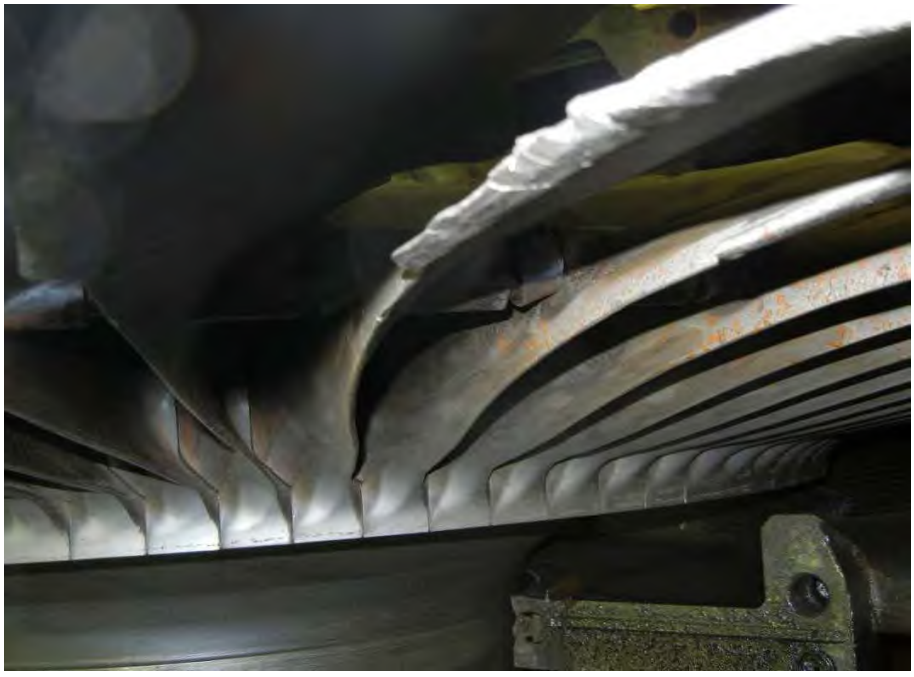

Fig. 74. Photograph of low pressure turbine "B" generator end last stage blades showing damage to stellited leading edges.

Fig. 75. Photograph of low pressure turbine "B" rotor L-2 stage diaphragm showing radial crack (arrow) through center section and inner wall.

Fig. 76. Close-up photograph of radial crack shown in low pressure turbine "B" turbine end L-2 diaphragm shown in Fig. 75.

Fig. 77. Photograph of turbine end last stage diaphragm from low pressure turbine "B" rotor showing extent of damage.

Fig. 78. Photograph of turbine end L-1 stage diaphragm from low pressure turbine "B" rotor showing extent of damage.

Fig. 79. Close-up photograph of diaphragm fracture surface shown in Fig. 78.

Fig. 80. Photograph of low pressure turbine "B" turbine end L-3 stage diaphragm showing extent of impact damage.

Fig. 81. Photograph of low pressure turbine "B" generator end L-4 stage diaphragm showing extent of impact damage to vane airfoils.

Fig. 82. Photograph of low pressure turbine "B" L-1 stage fractured disk rim with bubble wrap protection.

Fig. 83. Photograph of low pressure turbine "B" rotor with wooden protective box built around the fractured L-1 stage disk rim.

Fig. 84 Photograph of low pressure turbine "B" rotor at the GE Repair Facility in Chicago, IL., showing protective taping of fractured L-1 stage disk rim.

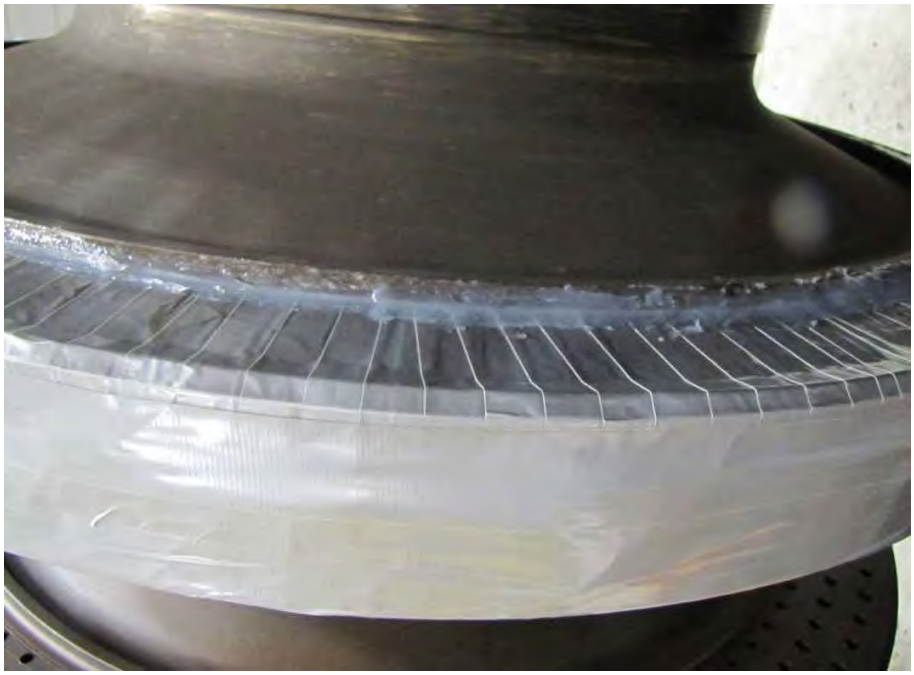

Fig. 85. Close-up of protective tape on fractured L-1 disk rim.

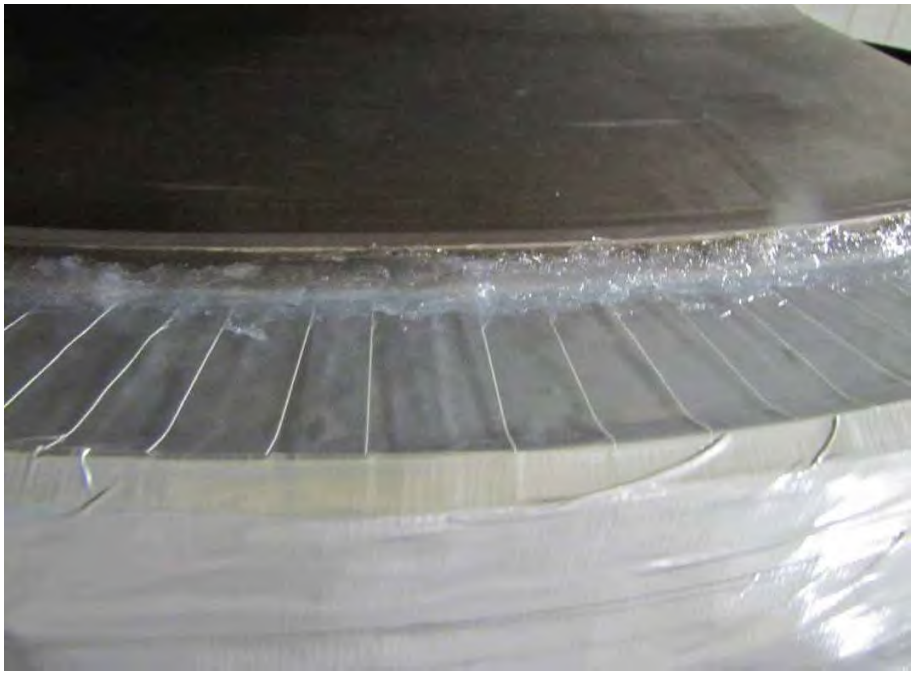

Fig. 86. Close-up of protective tape on fractured L-1 disk rim.

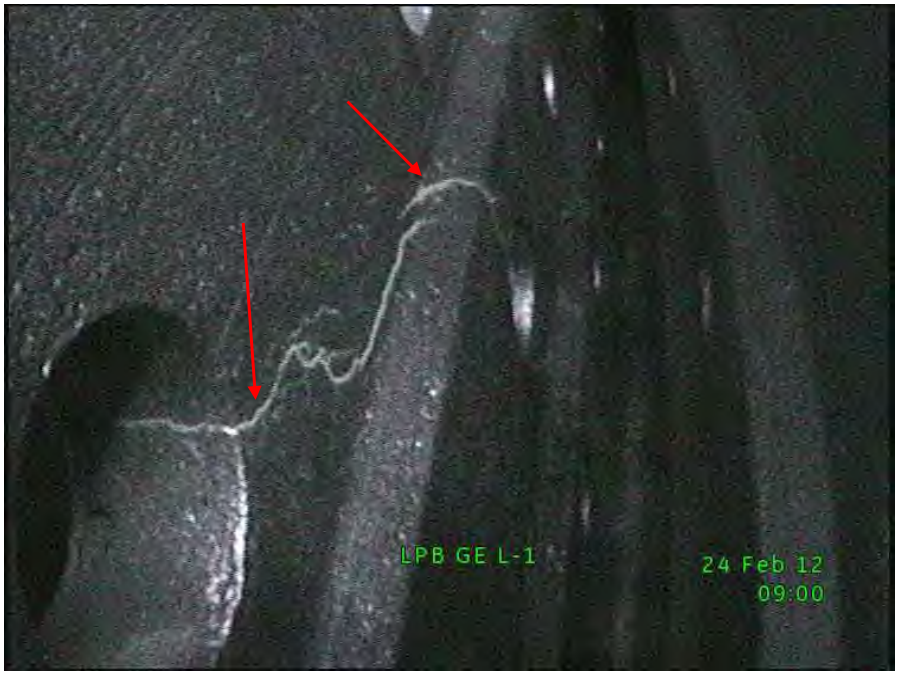

Fig. 87 Close-up blacklight photograph of low pressure turbine "B" L-1 disk rim showing MPI indications (arrows) in finger-root attachment.

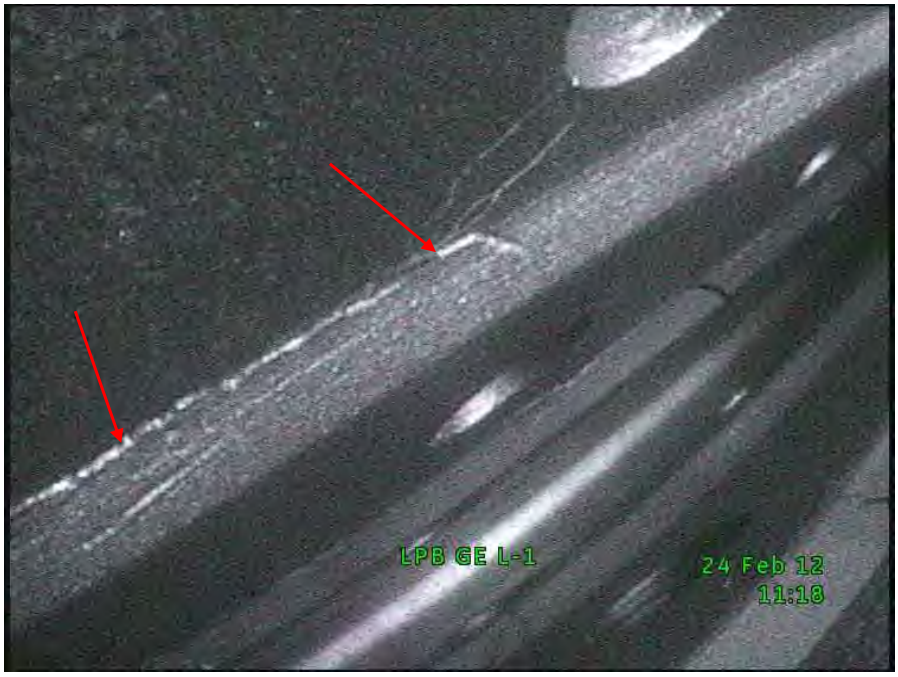

Fig. 88 Close-up blacklight photograph of Low Pressure Turbine "B" L-1 disk rim showing MPI indications (arrows) in finger-root attachment.

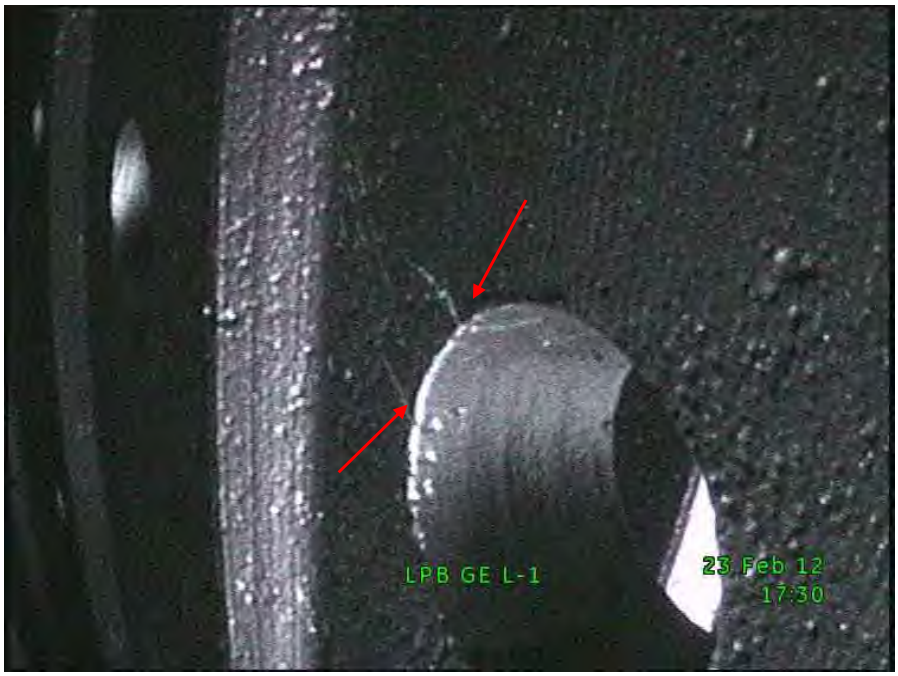

Fig. 89 Close-up blacklight photograph of low pressure turbine "B" L-1 disk rim showing MPI indication (arrows) in finger-root attachment.

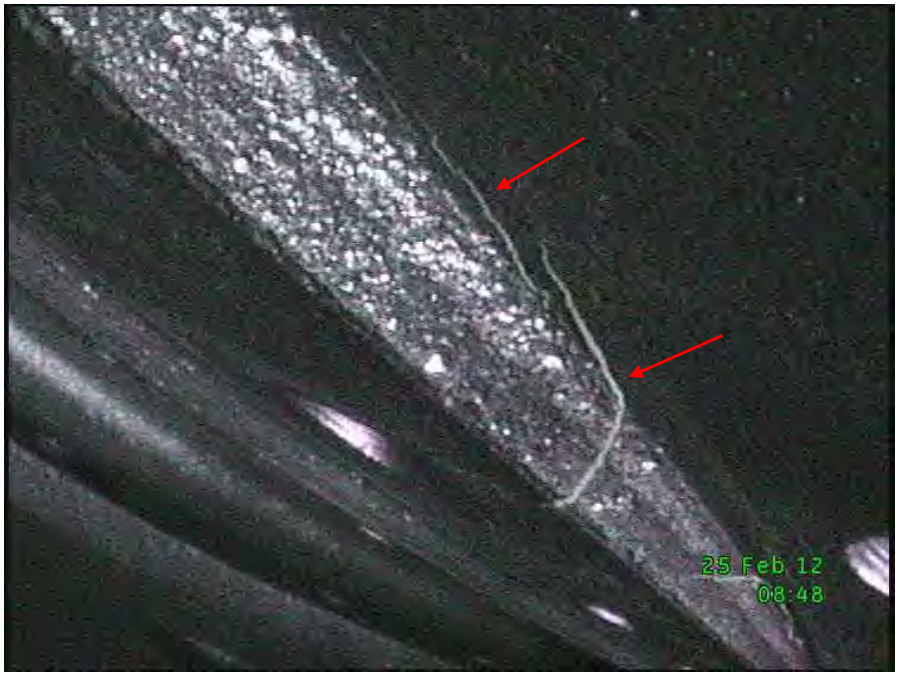

Fig. 90 Close-up blacklight photograph of low pressure turbine "A" L-1 disk rim showing MPI indications (arrows) in finger-root attachment.

Fig. 91 Close-up blacklight photograph of low pressure turbine "A" L-1 disk rim showing MPI indication (arrows) in finger-root attachment.

Fig. 92. Close-up blacklight photograph of low pressure turbine "A" generator end L-2 stage disk on inlet side of the blade dovetail showing indication (arrow).

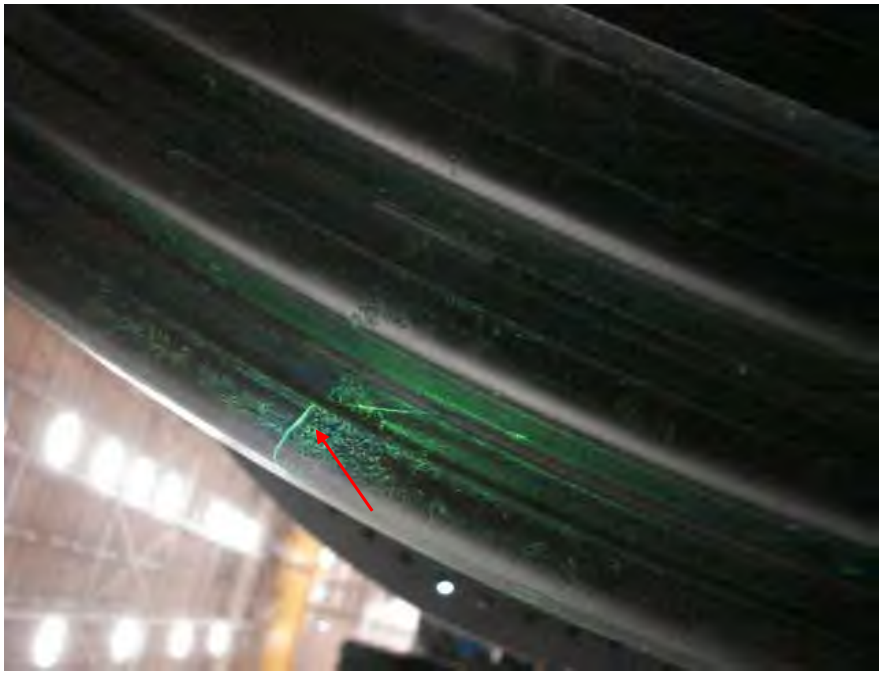

Fig. 93. Close-up blacklight photograph of low pressure turbine "A" generator end L-2 stage disk on inlet side of the blade dovetail showing indication (arrow).

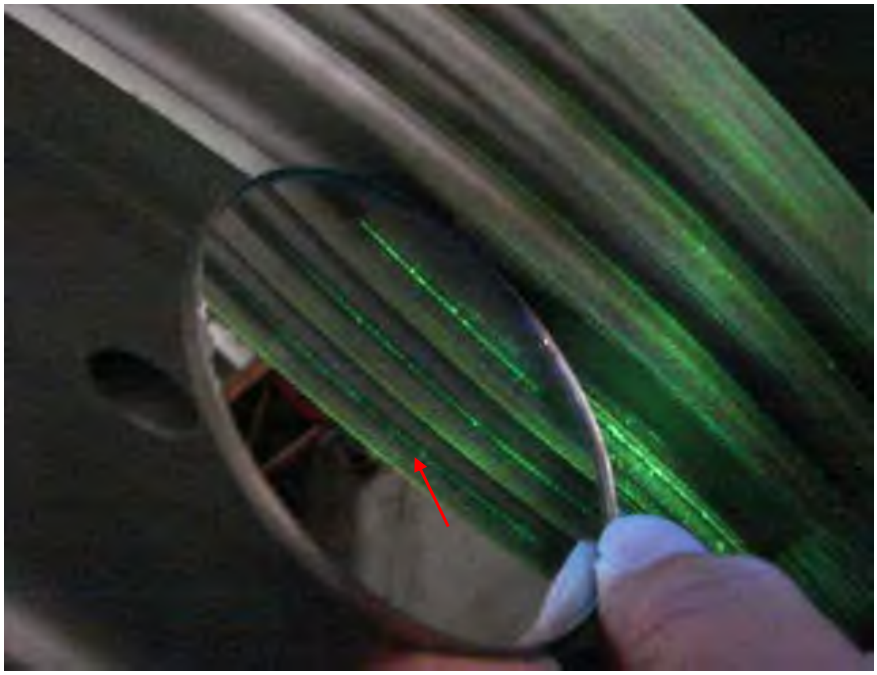

Fig. 94. Close-up blacklight photograph of low pressure turbine "A" generator end L-3 stage disk on exit side of the blade dovetail showing indication (arrow).

Fig. 95. Close-up blacklight photograph of low pressure turbine "A" generator end L-4 stage disk on the inlet side of the blade dovetail showing indication (arrow).

Fig. 96. Close-up blacklight photograph of low pressure turbine "A" generator end L-4 stage disk on exit side of the blade dovetail showing indication (arrow).

Fig. 97. Close-up blacklight photograph of low pressure turbine "A" generator end L-4 stage disk on inlet side of the blade dovetail showing indication (arrow).

Fig. 98. Close-up blacklight photograph of low pressure turbine "A" generator end L-5 stage disk on inlet side of the blade dovetail.

Fig. 99. Close-up blacklight photograph of low pressure turbine "A" generator end L-5 stage disk on inlet side of the blade dovetail.

Fig. 100. Close-up photograph of low pressure turbine "A" generator end L-2 stage disk rim showing excavation of indication at 330° location. Viewed from side.

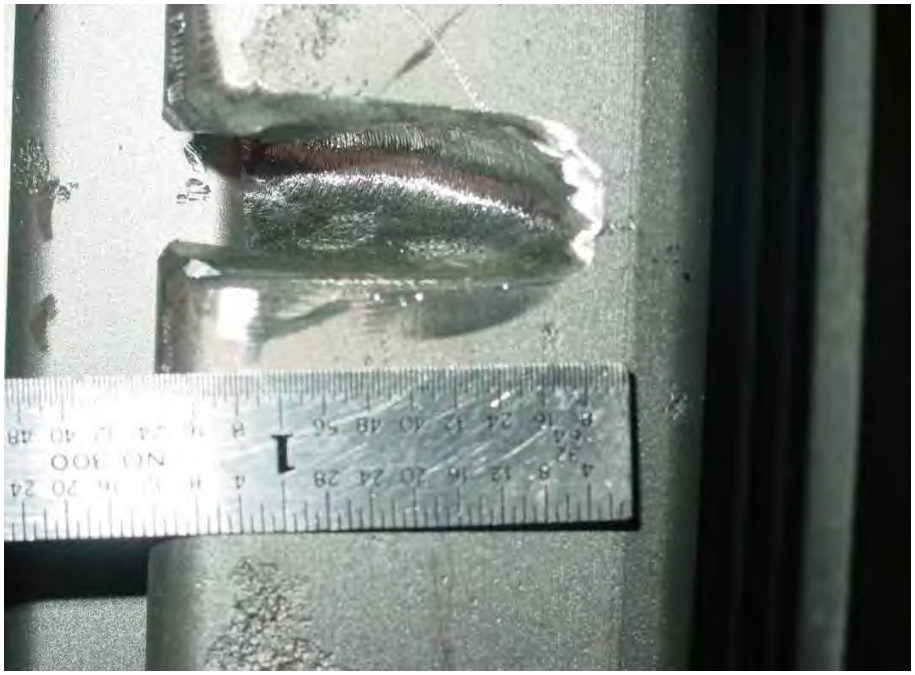

Fig. 101. Close-up photograph of low pressure turbine "A" generator end L-2 stage disk rim showing excavation of indication at 330° location. Viewed from top.

Fig. 102. Close-up photograph of low pressure turbine "A" generator end L-2 stage disk rim showing excavation of indication at 155° location.

Fig. 103. Close-up photograph of low pressure turbine "A" generator end L-2 stage disk rim showing excavation of indication at 155° location.

Fig. 104. Photograph of exciter doghouse showing portion of fractured generator shaft (arrow A) and portion of fractured exciter shaft (arrow B).

Fig. 105. Photograph of portion of fractured generator shaft shown in Fig. 104.

Fig. 106. Photograph of coupling from generator shaft end.

Fig. 107. Photograph of portion of fractured exciter shaft.

Fig. 108. Photograph of second fracture through exciter shaft.

Fig. 109. Photograph of third fracture through exciter shaft at collector end.

Fig. 110. Photograph of liberated exciter collector which came to rest in operator's room.

Fig. 111. Photograph of generator stator showing extent of rub damage.

Fig. 112. Generator rotor rub damage.

Fig. 113. Generator rotor rub damage.

Fig. 114. Generator rotor CE oil seal journal showing extent of rub damage.

Fig. 115. Photograph of No. 10 bearing.

Fig. 116. Photograph of No. 7 bearing.

Fig. 117. Photograph of No. 2 bearing.

Fig. 118. Photograph of bearing from Unit 3 (bearing No. unknown).

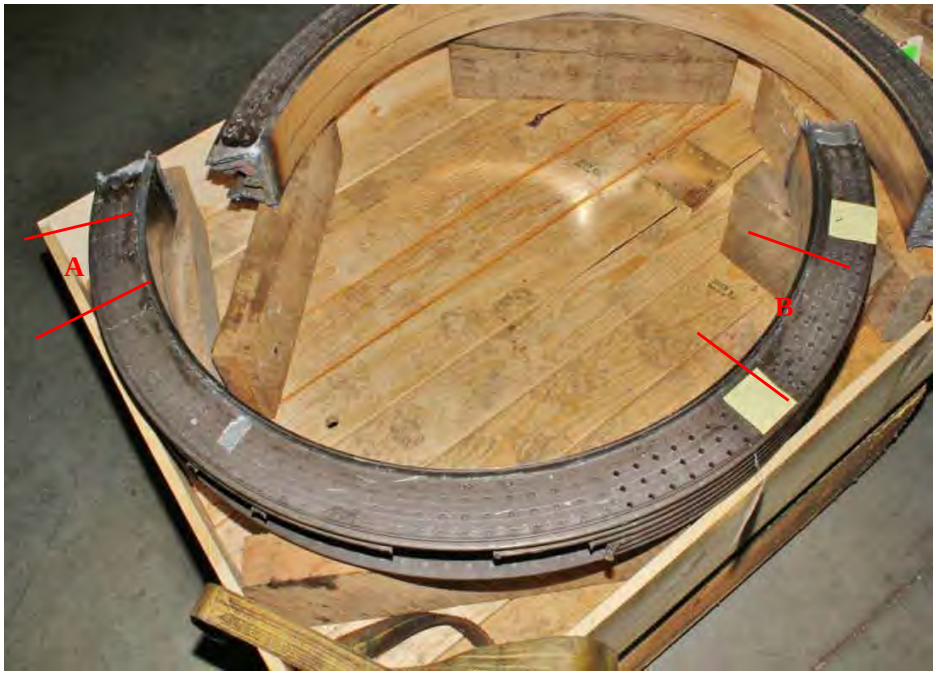

Fig. 119. Photograph of one half of sectioned low pressure turbine "B" fractured L-1 disk rim received from the GE Repair Facility. Identified by Engel Metallurgical as SID 14874.

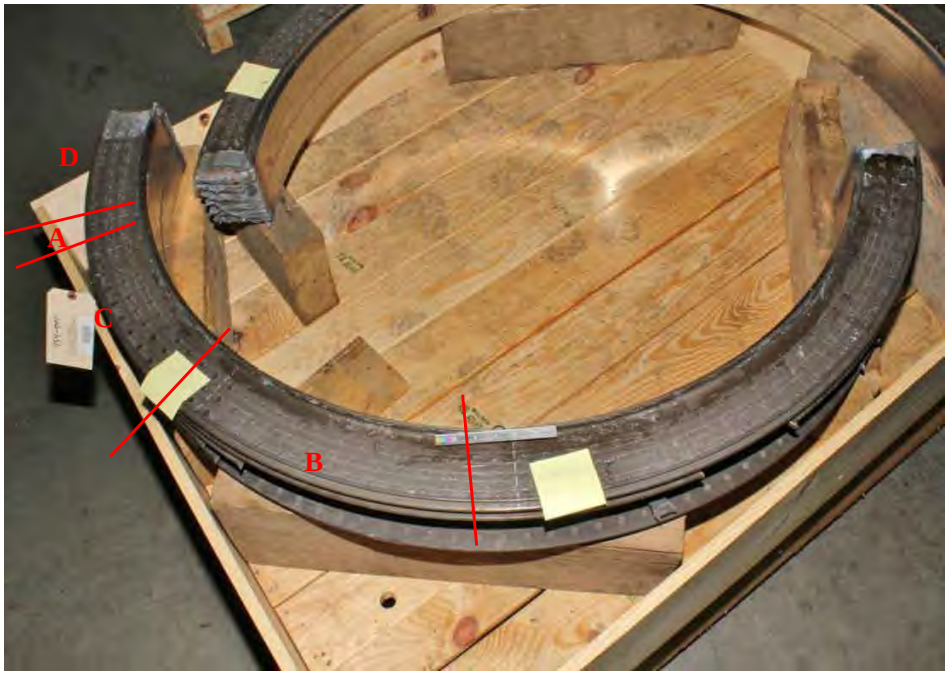

Fig. 120. Photograph of one half of sectioned low pressure turbine "B" fractured L-1 disk rim received from the GE Repair Facility. Identified by Engel Metallurgical as SID 14875.

Fig. 121. Close-up photograph of fractures through internal finger pinned blade attachments of the low pressure turbine "B" L-1 disk rim.

Fig. 122. Close-up photograph of fractures through internal finger pinned blade attachments of the low pressure turbine "B" L-1 disk rim.

Fig. 123. Close-up photograph of fractures through internal finger pinned blade attachments of the low pressure turbine "B" L-1 disk rim.

Fig. 124. Close-up photograph of fractures through internal finger pinned blade attachments in low pressure turbine "B" L-1 disk rim.

Fig. 125. SID 14874 subsegment "A" after circumferential sectioning.

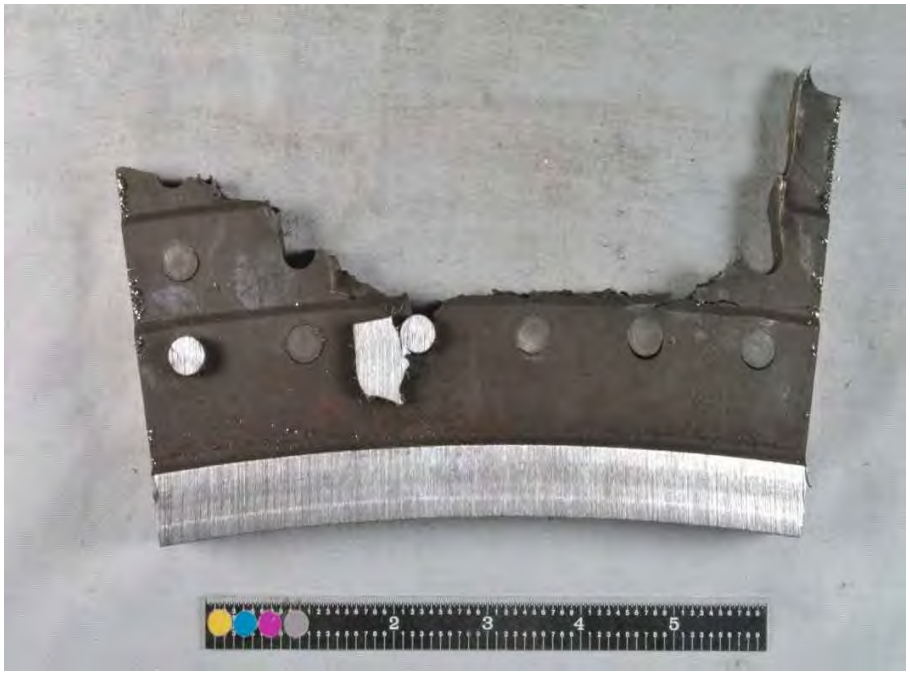

Fig. 126. SID 14874 subsegment "A3" finger pinned blade attachment.

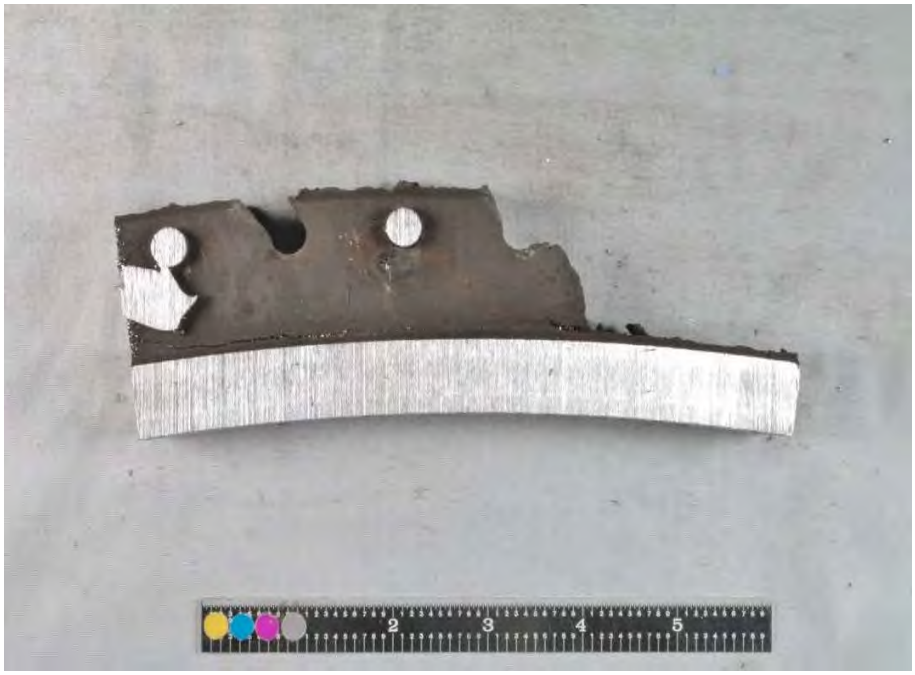

Fig. 127. SID 14874 subsegment "A4" finger pinned blade attachment.

Fig. 128. SID 14874 subsegment "A3" finger pinned attachment fracture surface.

Fig. 129 Close-up of SID 14874 subsegment "A3" fracture surface shown in Fig. 128.

Fig. 130. Close-up of SID 14874 subsegment "A3" fracture surface shown in Fig. 128.

Fig. 131. Close-up of SID 14874 subsegment "A3" fracture surface shown in Fig. 128.

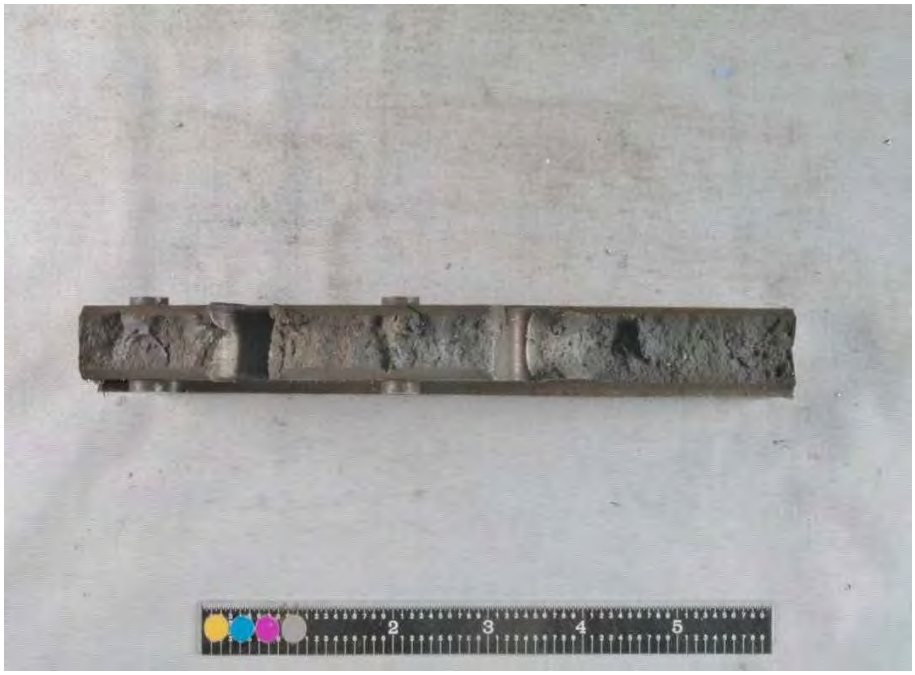

Fig. 132. SID 14874 subsegment "A4" finger pinned attachment fracture surface.

Fig 133. Close-up of SID 14874 subsegment "A4" fracture surface shown in Fig. 132.

Fig. 134. Close-up photograph of SID 14874 subsegment "A4" fracture surface shown in Fig. 132.

Fig. 135. Close-up photograph of SID 14874 subsegment "A4" fracture surface shown in Fig. 132.

Fig 136. SID 14875 subsegment "B" after circumferential sectioning.

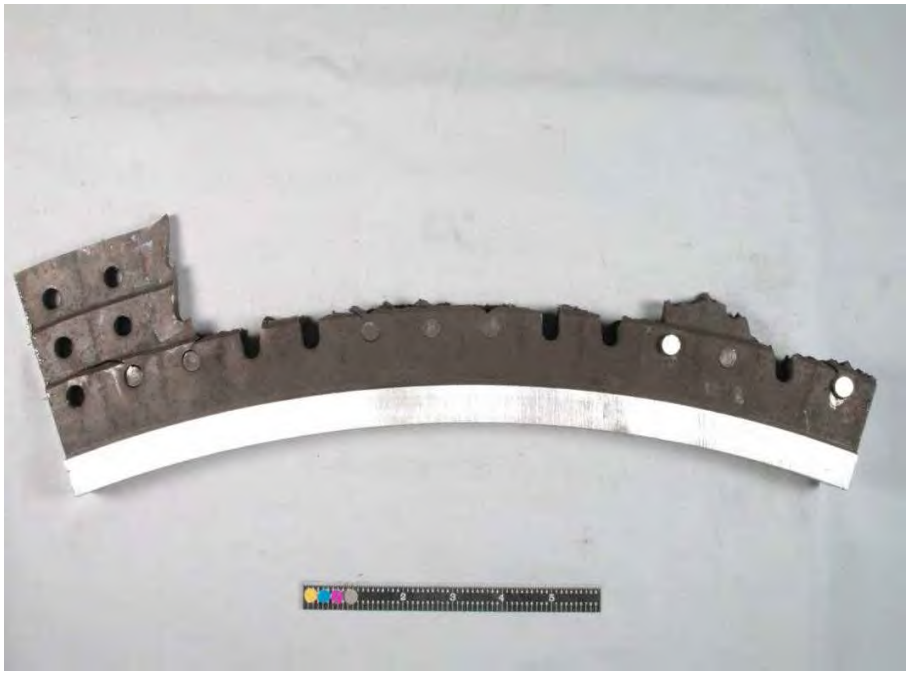

Fig. 137. SID 14875 subsegment "B3" finger pinned blade attachment, outlet side.

Fig. 138. SID 14875 subsegment "B4" finger pinned blade attachment, outlet side.

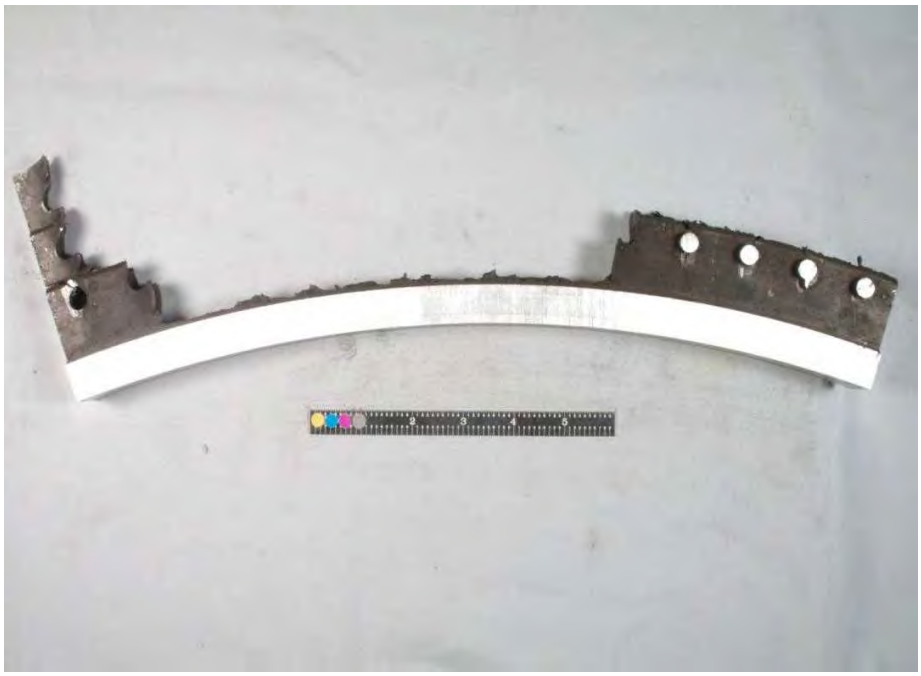

Fig. 139. SID 14875 subsegment "B5" finger pinned blade attachment, outlet side.

Fig. 140. Close-up of SID 14875 subsegment "B3" fracture surface.

Fig. 141. Close-up of SID 14875 subsegment "B3" fracture surface.

Fig. 142. Close-up of SID 14875 subsegment "B3" fracture surface.

Fig. 143. Close-up of SID 14875 subsegment "B3" fracture surface shown in Fig. 140.

Fig. 144. Close-up of SID 14875 subsegment "B3" fracture surface shown in Fig. 141.

Fig. 145. Close-up of SID 14875 subsegment "B3" fracture surface shown in Fig. 142.

Fig 146. Close-up of SID 14875 subsegment "B4" fracture surface.

Fig. 147. Close-up of SID 14875 subsegment "B4" fracture surface shown in Fig. 146.

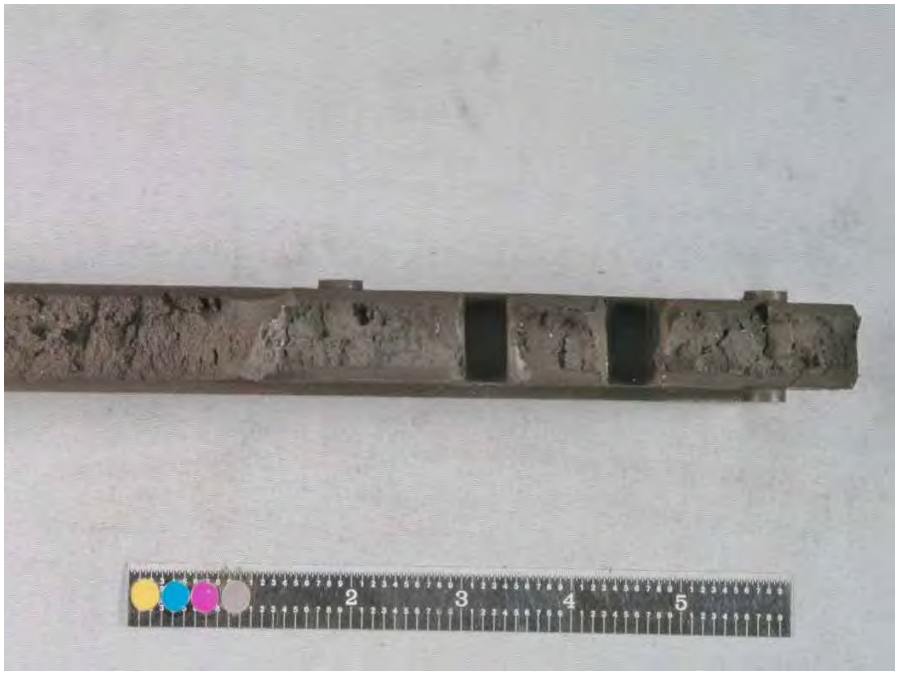

Fig. 148 Close-up of SID 14875 subsegment "B4" fracture surface.

Fig. 149. Close-up of SID 14875 subsegment "B4" fracture surface shown in Fig. 148.

Fig. 150. Close-up of SID 14875 subsegment "B5" fracture surface.

Fig. 151. Close-up of SID 14875 subsegment "B5" fracture surface.

Fig. 152. Close-up of SID 14875 subsegment "B5" fracture surface shown in Fig. 150.

Fig 153 Close-up of SID 14875 subsegment "B5" fracture surface shown in Fig. 151.

Fig. 154. SID 14875 subsegment "C" after circumferential sectioning.

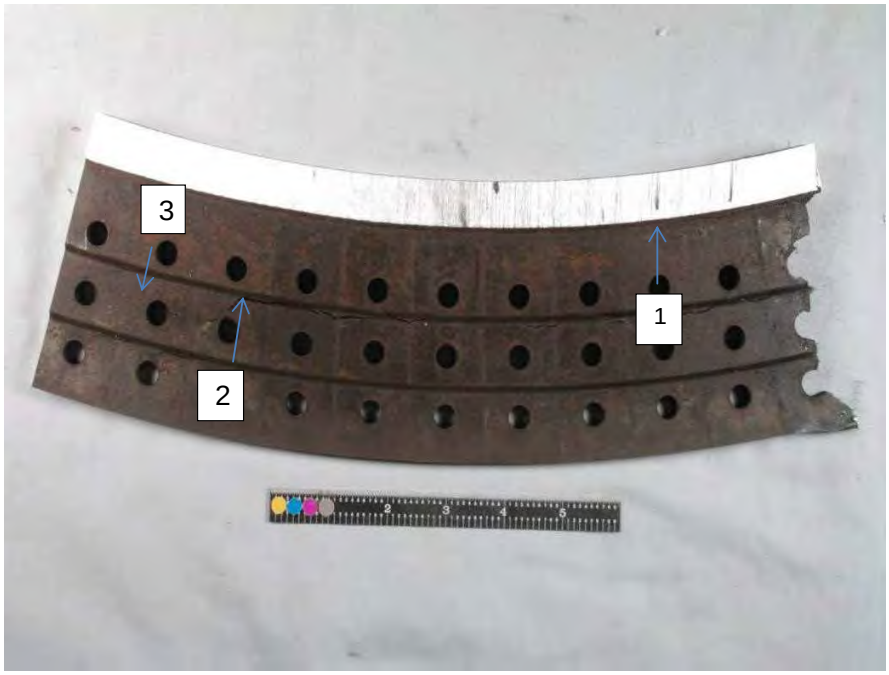

Fig. 155. SID 14875 subsegment "C4" finger pinned blade attachment showing location of three examined cracks, viewed from inlet side.

Fig 156 Close-up of SID 14875 subsegment "C4"finger pinned blade attachment shown in Fig. 155, viewed from inlet side.

Fig. 157 Close-up of SID 14875 subsegment "C4" finger pinned blade attachment shown in Fig. 155, viewed from inlet side.

Fig 158. Close-up of SID 14875 subsegment "C4" crack 1 identified in Fig. 155, viewed from inlet side.

Fig 159. Close-up of SID 14875 subsegment "C4" crack No. 1 shown in Fig. 158, viewed from inlet side.

Fig 160. Close-up of SID 14875 subsegment "C4" crack No. 1 shown in Fig. 158, viewed from inlet side.

Fig 161. Close-up of SID 14875 subsegment "C4" crack No. 2 identified in Fig. 155, viewed from inlet side.

Fig 162. Close-up of SID 14875 subsegment "C4" crack No. 2 shown in Fig. 161, viewed from inlet side.

Fig 163. Close-up of SID 14875 subsegment "C4" crack No. 2 shown in Fig. 161, viewed from inlet side.

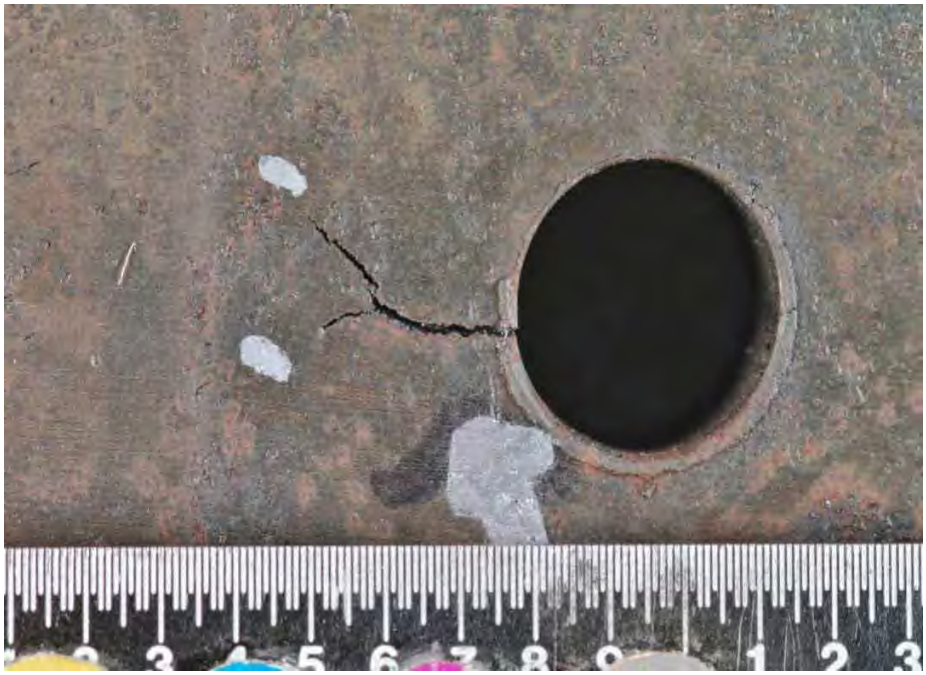

Fig 164. Close-up of SID 14875 subsegment "C4" crack No. 3 identified in Fig. 155, viewed from the inlet side.

Fig 165. Close-up of SID 14875 subsegment "C4" crack No. 3 shown in Fig. 164, viewed from inlet side.

Fig 166. Close-up of surface of fracture through crack No. 1 from SID 14875 subsegment "C4".

Fig 167. Close-up of surface of fracture through crack No. 1 from SID 14875 subsegment "C4" shown in Fig. 166.

Fig. 168. Close-up of surface of fracture through crack No. 2 from SID 14875 subsegment "C4".

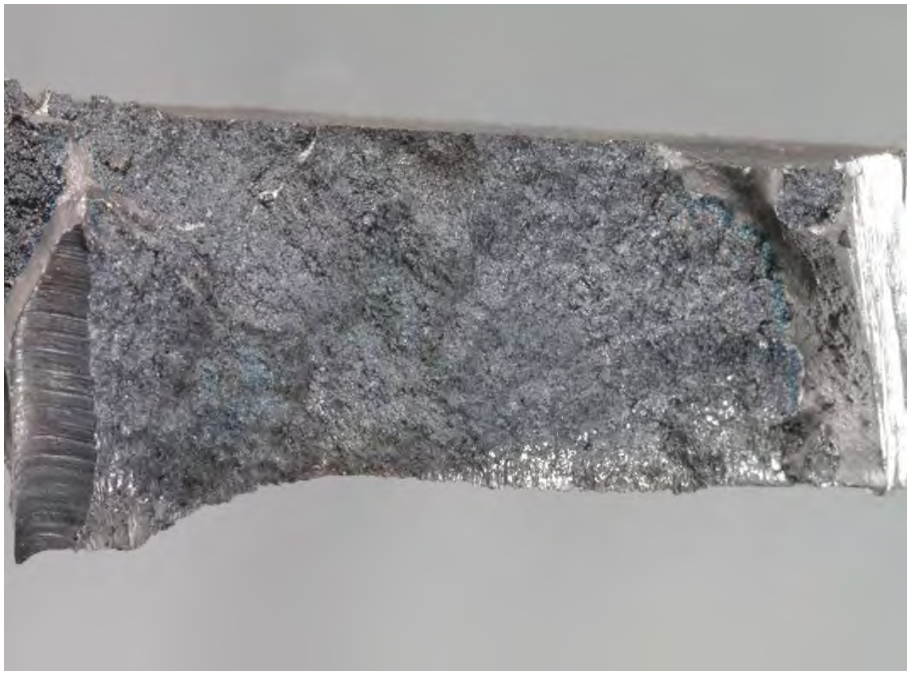

Fig 169. Close-up of surface of fracture through crack No. 2 from SID 14875 subsegment "C4" shown in Fig. 168.

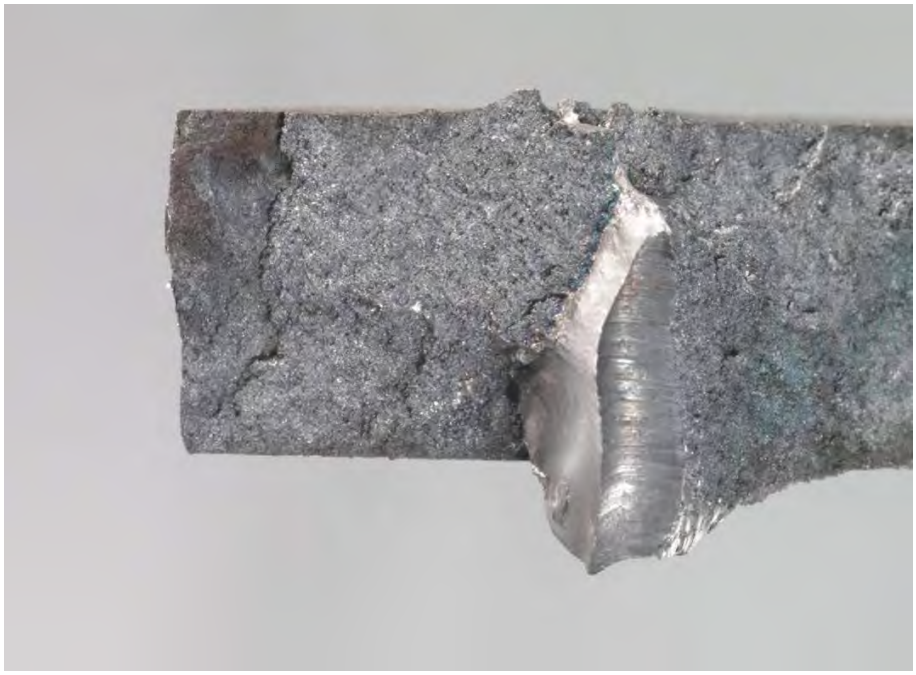

Fig 170. Close-up of surface of fracture through crack No. 2 from SID 14875 subsegment "C4" shown in Fig. 168.

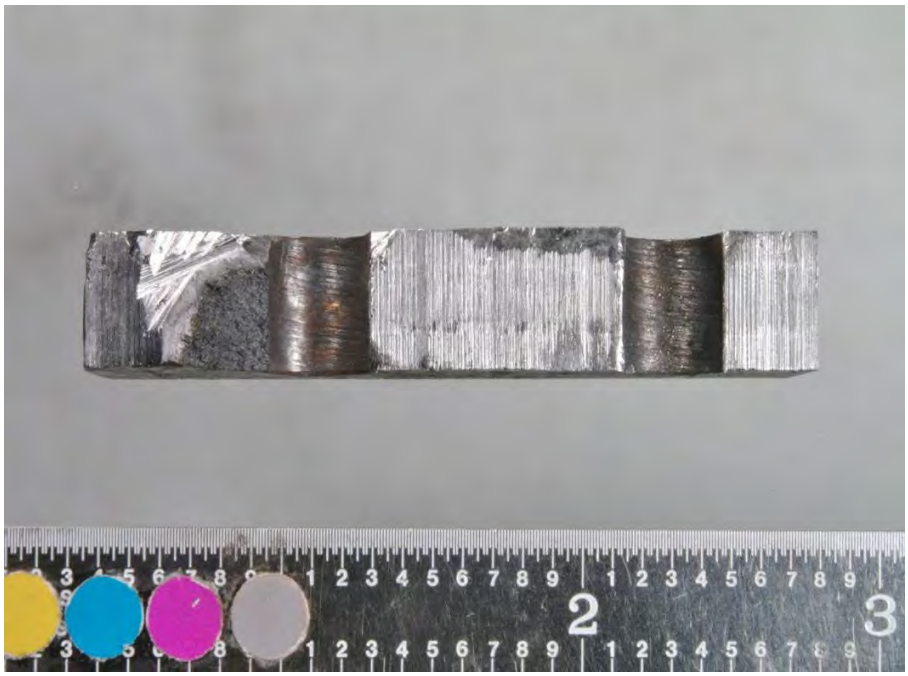

Fig 171. Close-up of surface of fracture through crack No. 3 from SID 14875 subsegment "C4".

Fig 172. Close-up of surface of fracture through crack No. 3 from SID 14875 subsegment "C4" shown in Fig. 171.

Fig 173. Close-up of finger pinned blade attachment from SID 14875 subsegment "C4" showing extent of corrosion/oxidation, viewed from inlet side.

Fig 174. Close-up of finger pinned blade attachment from SID 14875 subsegment "C4" shown in Fig. 173.

Fig. 175. Close-up photograph of fracture surface from SID 14875 "B4" subsegment identifying two areas examined by scanning electron microscope.

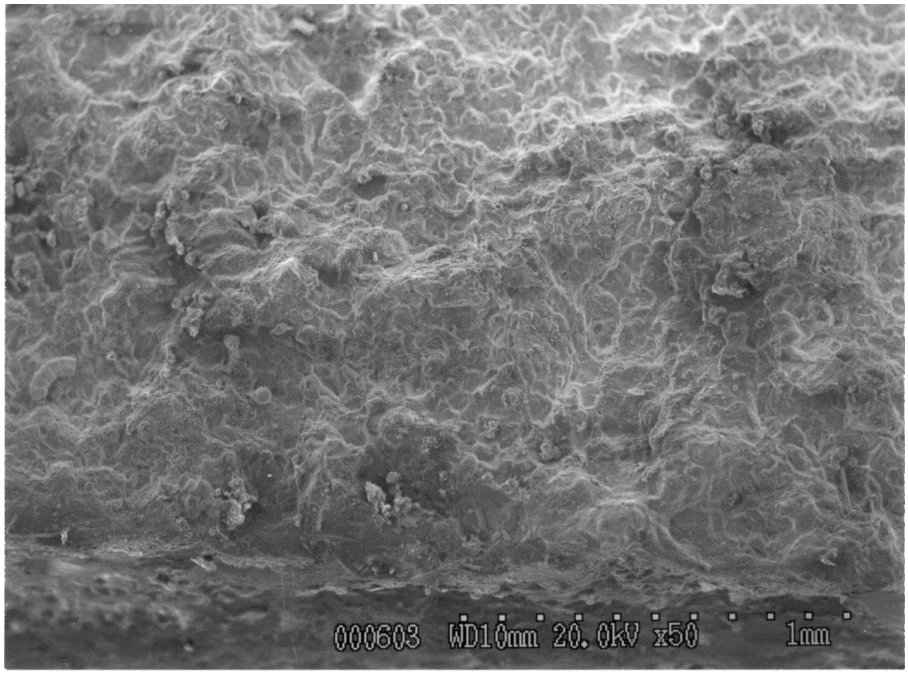

Fig. 176. Scanning electron microscope fractograph of SID 14875 "B4" Area "A" in the as-received condition.

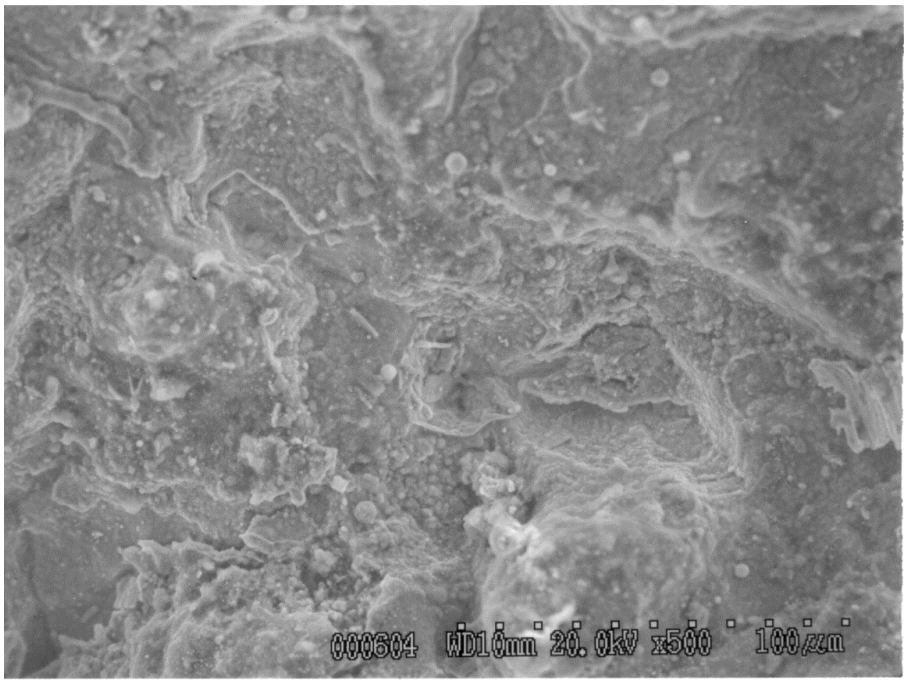

Fig. 177. Scanning electron microscope fractograph of SID 14875 "B4" Area "A" shown in Fig. 176.

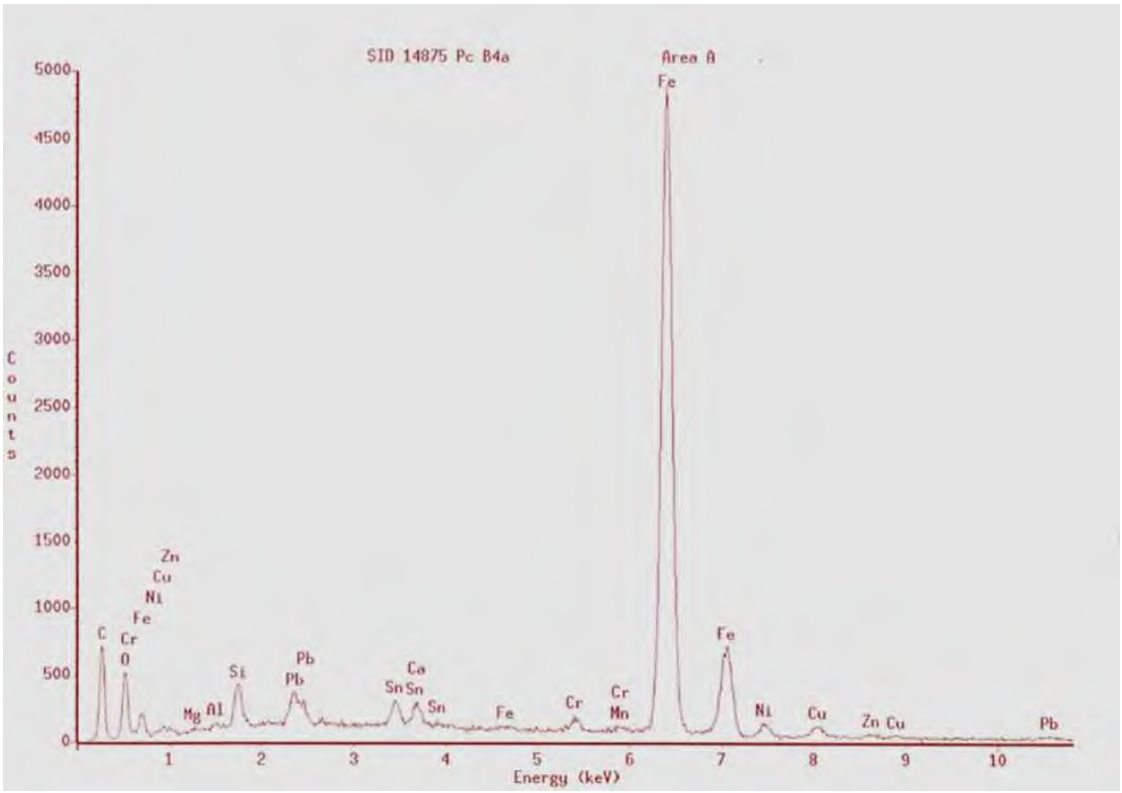

Fig. 178. X-Ray Energy Dispersive Spectrograph of SID 14875 "B4" Area "A" in the as-received condition.

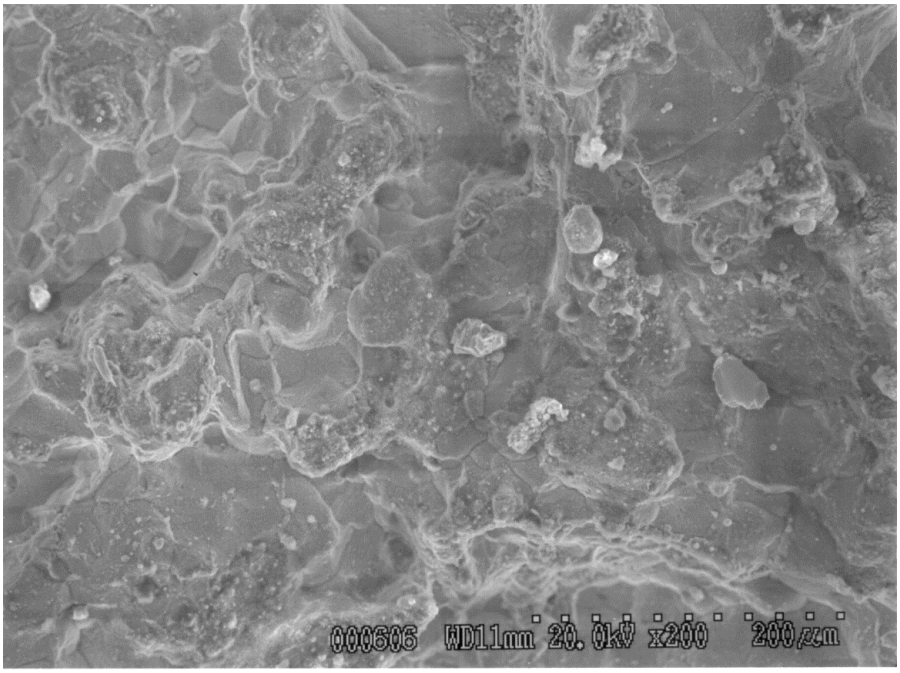

Fig. 179. Scanning electron microscope fractograph of SID 14875 "B4" Area C in the as-received condition.

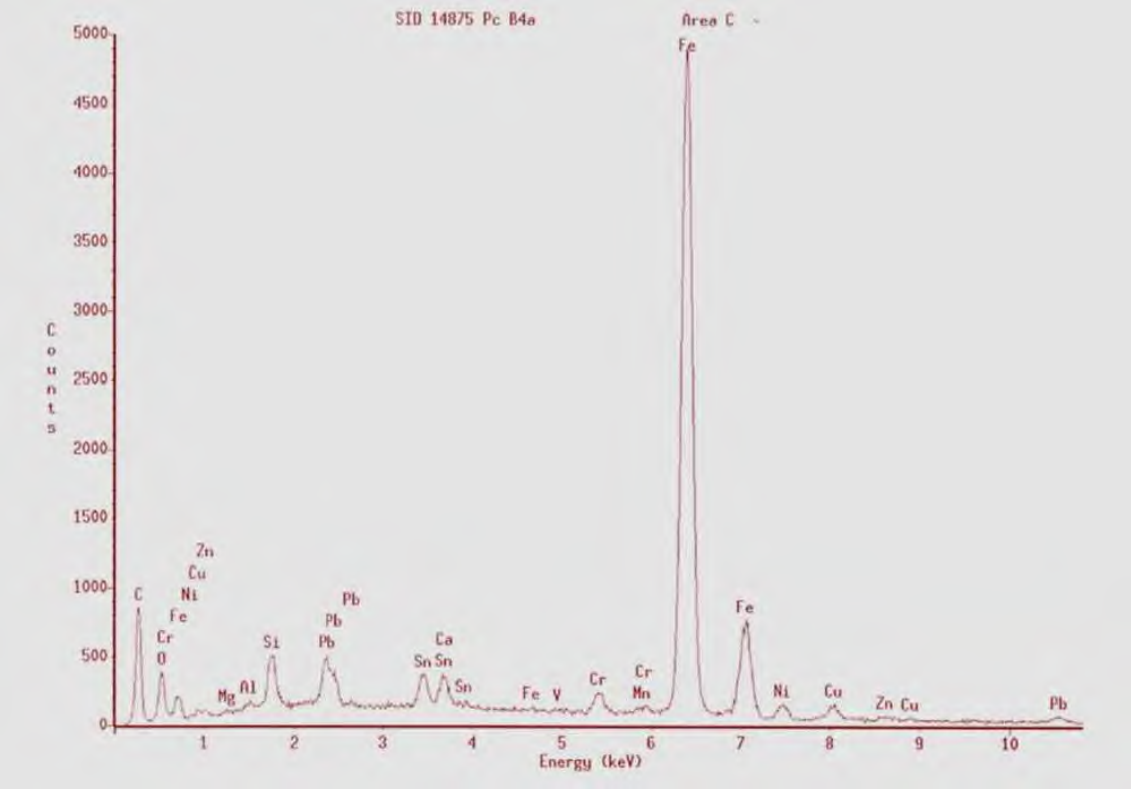

Fig. 180. X-Ray Energy Dispersive Spectrograph of SID 14875 "B4" Area "C" in the as-received condition.

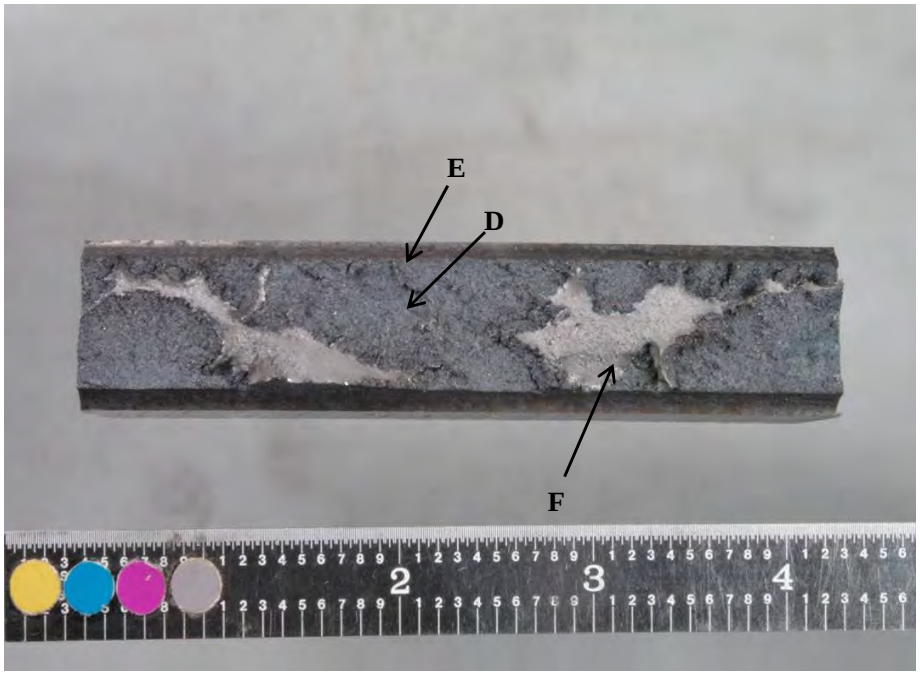

Fig. 181 Close-up photograph of SID 14875 "B4" fracture surface after cleaning identifying the three areas examined by scanning electron microscope.

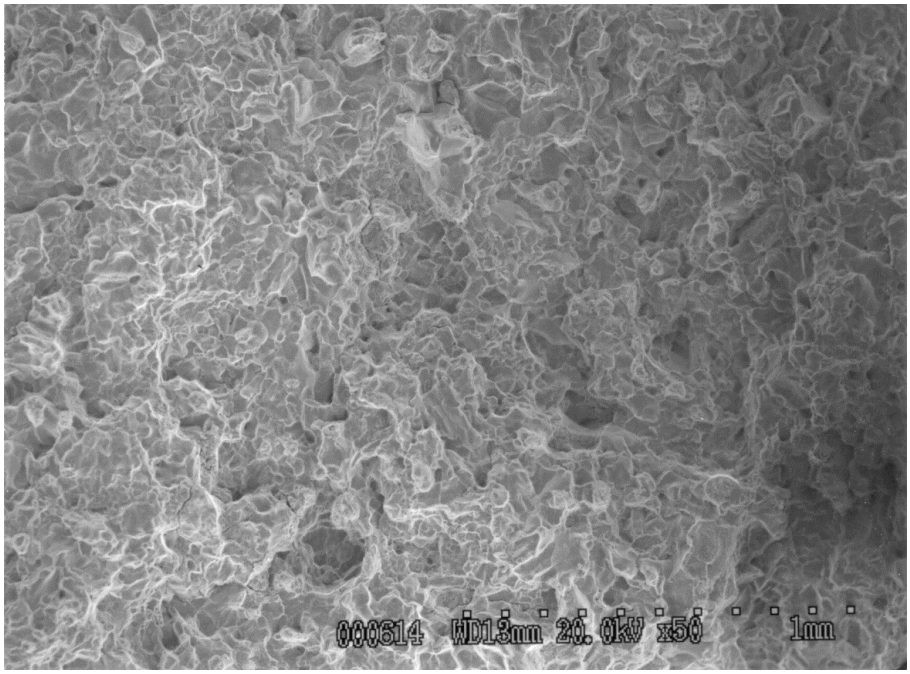

Fig. 182. Scanning electron microscope fractograph of SID 14875 "B4" Area "D".

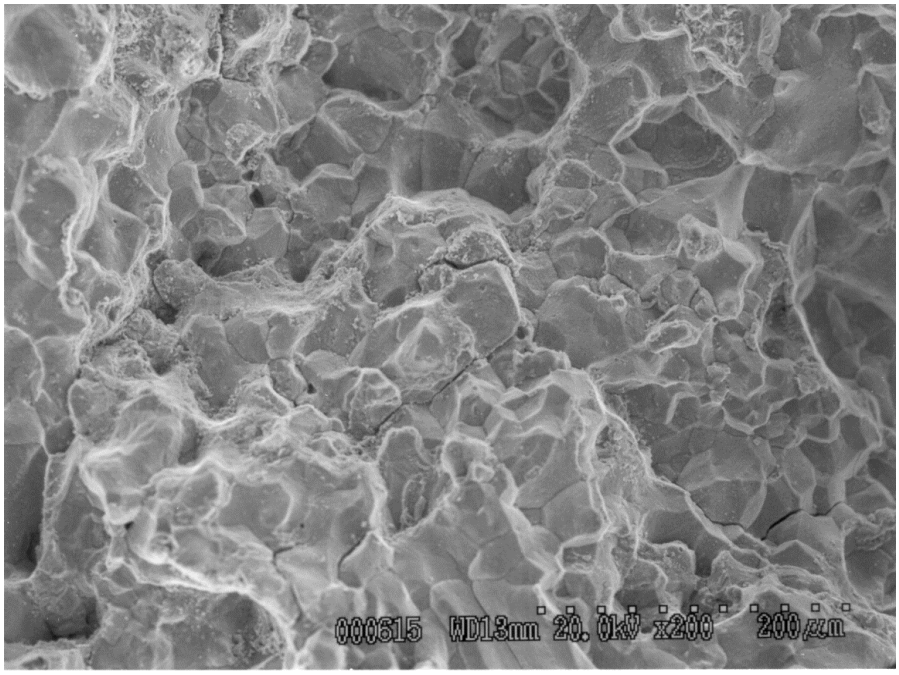

Fig. 183. Scanning electron microscope fractograph of SID 14875 "B4" Area "D".

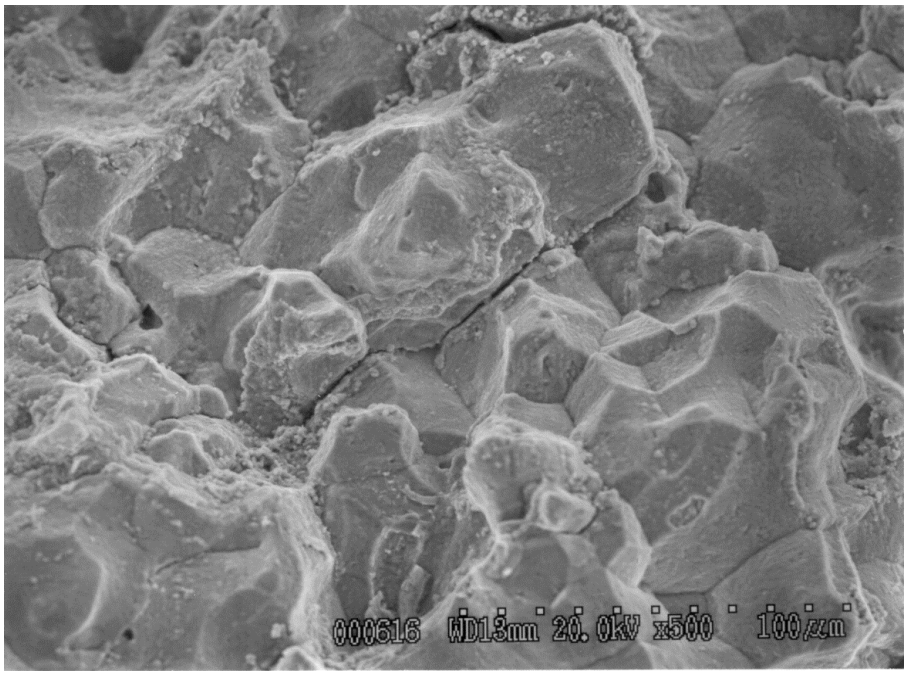

Fig. 184. Scanning electron microscope fractograph of SID 14875 "B4" Area "D".

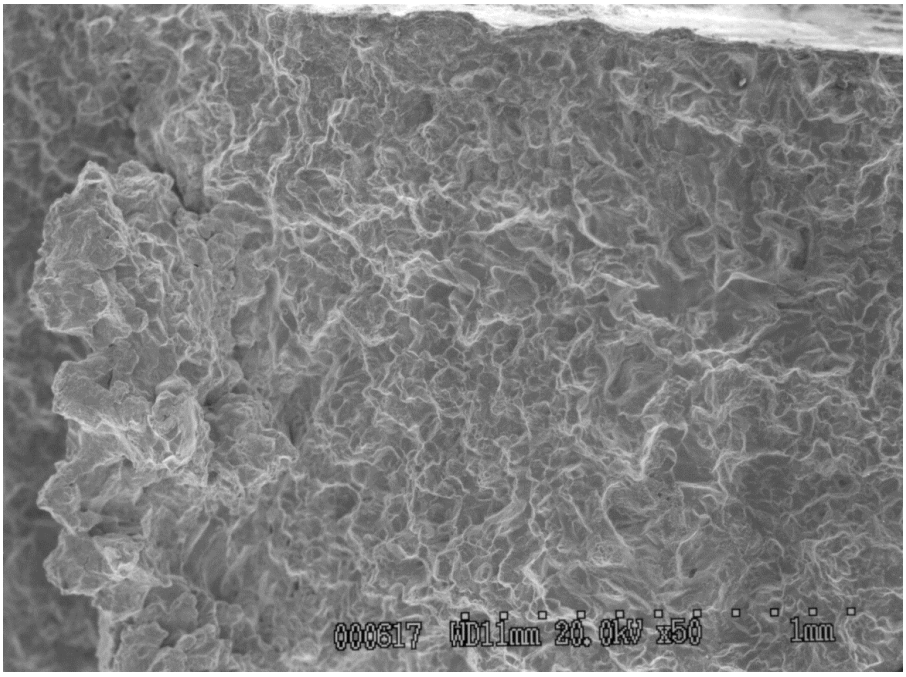

Fig. 185. Scanning electron microscope fractograph of SID 14875 "B4" Area "E".

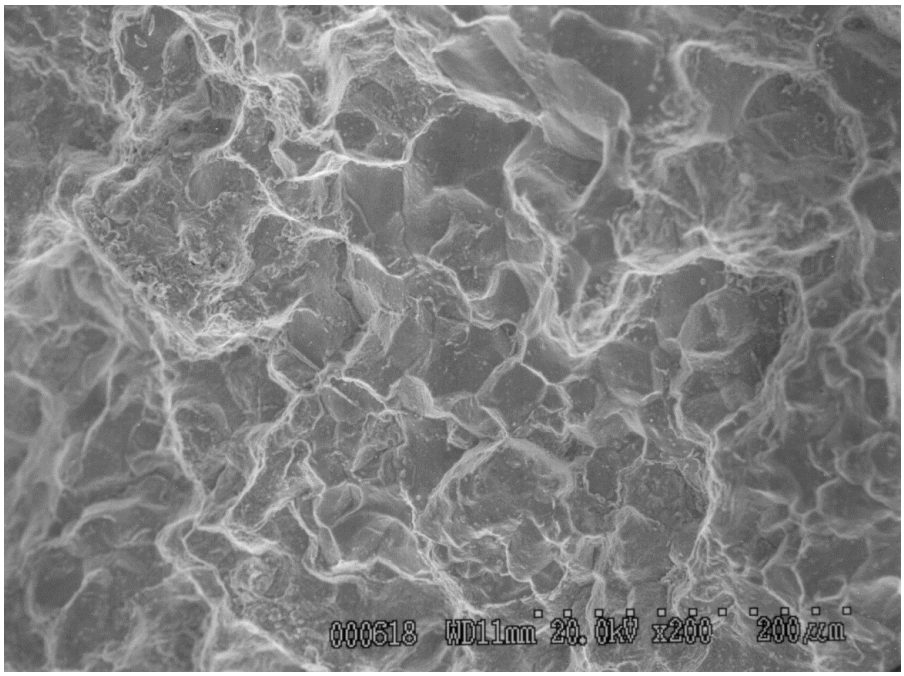

Fig. 186. Scanning electron microscope fractograph of SID 14875 "B4" Area "E".